Report No. 234

epaResearch
Climate - Water - Sustainability
Identifying pressures • Informing policy • Developing solutions

One-step Drinking Water Treatment Using Filtration and Nanostructured Composites

Authors: Anne Morrissey, Declan McGlade, Kieran Nolan, Brid Quilty and Jenny Lawler

Roinn Cumarsáide, Gníomhaithe ar son na hAeráide & Comhshaoil
Department of Communications, Climate Action & Environment

www.epa.ie

EPA RESEARCH PROGRAMME 2014–2020

One-step Drinking Water Treatment Using Filtration and Nanostructured Composites

(2011-W-MS-8)

EPA Research Report

Prepared for the Environmental Protection Agency

by

Dublin City University

Authors:

Anne Morrissey, Declan McGlade, Kieran Nolan, Brid Quilty and Jenny Lawler

ENVIRONMENTAL PROTECTION AGENCY
An Ghníomhaireacht um Chaomhnú Comhshaoil
PO Box 3000, Johnstown Castle, Co. Wexford, Ireland

Telephone: +353 53 916 0600 Fax: +353 53 916 0699
Email: info@epa.ie Website: www.epa.ie

© Environmental Protection Agency 2017

ACKNOWLEDGEMENTS

This report is published as part of the EPA Research Programme 2014–2020. The programme is financed by the Irish Government. It is administered on behalf of the Department of Communications, Climate Action and Environment by the EPA, which has the statutory function of co-ordinating and promoting environmental research.

The authors are grateful to all those who contributed to the success of this project. The project team acknowledge the support, encouragement and advice from the chairs of the steering committee, Lisa Sheils, Niamh Connolly, Eamonn Merriman and Dr Aisling O'Connor, and the other members of the steering committee, Dr John Gray (Consultant) and Darragh Page (EPA).

The authors are particularly grateful to the team from T.E. Laboratories, Mark Bowkett and Breda Moore, who were our project partners for the duration of the project and were invaluable in providing the water samples.

Other contributors to the project who should be acknowledged are Dr Alexander Yavorskyy, who developed and characterised the graphene composite used in the research; Dr Mahendra Kumar, who assisted the project team with the development of the graphene filters and the work on humic acids and membrane antifouling; Greg McNamara for his help with the Life Cycle Assessment work; and Dr Zahra Gholamvand, who introduced the team to the world of graphene and whose knowledge and support were invaluable at the early stages of the project. The project team would also like to acknowledge the contribution to the funding of the project from Environtech University Designated Research Initiative at Dublin City University and the Schools of Biotechnology and Chemical Sciences for funding the final year undergraduate students whose work contributed to some of the results of the filtration studies.

Cover image: the Boyle River, courtesy of Ecofact.

DISCLAIMER

Although every effort has been made to ensure the accuracy of the material contained in this publication, complete accuracy cannot be guaranteed. The Environmental Protection Agency, the authors and the steering committee members do not accept any responsibility whatsoever for loss or damage occasioned, or claimed to have been occasioned, in part or in full, as a consequence of any person acting, or refraining from acting, as a result of a matter contained in this publication. All or part of this publication may be reproduced without further permission, provided the source is acknowledged.

The EPA Research Programme addresses the need for research in Ireland to inform policymakers and other stakeholders on a range of questions in relation to environmental protection. These reports are intended as contributions to the necessary debate on the protection of the environment.

EPA RESEARCH PROGRAMME 2014–2020
Published by the Environmental Protection Agency, Ireland

ISBN: 978-1-84095-755-6 December 2017

Price: Free Online version

Project Partners

Anne Morrissey
School of Biotechnology
Dublin City University
Dublin 9
Ireland
Email: anne.morrissey@dcu.ie

Jenny Lawler
School of Biotechnology
Dublin City University
Dublin 9
Ireland
Email: jenny.lawler@dcu.ie

Brid Quilty
School of Biotechnology
Dublin City University
Dublin 9
Ireland
Email: brid.quilty@dcu.ie

Kieran Nolan
School of Chemical Sciences
Dublin City University
Dublin 9
Ireland
Email: kieran.nolan@dcu.ie

Mark Bowkett
T.E. Laboratories
Loughmartin Business Park
Tullow
Co. Carlow
Ireland
Email: mbowkett@tellab.ie

Alexander Yavorskyy
School of Chemical Sciences
Dublin City University
Dublin 9
Ireland
Email: alexander.yavorskyy@dcu.ie

Declan McGlade
School of Biotechnology
Dublin City University
Dublin 9
Ireland
Email: declan.mcglade2@mail.dcu.ie

Contents

List of Figures

List of Tables

Executive Summary

Background

Sustainable access to clean, safe drinking water has been a key concern in Ireland in recent years, with instances of boil water notices due to the presence of microbial contaminants such as *Cryptosporidium parvum* and *Escherichia coli* being all too frequent. Many drinking water treatment plants do not have the technical capacity to fully eliminate these microbial contaminants. A commonly used disinfection method, chlorination, can also lead to further problems, including the presence of toxic chlorine by-products in the finished drinking waters. In addition, emerging micropollutants of concern, such as pharmaceuticals and personal care products (PPCPs) and hazardous organic pollutants (HOPs), are also not fully eliminated in a drinking water treatment process. While levels found in drinking water sources are typically very low (of the ng/L to µg/L order of magnitude), the effects of long-term exposure to low levels of these chemicals is unknown.

In order to assure water quality and future-proof the potential for reclaimed water use for potable purposes, the development and application of treatment technologies that are capable of removing microbial contaminants, PPCPs and HOPs is needed. While community access to drinking water varies between public water supplies, group water schemes and private water supplies, there is a need for a variety of drinking water treatment technologies that can remove both microbial and other micropollutants in the same system, particularly for small water supply schemes.

Graphene has attracted significant attention in recent years as a uniquely structured carbon with attractive adsorbent properties suitable for the capture of low-concentration pollutants. Composites containing graphene-based structures have been shown to have antimicrobial and antibacterial properties, indicating that these composites could couple enhanced bacterial removal and strong disinfection activity to enable very effective drinking water treatment. In addition, the development of improved membrane filtration systems for the rejection of micro-organisms and compounds such as pharmaceuticals is vital.

Objectives

Arising from the identified need to develop an improved drinking water treatment system, particularly for small-scale systems, the aim of this project is to design an innovative drinking water treatment technology that can remove inorganic, organic and microbiological contaminants with great effectiveness and reduce the discharge of chemicals to the environment. This technology is based on combining the adsorption properties of graphene, the biocidal properties of a graphene–copper composite and a modular filtration system that is suitable for drinking water treatment in small- and middle-scale group water schemes, where the small volume of drinking water supplied per day makes conventional technology less effective and more expensive.

Key Outputs

The key output from this project is an innovative drinking water treatment system that can be used for small-scale drinking water treatment. This modular system incorporates a novel graphene–copper composite immobilisation technique, which was tested and validated, and the integrated system was shown to remove key pathogens associated with drinking water, e.g. *E. coli* and cryptosporidum, as well as PPCPs.

Secondary outputs and discoveries include:

- Graphene and graphene oxide were shown not to be biocidal, despite reports in the literature to the contrary, while the combination of copper and graphene as a nanostructured composite was shown to be biocidal.
- Positively and negatively charged ultrafiltration membranes with improved characteristics were fabricated using graphene oxide and graphene oxide–titanium dioxide (TiO_2) composites.
- Acid-activated alginate–graphene oxide adsorptive beads were fabricated, and these beads exhibit

strong potential for use in the removal of organic pollutants.

- Public awareness of the importance of the treatment of contaminated drinking water supplies was created through a mini-symposium, international and national scientific meetings, publications in peer-reviewed journals, book chapters and industry publications.

1 Background and Objectives

1.1 Introduction

Sustainable access to clean, safe drinking water has been a key concern in Ireland in recent years, with instances of boil water notices being all too frequent. Even developed countries such as Ireland suffer from microbiological issues in water bodies, with *Escherichia coli* being detected at least once in 76 small private supplies and 24 private group water schemes (EPA, 2015). Current disinfection methods, including chlorination, have been shown to be ineffective for certain microbial contaminants such as *Cryptosporidium parvum* (Giannakis *et al.*, 2016) and to lead to further problems, including the presence of toxic chlorine by-products in the finished drinking waters (Villanueva *et al.*, 2003). At the same time, the release of wastewater treatment plant (WWTP) effluent can be considered a major source of pollution in drinking water sources, along with contamination from landfill leachate, sewage system or septic tank leakage, and contamination from agricultural runoff, as surface and ground waters account for a significant proportion of drinking water sources. One group of compounds that has attracted increasing interest in recent years is that of so-called contaminants of emerging concern, such as pharmaceuticals and personal care products (PPCPs) and hazardous organic pollutants (HOPs). The concentration of PPCPs in drinking water sources will typically be at least an order of magnitude less than that observed in WWTP effluents, on account of the processes of dilution and sorption to solids, but the degradation of these compounds is unlikely (Gómez *et al.*, 2012). While levels found in drinking water sources are typically very low (of the ng/L to µg/L order of magnitude), the effects of long-term exposure to low levels of these chemicals is unknown (Nicolopoulou-Stamati *et al.*, 2015; Sweeney *et al.*, 2015). In addition, certain compounds such as diclofenac have been found in mg/L levels (Praskova *et al.,* 2014). Many of the transformation products or metabolites of these substances can themselves be considered contaminants of concern (Evgenidou *et al.*, 2015).

A number of studies on the occurrence of PPCPs in various matrices within the Irish environment have been carried out under previous EPA-funded projects. A wide variety of pharmaceuticals at varying concentrations have been found in WWTP effluents (Luo *et al.*, 2014), in Irish WWTP influent and effluent streams (Lacey *et al.*, 2008, 2012), in Irish sewage sludge and sludge-enriched soils (Barron *et al.*, 2009), and in the marine and wider aquatic matrices in Ireland (McEneff *et al.*, 2015; Quinn *et al.*, 2015). In some cases (e.g. carbamazepine), the effluent concentrations from WWTPs were found to be higher than the influent concentrations (Lacey *et al.*, 2012).

WWTP effluents containing PPCPs are a good indication that the local drinking water sources may be contaminated. Many drinking water treatment plants do not have the technical capacity to remove micropollutants such as pharmaceuticals and other trace organic compounds (Wang *et al.*, 2015) or to fully eliminate microbial contaminants (Giannakis *et al.*, 2016). In order to assure water quality and future-proof the potential for reclaimed water use for potable purposes, the development and application of treatment technologies that are capable of removing PPCPs (Azaïs *et al.*, 2014) and microbial contaminants (EPA, 2015) is needed. With community access to drinking water varying between public water supplies, group water schemes and private water supplies, there is a need for a variety of drinking water treatment technologies, according to the size of the water supply, the variability in water demand and the seasonal variations in drinking water quality, particularly for small water supply schemes, that can remove both microbial and other micropollutants in the same system.

Graphene has attracted significant attention in recent years as a uniquely structured carbon with attractive adsorbent properties suitable for the capture of low-concentration pollutants (Speltini *et al.*, 2016). Composites of graphene with titanium dioxide (TiO_2) have been shown to have antimicrobial and antibacterial properties (Akhavan and Ghaderi,

2010), indicating that these composites could couple enhanced bacterial removal and strong disinfection activity to provide very effective drinking water treatment. In addition, developing an improved membrane filtration system that can act on the basis of size exclusion for the rejection of micro-organisms and compounds such as pharmaceuticals is vital. Ultrafiltration (UF) systems have been shown to retain micro-organisms, but not low molecular weight organic compounds, leading to the repopulation of contaminants on the permeate side (Peter-Varbanets *et al.*, 2011), i.e. an unacceptable biostability level, while reverse osmosis (RO) systems have high energy costs (Kosutic *et al.*, 2005). As such, the use of nanofiltration (NF) membranes or combination hybrid systems incorporating NF is recommended for effective drinking water treatment. The choice of membrane, based on empirical studies (Garcia *et al.*, 2006), should take a variety of contaminants into account. The complete rejection of contaminants is not always achieved (Radjenović *et al*., 2008), particularly during long-term operation; therefore, an assessment of the effectiveness of a hybrid system incorporating NF and graphene nanocomposites is proposed.

1.2 Background

1.2.1 The biocidal properties of graphene-related materials

Carbon is one of the most versatile and important elements in the periodic table and can form a very large range of compounds. Two naturally occurring forms of carbon are diamond and graphite (used in pencils) (Figure 1.1). Graphite is composed of layers of carbon atoms held together by van der Waals forces, and each individual layer or sheet is graphene. Until its discovery by Nobel prize winners Geim and Novoselov in 2004 (Novoselov *et al.*, 2004), planar graphene was widely thought to be thermodynamically unstable, as it readily forms curved structures, such as soot, fullerenes and nanotubes (Figure 1.1). However, it is now known that this material has extensive applications, such as in the electronics industry (Sharma and Ahn, 2013), controlled drug delivery (Yang *et al*., 2009) and photo-catalysis (Putri *et al*., 2016). Initiatives such as the Graphene Flagship also research graphene and are discovering new applications all the time (Graphene Flagship, 2016). What makes graphene special is its remarkable

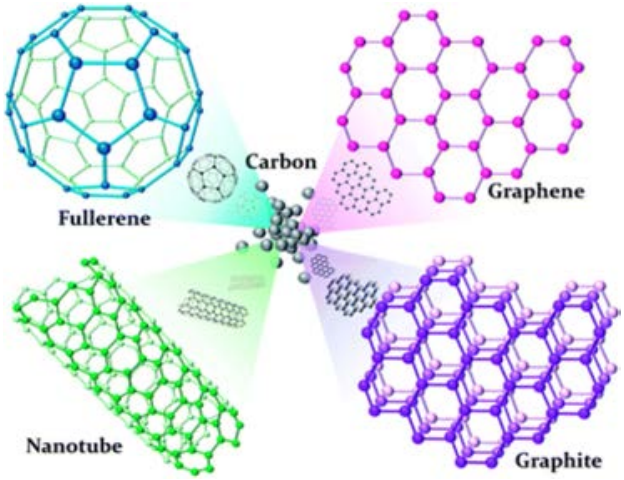

Figure 1.1. Allotropes of carbon. Reproduced from Cheng *et al.* (2013) with permission of the Royal Society of Chemistry.

properties: it is the best conductor of electricity known (up to 200,000 cm^2/V per s, which is higher than silicon, the material traditionally used in electronic devices), it is the strongest compound yet to be discovered (100–300 times stronger than steel), it is the lightest material known (with 1 m^2 coming in at around 0.77 mg) and the best conductor of heat at room temperature (RT) (~5000 W/m per K), among other things. Graphene can be also be added to polymers and metals in very small amounts as a reinforcement filler to enhance materials' existing properties and to make light and tough composite materials.

The high surface-to-volume ratio of graphene gives it a high adsorptive capacity and has led to its application in the removal of contaminants and other undesirable components from water (Nguyen *et al.*, 2012; Kemp *et al.*, 2013).

There are several ways to make graphene (Table 1.1). The mechanical exfoliation or micromechanical cleavage method – also known as the Scotch tape method (Novoselov *et al*., 2004) – involves separating the layers of carbon in graphite into monolayers using an adhesive, such as tape. However, while very high-quality graphene can be produced in this way, this method is very slow and producing large-scale quantities is unrealistic. Similarly, it is possible to produce single layers of very pure graphene, with minimal impurities, using the chemical vapour deposition method (Novoselov and Neto, 2012), but this method is also very slow and expensive. Graphene (top right in Figure 1.1) consists of a

Table 1.1. Graphene production techniques [adapted from Gholamvand (2016)]

Method	Advantages	Disadvantages
Mechanical exfoliation or micromechanical cleavage – also known as the Scotch tape method (Novoselov *et al.,* 2004)	Low cost No special equipment required High quality, no functional groups, defect-free basal plane Large area flakes	Slow process Extremely low yield No mass production possibility Limited to single flake fundamental experiments
Epitaxial growth (Berger *et al*., 2006)	Compatible with CMOS processing	Intensive surface preparation required Largely multi-layer graphitic domain High-temperature processing Limited substrate choice
Chemical vapour deposition growth (Novoselov and Neto, 2012)	Large area graphene coatings Compatible with CMOS High-quality graphene High monolayer yield Easy to transfer to other substrates Useful in transparent electronic applications	Limited scalability potential, dictated by furnace and substrate sizes Not suitable for composite application High-temperature processing Damage possibility during transfer Metal substrates impose high cost
Liquid phase exfoliation by sonication (Nicolosi *et al*., 2013)	High-quality graphene Low process capital cost Scale-up possibility Screening possibility to the range of sizes and thicknesses Environmentally friendly	Low throughput Low concentration dispersion Solvent recovery problem Low content of monolayer Small flake size due to breakage by high-power ultrasound
Graphite oxidation–reduction; chemical synthesis methods (Hummers and Offeman, 1958; Park and Ruoff, 2009)	Scalable liquid phase route High monolayer yield possible Water-processable graphene oxide intermediate High concentration (~10 mg/mL) Useful for composite application	Defected with holes and persistent functional groups Electronically altered Strong acid needed (not sustainable) Non-trivial reduction step requiring reducing chemicals or high temperature

CMOS, complementary metal-oxide semiconductors.

two-dimensional lattice of carbon atoms. Graphite (bottom right) is a stack of graphene layers, whereas carbon nanotubes (bottom left) are rolled-up cylinders of graphene. Buckminsterfullerene (top left) is made up of graphene balled into a 12-sided sphere.

The most effective methods for large-scale production (gram quantities) of graphene are the graphite oxidation–reduction methods, i.e. the Hummers and Offeman method and/or its variants (Hummers and Offeman, 1958), as listed in Table 1.1. This involves the heating of graphite flakes to produce expanded graphite, which is then oxidised using sulfuric acid and potassium permanganate ($KMnO_4$) to form a green paste. Water and hydrogen peroxide (H_2O_2) are then added to obtain golden-yellow suspended graphite oxide flakes. Washing these with hydrochloric acid (HCl) and water and centrifuging the solution causes the gradual splitting of the layers (exfoliation) of graphite oxide into a paste-like graphene oxide (GO) solution. However, the problem with GO is that it contains residual oxygen and is very different from pristine graphene (Chua and Pumera, 2013). For this reason, GO is thermally reduced to reduced GO (rGO). The quality of the graphene produced using this method is not as high as that made using other methods. However, the presence of the functional groups, while undesirable for the electronics applications of graphene, is very useful if the application is water treatment (including antibacterial applications), as such functional groups provide adsorption sites for pollutants. In addition, once rGO has been produced, there are numerous ways to functionalise rGO for use in different applications. This also makes the chemical synthesis method of graphene composites quite straightforward. Therefore, in practice, GO and rGO are used in water treatment applications, rather than pristine graphene, although

the three terms are often used interchangeably in the literature.

One further consideration is the fact that the resulting surface functionalisation and the average sheet size produced using the graphite oxidation–reduction methods are not homogenous. Rather, the product is a colloidal suspension of oxidised graphene sheets of varying lateral size, thickness and surface functionalisation. This gives rise to issues when considering biological applications of these materials, as batch-to-batch variations in their fundamental characteristics will impact significantly on their interaction with biological systems. This also represents a potential problem when attempting to provide definitive information as to the toxicity and biological availability of graphene-related materials (GRMs), such as composites of metals, polymers and other additives. It should also be noted that there is currently no standard or guidelines for the characterisation of GRMs and those sold commercially will often be certified/characterised on a batch-to-batch basis. The biological availability and potential toxicity of GRMs is dependent on their surface functionalisation as well as on several other physical and chemical characteristics, including particle size and oxidative potential.

Having said that, prior to the research in this current project, the actual toxic effect or the biocidal mechanism of GRMs on biomaterials was not fully known or understood. What is emerging is that the cytotoxic potential of a carbon nanomaterial is inversely proportional to its mass, i.e. single-walled carbon nanotubes are more effective at inactivating *E. coli* than their multi-walled counterparts (Jia *et al*., 2005; Kang and Mauter, 2009). Furthermore, in the cases where biocidal activity has been observed, there are a number of theories in the literature explaining the mechanism. These are summarised below.

Lateral size of graphene oxide sheets

Direct contact between cells and relatively large graphene sheets causes oxidative stress to cellular components as a result of the graphene wrapping the cells (Figure 1.2a), thereby isolating them from the environment and inhibiting normal function (Akhavan *et al.*, 2011; Liu *et al.*, 2012a).

Cell disruption by the sharp edges of graphene sheets

While several researchers agree that cell membrane damage is a key feature of the antibacterial action of graphene materials, the exact mechanism is still not fully understood. One theory is that the sharp edges of relatively small graphene sheets disrupt the bacterial cell walls (Figure 1.2b) (Akhavan and Ghaderi, 2010; Hu *et al.*, 2010; Liu, Hu *et al.*, 2012).

Lipid extraction model

The antibacterial activity of GO sheets is based not only on kinetic membrane damage but also on the gradual dissolution of the cellular membrane due to the interaction with the graphene sheets (Tu *et al.*, 2013), resulting in the extraction of lipids from the phospholipid bi-layer by van der Waals forces in the cellular envelope (Figure 1.2c).

The availability of basal planes on the graphene sheet

Some researchers believe that other factors, such as the availability of basal planes of graphene, are also involved (Hui *et al.*, 2014). The Langmuir–Blodgett deposition method employed by Mangadlao *et al.* (2015) showed that GO sheets deposited on a flat surface with no edges available were still capable of producing an antibacterial effect against *E. coli*, suggesting that the flat planes of GO alone could be antibacterial. The lack of a required edge interaction is in contrast to the lipid extraction model proposed by Tu *et al.* (2013), which, while robust as a mode of action, is dependent on the insertion of the edge of the graphene sheets into the membrane.

Other considerations that need to be understood are the effect of the type of matrix (growth media or not) in which the organism is found (Hu *et al.*, 2010; Ruiz *et al.*, 2011; Liu *et al.*, 2011), the state of the organism at the time of exposure to the antibacterial action of the GRMs (Das *et al.*, 2013; Bao *et al.*, 2011; Tai *et al.*, 2012), the strain of the organism (Gram positive or Gram negative) used in the study (Ruiz *et al.*, 2011; Krishnamoorthy *et al.*, 2012) and the washing procedure used to remove residual material from the GRMs production step (Ruiz *et al.*, 2011; Bao *et al.*,

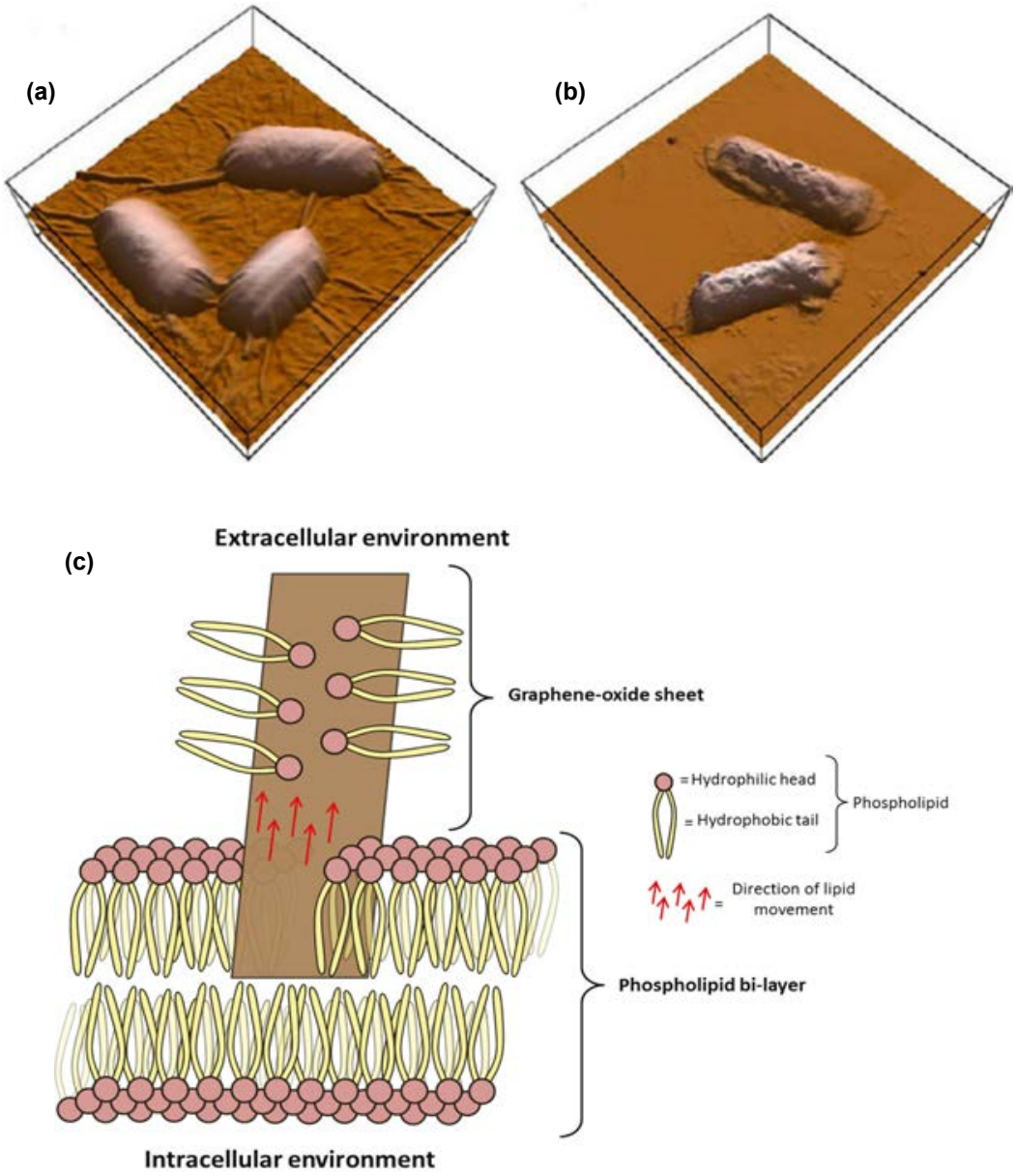

Figure 1.2. How cells are damaged by GO: (a) cell wrapping (Akhavan *et al.*, 2011), (b) cell disruption (Liu *et al.*, 2012a) and (c) extraction of lipids from the cell (Tu *et al.*, 2013).

2011; Tai *et al.*, 2012; Das *et al.*, 2013), as conflicting results on the biocidal effect of GRMs have been found in the literature. However, what does seem to be clear is that both laterally large and small GO sheets can have an antibacterial effect and that the relationship is proportional to the available basal planes and not just the edges alone.

In parallel with the studies on the antibacterial effects of stand-alone graphene, there is a growing interest in the development of composite materials for antibacterial purposes. Graphene composites containing a biocidal metal, such as silver or copper (Cu), have been found to be more effective at killing cells than either the metals or graphene on their own (Shen *et al.*, 2010; Bao *et al.*, 2011; Ma *et al.*, 2011). The number of studies on graphene–silver composites is growing (Song *et al.*, 2016), but concern over the cytotoxic effect of silver nanoparticles (Jiravova *et al.*, 2016) and the high cost associated with silver are limiting factors. On the other hand, Cu has been shown to be an effective antibacterial material and to be almost as effective as silver nanoparticles in terms of antibacterial efficacy in some cases (Yoon *et al.*, 2007). To date, there has been very little investigative

work into the application of a graphene–Cu composite (GCC) as an antibacterial agent. Graphene has also been shown to be an effective agent for the adsorption of organic and environmental pollutants from water, much like other carbonaceous materials (Yang *et al.*, 2011; Maliyekkal *et al.*, 2013; Wang *et al.*, 2013), and represents a potential agent for water remediation. Combining the adsorptive potential of graphene materials for pollutant removal with the antibacterial potential of Cu represents a niche line of investigation that has not been carried out up to now and is the main focus of this project.

1.2.2 Filtration strategies used in drinking water treatment – a focus on PPCPs

Typical drinking water treatment plants consist of a number of stages, including chemical coagulation/settling, sand filtration, adsorption using granular-activated carbon (GAC), and disinfection using chlorination, ozone, ultraviolet (UV) light or a combination of these technologies. Chemical coagulation has shown limited potential for the removal of pharmaceuticals, reducing the concentrations of ionisable pharmaceuticals only, but not removing them completely, while non-ionisable pharmaceuticals, such as carbamazepine, were unaffected (Vieno *et al.*, 2006, 2007). Sand filtration has been shown to be ineffective for the removal of pharmaceuticals such as bezafibrate, clofibric acid, carbamazepine and diclofenac, and a high dose of ozone (3 mg/L) was not capable of removing clofibric acid (Ternes *et al.*, 2002). UV light was shown to be ineffective for the removal of antibiotics, although chlorination and ozone were able to reduce concentrations to a reasonable level (Adams *et al.*, 2002). Residual free chlorine in a drinking water treatment system was shown to be capable of further degrading approximately 50% of a cohort of 98 studied pharmaceuticals in treated drinking water (Gibs *et al.*, 2007). However, on account of the nature of many pharmaceuticals (polar, with acidic or basic functional groups), ozonation or chlorination can result in the transformation of compounds rather than their removal (Snyder *et al.*, 2003). Thus, there is a need for physical removal rather than transformation, a function that membrane separation processes such as NF could reasonably perform. There has been very little research on the application of graphene-enhanced filtration membranes for the removal of PPCPs from drinking water or wastewater streams and, given the promising results in other areas such as desalination, this is an area that is worthy of more attention. The background to the issue and the limited research that has been carried out in the area are presented in this section.

Membrane separation is the umbrella term typically given to operations including microfiltration (MF), UF, NF, RO (Table 1.2), forward osmosis (FO), membrane distillation (MD) and pervaporation (PV). These technologies are widely employed in a diverse number of industries, for example the purification of proteins in the pharmaceutical industry (UF), the treatment of wastewater (MF, UF) and drinking water (MF, UF, NF, RO), the desalination of seawater and brackish water (NF, RO, FO, PV), the cleaning of blood during haemodialysis (UF), solvent separation (PV) and many more. Two primary, common goals in all settings are enhanced productivity (i.e. the flux of treated permeate) and enhanced selectivity (e.g. the retention of valuable proteins and the rejection of unwanted compounds or organic matter and micro-organisms). A complete introduction to membranes and the physics underlying these different and distinct separation systems can be found in a number of key publications and textbooks (Cheryan, 1998; Baker, 2004; Foley, 2013).

Table 1.2. Typical membrane filtration processes

Technique	Size classification	Smallest particle typically rejected	Membrane type	Pressure range (bar)	Applications
MF	0.1–10 µm	Bacteria	Porous	0.5–3	Separation of cells/bacteria from liquid
UF	1–100 nm	Viruses	Microporous	1–10	Separation of proteins
NF	0.5–5 nm	Divalent ions	Microporous/dense	7–40	Separation of dyes, water softening
RO	<1 nm	Monovalent ions	Dense	25–100	Desalination of sea and brackish water

Graphene derivatives such as GO are attractive because of their ease and low cost of manufacture in comparison with pristine graphene. As described in section 1.2, GO is typically produced from an aqueous dispersion of graphite oxide, followed by exfoliation in a solvent, typically using a Hummers or modified Hummers and Offeman method. The pore size/nanosheet spacing is adjustable by tuning the properties of the GO nanosheets, including by the inclusion of filler molecules such as TiO_2 or other nanoparticles (Hu and Mi, 2013; Xu *et al.*, 2013; Mi *et al.*, 2014; Kumar *et al.*, 2016).

The fabrication of many nanocomposite membranes is based on phase inversion [e.g. the non-solvent induced phase separation (NIPS) method or thermally induced phase separation method], in which nanosheets are dispersed in polymer solutions prior to the casting of porous or microporous membranes, and can be prepared in either flat-sheet or hollow-fibre configurations. During the NIPS process, the hydrophilic nature of GO sheets means that the GO converges to the membrane and pore surfaces (Ganesh *et al.*, 2013) during precipitation in aqueous solution. This is the most commonly used type of membrane in MF or UF processes on account of its typically porous structure, and the structure most often consists of a thin dense skin layer over a more macroporous sublayer (asymmetric structure), formed as a result of the slower precipitation of the polymer below the skin layer (Kumar *et al.*, 2015). More dense membranes, such as NF or RO membranes, are typically of a thin film composite (TFC), multi-layer-type structure, composed of a thin dense polymer film or barrier layer on top of one or more porous support layers (Kang *et al.*, 2008) (Figure 1.3). The porous membranes previously outlined often form the porous support layer for TFC membranes, and carbon nanosheets can be incorporated into either the support layer or the thin barrier layer. The fabrication of GO membranes by vacuum filtration or layer-by-layer deposition of GO suspension has also been widely studied for the separation of gases or liquids (Feng *et al.*, 2016), while membranes have also been prepared by electrospinning, spin coating or drop casting (Sun *et al.*, 2013; Nazarpour and Waite, 2016). Although vacuum/solution filtration for deposition of pure GO membrane layers appears attractive, the mechanical stability under hydrated conditions can be insufficient, with GO layers tending to slough off the support layer under typical crossflow/pressurised conditions. In an aqueous environment, the layers become negatively charged, leading to electrostatic repulsion that can exceed the van der Waals or hydrogen bonding forces that hold the GO layers together (Hu and Mi, 2013; Huang *et al.*, 2013). As such, the surface layer deposited GO must generally be crosslinked to maintain membrane integrity (Safarpour *et al.*, 2015; Feng *et al.*, 2016) and this is often an approach taken for the immobilisation of GO on the surface of ceramic membranes.

While RO is an established unit operation in the advanced treatment of water, the application of NF is a membrane separation process that is gaining increased attention in the literature for the removal

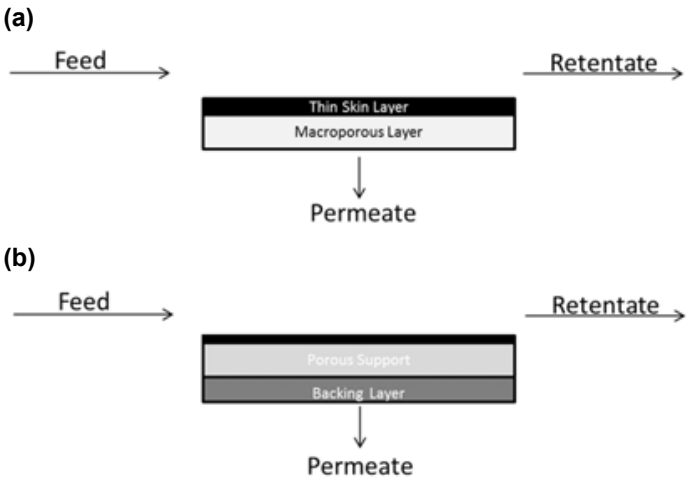

Figure 1.3. Membrane structure. (a) Asymmetric macroporous membrane. (b) TFC membrane. The top layer is the thin barrier layer.

of trace organic contaminants from drinking water. NF is a medium- to high-pressure (7–40 bar) crossflow membrane filtration process employing membranes with pore sizes in the range of 0.5–5 nm and molecular weight cut-offs (MWCOs) in the range of 200–2000 Da. It is has been shown to remove protozoa (including oocytes), bacteria and viruses, as well as natural organic matter (NOM), organohalides, pesticides and pharmaceuticals (Van der Bruggen and Vandecasteele, 2003; Shannon *et al.*, 2008). NF compares favourably with RO, in that it can be operated at a lower applied pressure and rejects fewer mineral ions, meaning that the energy requirements are lower and that the permeate needs less post treatment (Plumlee *et al.*, 2014; Wang *et al.*, 2015).

The rejection or retention of pharmaceuticals on NF membranes is governed by the operating parameters (e.g. crossflow velocity, operating temperature, transmembrane pressure), solute properties (e.g. charge, hydrophilic/hydrophobic, polar/non-polar), membrane properties [e.g. surface roughness, charge, pore size/MWCO, functional groups (acidic/basic)] and feed composition [(e.g. pH, ionic strength, presence of other substances such as humic acids (HAs)] (Radjenović *et al.*, 2008; Simon *et al.*, 2013; Wang *et al.*, 2015). The most well understood mechanism of rejection of solutes by NF is the physical sieving of solutes larger than the MWCO of the membrane, while steric effects will also lead to rejection. Size exclusion may dominate the rejection in one membrane type; rejection for another membrane material, even with similar pore size, may be dominated by electrostatic interactions (Siegrist and Joss, 2012), and there is a large variation in the literature between reported rejection/retention values for pharmaceuticals (Vogel *et al.*, 2010). Other physico-chemical interactions, such as adsorption and electrostatic diffusion, are also important in rejection, as are charge exclusion effects (electrical and Donnan). Hydrophobic–hydrophobic interactions between the membrane and the solute, and the diffusion limitation of the solute are also thought to play a role (Bellona *et al.*, 2004; Kim *et al.*, 2007; Darvishmanesh *et al.*, 2009). Steric hindrance is the most likely mechanism for the rejection of uncharged, hydrophilic compounds, and a correlation between the molecular size/weight and the membrane pore size distribution has been seen in the rejection of solutes of this type (Kosutic, 2000; Van der Bruggen and Vandecasteele, 2002).

Molecules with a low dipole moment, such as diclofenac and ibuprofen, are more likely to be rejected than molecules such as carbamazepine (Vergili, 2013). Less polar (low dipole moment) molecules can be preferentially adsorbed to the membrane, particularly if they are also hydrophobic, resulting in a lower steady-state rejection and a time-dependent effect, as the adsorption capacity of the membrane is reached (Wang *et al.*, 2015). Removal efficiency of solutes is also related to their octanol water partition coefficient ($\log K_{OW}$), which is related to their hydrophobicity and interaction with hydrophobic membranes. High $\log K_{OW}$ compounds (such as diazepam, ibuprofen and diclofenac) and low solubility can lead to an increase in rejection, and this in turn can, in part, be attributed to hydrophobic adsorption to the membrane surface (Yoon *et al.*, 2006; Vona *et al.*, 2015). Ibuprofen, for example, in its neutral form, has a relatively high hydrophobicity and reasonably high levels of adsorption to hydrophobic membrane surfaces will typically be observed. In the presence of other solutes that also adsorb to the membrane surface (competitive adsorption), it may be observed that an increase in rejection occurs for compounds that sorb less than other compounds within a mixed matrix, in comparison with the rejection that would be observed in a single-component feed (Braeken *et al.*, 2005; Steinle-Darling *et al.*, 2010).

The pH and p*K*a values of the solutes have a significant effect on the retention of PPCPs on charged membranes, particularly for ionisable pharmaceuticals such as sulfamethoxazole and ibuprofen, whereas it is less important for non-ionisable compounds such as carbamazepine. Retention on negatively charged membranes can be seen to increase as the compound becomes negatively charged above its p*K*a value; for example, the rejection of amoxicillin was enhanced by 85% with an increase in pH above the p*K*a (Derakhsheshpoor *et al.*, 2013). The rejection of ibuprofen (hydrophobic and acidic) at pH values lower than the p*K*a led to a reduction in diffusion through the membrane due to partial adsorption on a negatively charged membrane surface, while electrostatic repulsion was dominant at higher pH (Bellona and Drewes, 2005). The speciation of pharmaceuticals can also lead to a change in retention as a function of pH (Nghiem *et al.*, 2005). For example, clonazepam and diclofenac are protonated under acidic conditions and become neutral when the pH is increased to 6 and

4, respectively. However, under alkaline conditions clonazepam changes to its enolic form, which has an enhanced water affinity due to the charge on the molecule; this in turn leads to a reduction in retention (Vona *et al.*, 2015).

The effect of organic fouling on membrane characteristics is typically found to be membrane dependent, with pore size deemed to be the dominant factor. For example, fouled, tight NF membranes have been shown to become more hydrophilic and negatively charged, whereas loose NF membranes became more hydrophobic and less negatively charged. The physical characteristics of the membrane also play a role, with hydrophobic membranes with a high degree of surface roughness being subject to increased levels of adsorption of organics over smooth, hydrophilic membranes (Chang *et al.*, 2012). The major compounds in drinking water sources that have the tendency to foul NF membranes include HAs and polysaccharides, and model foulants that mimic typical organic fractions and colloidal materials in treated secondary wastewater and surface water are often approximated in laboratory studies using a combination of HAs, bovine serum albumin (BSA), alginate and colloidal silica (Her *et al.*, 2008; Nghiem *et al.*, 2010). A fouling layer can build up on the surface of the membrane and within the pores, and this can modify the membrane properties, such as hydrophobicity and surface charge, and can also lead to cake-enhanced concentration polarisation (Nghiem and Hawkes, 2007). Membrane fouling and its effect on the retention of PPCPs is complex, and both enhancements, and decreases in rejections have been reported in the literature (Contreras *et al.*, 2009; Wei *et al.*, 2010; Vergili, 2013; Azaïs *et al.*, 2014; Feng *et al.*, 2014).

Improved rejection of pharmaceuticals can be achieved by the tailored fabrication of membranes or the modification of commercially available NF membranes. Enhanced rejection by the modification of the support layer by polymer blending has been investigated (Derakhsheshpoor *et al.*, 2013), while the incorporation of molecules to enhance charge or hydrophilicity is a common approach for improving the separation capabilities and reducing fouling (Rana *et al.*, 2012). The use of charged molecules within the membrane matrix will generally lead to superior removal of charged molecules such as ibuprofen, cephalexin and sulfamethoxazole, with difficulties in the removal of uncharged molecules such as carbamazepine or caffeine (Narbaitz *et al.*, 2013; Yang *et al.*, 2016).

Integrated systems for PPCP removal have been explored extensively in the literature, including the use of NF with advanced oxidation processes (AOPs) such as ozone, peroxide, UV, photo-Fenton, photocatalysis, electrocoagulation (Chaabane *et al.*, 2013) and electrochemical AOPs (Ganiyu *et al.*, 2015), and have in many cases shown enhanced performance of NF in terms of enhanced flux and removal of organic contaminants (Szép *et al.*, 2012). Ozonation, for example, can be efficient for the removal of polar compounds such as diclofenac and carbamazepine, although it is not effective for clofibric acid or bezafibrate (Ternes *et al.*, 2002). While GAC operations alone are not particularly useful for the removal of hydrophilic, polar/charged high molecular weight compounds (including clofibric acid, diclofenac and carbamazepine), the inclusion of an NF step prior to the GAC step removes the majority of NOM that is present for competitive adsorption, leading to enhanced removal of PPCPs by GAC (Verliefde *et al.*, 2007). The adsorption capacity of GO and rGO has also shown promise for the removal of PPCPs, with membranes prepared for adsorptive removal of cations, anions and BPA developed with selective adsorption characteristics on UF membranes (Zhang *et al.*, 2015). A photocatalytic cubic Ag/AgBr/GO nanocomposite showed complete degradation of diclofenac within 6 min under visible light irradiation (Esmaeili and Entezari, 2015) – integration of this type of composite within a membrane would be of great interest.

UF has also been explored to some extent for the removal of PPCPs. While UF of PPCPs themselves would be expected to achieve only moderate removal (Benitez *et al.*, 2011), on account of the typical MWCO of UF membranes being far larger than that of PPCPs, the interaction between NOM and PPCPs means that some proportion of these chemicals can be successfully removed. More polar, less volatile and less hydrophobic compounds have been shown to be more poorly retained than less polar, more volatile and more hydrophobic compounds, which indicates that retention by UF is clearly governed by hydrophobic adsorption, with size exclusion shown to be dominant

once steady-state operation is established in the filtration of natural waters, demonstrating the key role of NOM and natural water characteristics (Yoon *et al.*, 2006). Strong interactions have been shown between humic substances and diclofenac and ibuprofen, leading to retention of up to 80% of these compounds on 5 kDa MWCO UF membranes; however, on account of the charge/electrostatic interactions already discussed, sulfamethoxazole and carbamazepine were not removed because of the lack of adsorption onto HA (Burba *et al.*, 2005). Adsorption has been shown to be a governing mechanism for the retention of hydrophobic compounds and is also dependent on the $\log K_{ow}$ of the PPCP as well as the charge/speciation. NOM presence significantly enhanced the removal of bisphenol A and 17β-estradiol, even with MWCOs up to 30 kDa (Heo *et al.*, 2012). As such, an integrated system comprising a pre-treatment UF step for natural waters shows real promise as a means of reducing fouling of NF membranes due to NOM and also as a means of potentially removing a proportion of the PPCPs present. An adsorption-based filtration strategy can further remove PPCPs, and the appropriate choice of NF membranes for final polishing means that there is the potential for almost complete removal.

1.3 Project Objectives

The aim of this project was to develop an innovative drinking water treatment technology, which can remove inorganic, organic and microbiological contaminants with great effectiveness and reduce the discharge of chemicals to the environment, compared with the chlorination technology currently adopted. This technology is based on combining the adsorption properties of graphene, the biocidal properties of a GCC and a modular filtration system, and will be suitable for drinking water treatment in small- and middle-scale group water schemes, where the small volume of drinking water supplied per day makes conventional technology less effective and more expensive. The proposed disinfection strategy does not rely on chlorine, thus eliminating the emission of toxic by-products. While the proposed technology has been specifically designed to remove microbial and microcontaminants such as pharmaceuticals, it would also be expected to be effective against other common contaminants such as pesticides, arsenic, iron, manganese and aluminium.

Secondary objectives of the project are to build on the national expertise in membrane technology for drinking water treatment, which was identified in an EPA report (O'Dea and Duffy, 2011), and to give the postgraduate student assigned to the project an opportunity to perform cutting-edge research at the interface between chemistry, engineering and microbiology with direct support from industry. Finally, the outputs of this research will contribute to Ireland's reputation for scientific and technological capacity, since drinking water research is a priority in nearly all countries. In order to achieve these aims, a number of key technical objectives were identified:

- to undertake research into the design and operation of filtration systems for private water schemes;
- to add to the body of knowledge on understanding the mechanism of action for antibacterial activity with graphene and GRMs;
- to develop novel graphene composites for the removal of biological and emerging pollutants;
- to design a robust and easy-to-install barrier system for small supplies;
- to improve the processes for the removal of microbial pollution and emerging contaminants;
- to raise public awareness of the importance of ensuring that public water schemes do not cause health and environmental problems;
- to educate a new generation of young scientists/engineers.

2 Research Approach

2.1 Collaboration and Project Elements

This project was a 4-year medium-scale multidisciplinary collaboration involving academic staff from two schools at Dublin City University (DCU) and T.E. Laboratories based in Carlow. The project was managed by DCU, which was responsible for the allocation of the work packages, the co-ordination of the different elements of the project, writing of the reports and management of the budget. Specific on-site management of the separate elements of the project were supervised by relevant members of DCU academic staff. Water samples and advice on water sample analysis were provided by T.E. Laboratories. This end-of-project technical report provides details on the design, build and testing of the prototype unit for water treatment, which is the main output from this project. In addition, the significance of graphene and filtration – the key elements of the prototype – are explained in the introduction to this report (Chapter 1) as are the robust analytical methods used to test the elements of the prototype (the graphene composite, the membrane construction and the filtration studies). This research was composed of three streams, as shown in Figure 2.1, whose output fed into the final prototype design.

2.2 Research Methods

The analytical methods used in this project consisted of three elements, one for each of the project streams indicated in Figure 2.1. Furthermore, because a PhD student was being trained in microbiological techniques as part of this project, emphasis was placed on the evaluation of the effect of GRMs on

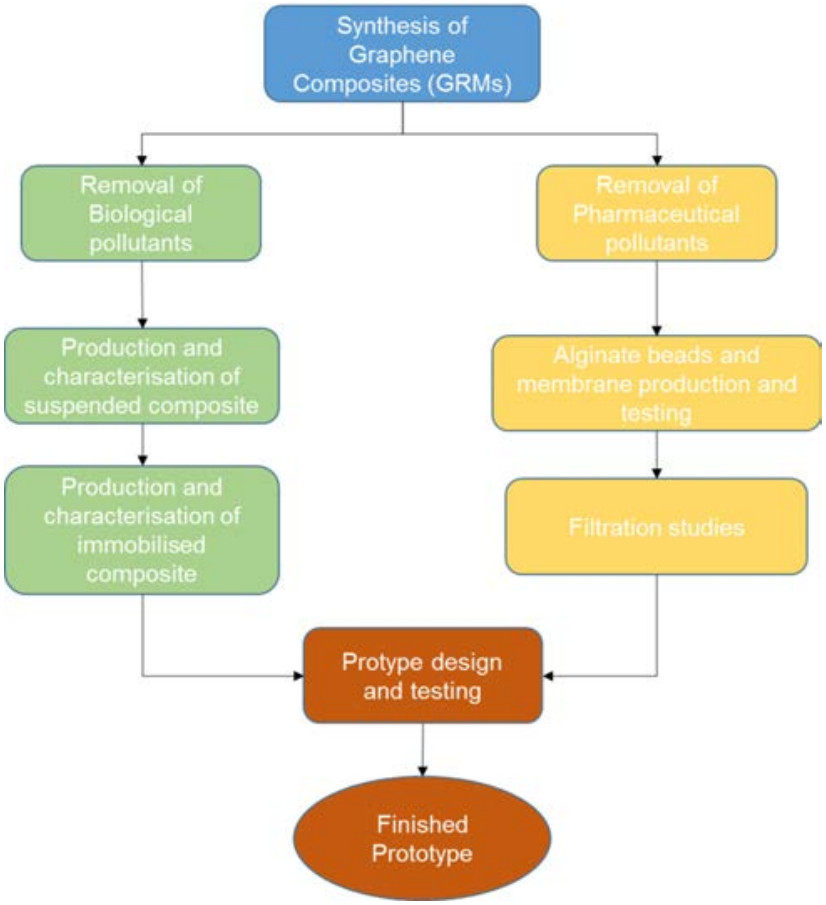

Figure 2.1. Plan showing distinct components of the project.

micro-organisms. This also had the added benefit of adding to the body of knowledge on the actual biocidal mechanism of GRMs, which heretofore had been ambiguous (see section 1.2.1).

2.2.1 Preparation and characterisation of graphene and graphene composites

The work for this project involved the production and characterisation of three graphene materials, GO, GCC [reduced graphene oxide-Cu composite (Cu-rGO)], rGO, Cu nanoparticles (CuNPs), a Cu-rGO film and Cu-rGO-impregnated glass fibre membranes.

Material preparation

Two grams of graphite flakes (Anthracite Industries Inc., Sunbury, USA) were placed in a 700 W microwave for 15 seconds to produce expanded graphite (EG) as the precursor for *GO* synthesis. Two grams of EG and 250 mL of sulfuric acid (H_2SO_4) were then mixed and stirred in a round-bottom flask. Next, 10 g of $KMnO_4$ was gradually added to the mixture. After 24 h of stirring at RT, the mixture was then transferred into an ice bath, and 500 mL of deionised (DI) water and 100 mL of H_2O_2 was added slowly to the mixture resulting in a colour change to golden brown. Following 30 min of stirring, the resulting oxidised EG particles were washed with a HCl solution (9:1 water to HCl) and centrifuged three times, and then centrifuged and washed with DI water. Repeated centrifugation washing steps with DI water were carried out until the solution had a pH > 5. During the washing process, oxidised EG particles were exfoliated to GO sheets with gentle shaking, resulting in a viscous aqueous solution with a concentration of 4.5 mg/mL.

A *GCC (Cu-rGO)* was subsequently produced via the sodium borohydride ($NaBH_4$) reduction method described by Zhang (2012). GO (30 mg), Cu chloride ($CuCl_2$) (18 mg) and DI water (200 mL) were mixed in a 500 mL round-bottom flask, the mixture was ultra-sonicated at low energy for 1 h. To this mixture, 10 mL of 1% $NaBH_4$ solution was then added slowly, and the reaction mixture was stirred at 100°C for 24 h. After being cooled to 50°C, the resulting composite was collected by centrifugation and dried at 100°C under vacuum to give the Cu-rGO composite.

Reduced graphene oxide was produced via the method described for Cu-rGO, without the addition of $CuCl_2$. The effect of the reduction process of the oxidative state of the Cu present in the composite was also investigated via the reduction of $CuCl_2$ in the absence of graphene to produce processed Cu (*CuNP*).

The preparation of *GCC films and impregnated glass fibre* membranes involved the addition of GO (20 mg) and $CuCl_2$ (150 mg) to 40 mL of DI water in a 250 mL round-bottom flask and sonicating for 40 min. To this mixture, 20 mL of ascorbic acid (0.1 M) was then added slowly and the mixture was stirred at 80°C for 24 h. The resulting mixture was then washed repeatedly with DI water and dried slowly at 60°C. To this mixture, 10 mg of Cu-rGO was added to 10 mL of sterile DI water and sonicated for 1 h. This was then vacuum-filtered onto a nitrocellulose membrane (Whatman), pore size 0.22 µm, and allowed to dry to make the Cu-rGO film, which was then peeled from the surface of the membrane. To make the Cu-rGO-impregnated glass fibre membranes, the sonicated mixture was drop cast onto glass-microfibre discs (Sartorius) and dried slowly at 60°C to create a graphene composite coating.

Material characterisation

The characterisation of graphene and graphene composites involved a number of steps. Firstly, the exfoliation of graphite to GO and the subsequent reduction to rGO were confirmed via ultraviolet-visible (UV-Vis) spectrophotometric analysis [UV-3100PC (VWR, Ireland) spectrophotometer] and thermogravimetric analysis (TGA; TGA Q50, TA Instruments, UK). Next, dynamic light scattering was used to establish the particle size distribution within aqueous suspensions of each material. The morphological profile of each material was evaluated via optical and scanning electron microscopic analysis. The presence of sheet-like structures, indicative of graphene exfoliation from graphite, was examined, as was the gossamer-like lustre, indicative of low-number graphene sheets. Energy-dispersive X-ray spectroscopy (EDX) was used to evaluate the elemental composition of GO and the Cu composite (Cu-rGO) to establish the level of oxidation and the percentage of Cu present in the composite, respectively (Table 2.1). Finally, scanning electron microscopy (SEM) was used to study the morphology of the materials by providing a three-dimensional

Table 2.1. Average results from the EDX analysis of graphene, Cu-rGO composite and CuNPs

Material	Carbon	Oxygen	Sulfur	Copper	Silicon
GO	50.1	46.3	3.6	–	–
Cu-rGO	37.2	22.4	–	40.4	–
CuNP	–	24.1	–	74.4	1.5

–, not detected.

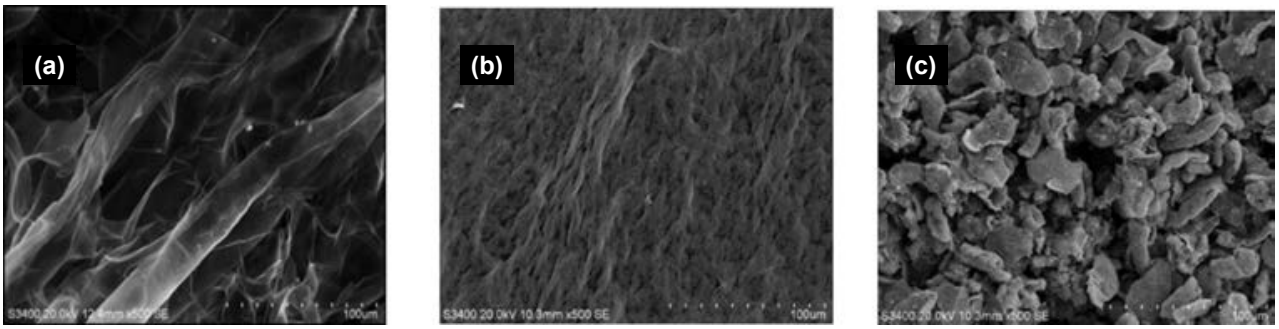

Figure 2.2. Scanning electron micrographs of (a) chemically exfoliated GO sheets, (b) exfoliated GO sheets following chemical reduction and (c) GCC (all at ×500 magnification).

image of the surface of each (Figure 2.2) by mounting the samples on aluminium stubs (AGG3313) using carbon conductive tape (G3939) purchased from Agar Scientific (Stansted, UK). Samples were imaged with a Hitachi-S3400 scanning electron microscope (Hitachi, Japan) for secondary electron imaging and a Hitachi S5500 FESEM (Hitachi, Japan) for both secondary and transmission electron imaging.

2.2.2 Microbiological studies

E. coli (T37-1) was isolated from water from the River Tolka and used as a model Gram-negative organism. Oxidase, indole, catalase and analytical profile index (API) 20E tests were conducted to confirm the identity of the organism. *Bacillus subtilis* (DSM-10) was used as a model Gram-positive organism. GO, rGO, CurGO and CuNPs materials were tested for antibacterial activity using the disc diffusion method to examine the potential diffusive nature of the materials (Figure 2.3) and liquid growth studies to determine minimum inhibitory concentrations and the antibacterial potential in a liquid medium (Figure 2.4). In order to examine the antibacterial efficacy of the vacuum-filtered graphene films, an agar slurry method, used to ascertain the antibacterial efficacy of surfaces, was employed (ASTM standard E2180–07, 2012). During the antibacterial investigations, two Cu-containing salts – $CuCl_2$ and Cu sulfate ($CuSO_4$) – and CuNPs were used as controls for comparison with the Cu-containing graphene composite. The CuNPs, produced via the same method, are analogous to the Cu present in the composite material.

Solid media studies

A loopful of bacterial culture was transferred from a maintained agar plate using a sterile inoculation loop to a 10 mL aliquot of nutrient broth and grown overnight on a shaking incubator at 150 rotations per minute (rpm) and 30°C. Following overnight growth, the broth was centrifuged at 4000 rpm for 15 min and the pellet washed twice and re-suspended in 10 mL of phosphate-buffered saline (PBS). Optical densities were adjusted to 0.5 McFarland standard, equating to a cell number of ~10^8 colony-forming units (CFU)/mL.

Subsequently, 1000 ppm (parts per million) suspensions of GO, rGO, Cu-rGO and CuNPs were prepared by adding 10 mg of each material to 10 mL of sterile DI water and sonicating for 1 h; 1000 ppm concentrations were used for these materials in all cases unless otherwise specified. Solutions of $CuCl_2$ and $CuSO_4$ were prepared by dissolving powders of each in sterile DI water.

- *Well diffusion assay*: 10 mm wells were cut into the agar using a heat-sterilised agar cutter. Of each material suspension, 200 µL was added at 1000 ppm, in triplicate, to wells on individual agar plates.

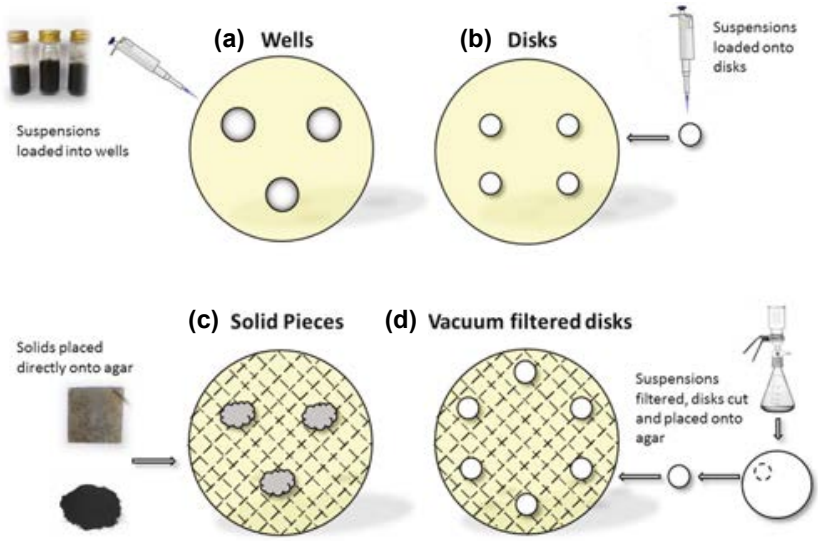

Figure 2.3. The four methods employed in examining the effect of materials in solid media: (a) suspensions added to wells cut into agar; (b) disks loaded with suspensions added onto the surface of the agar; (c) solid pieces of material added to agar with a bacterial lawn; and (d) suspensions are filtered and disks of membrane added to the surface of the agar.

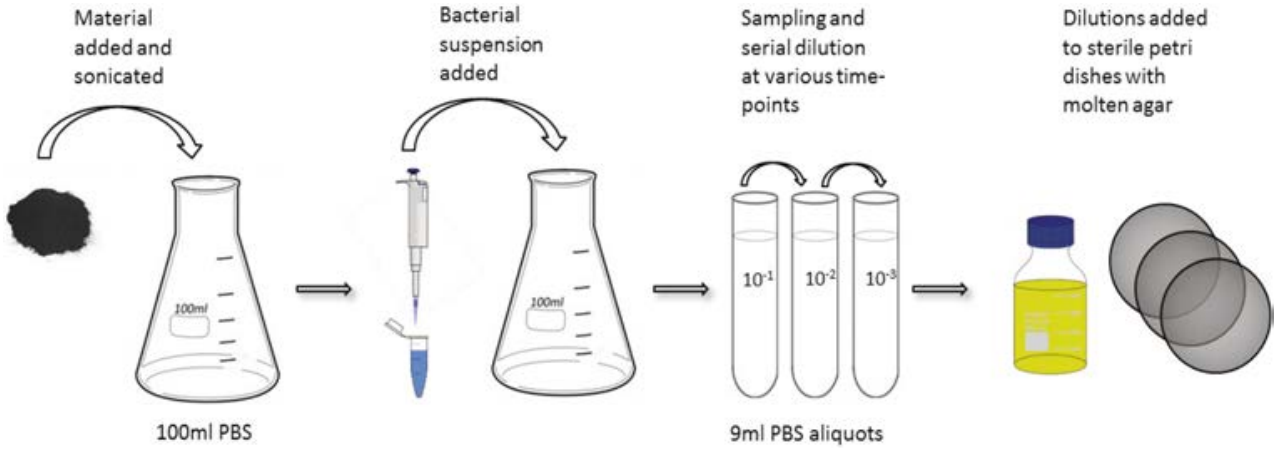

Figure 2.4. Liquid media studies.

- *Disk diffusion assay*: sterile 6 mm Whatman disks (Grade AA 2017–006) impregnated with 20 µL of each material suspension were placed onto the inoculated agar.
- *Solid exposure assay*: suspensions of GO and rGO were dried at 60°C in a fan-assisted oven to form films, and 5mm sections, which weighed ~5 mg each, were cut and applied directly to inoculated agar plates. For comparison, and as the other materials did not form free-standing films, 5 mg of each of Cu-rGO and CuNPs were placed, in triplicate, directly onto the surface of plates.
- *Vacuum-filtered disks*: 20 mL of each material suspension was filtered using a Supelco filtration apparatus (58062-U) onto Whatman cellulose acetate filters (pore size 0.2 µm) with a diameter of 35 mm. Then, 5 mm disks were cut and placed, face down, onto inoculated agar plates so that the material was in direct contact with the cells. The final concentration on each of the particulate-loaded disks was ~0.4 mg. Standard Whatman disks were loaded with equivalent quantities of $CuCl_2$ and $CuSO_4$ for comparative purposes. The concentration of material on each vacuum-filtered disk was 0.02 mg/mm^2 or 0.4 mg/disk. Results in all cases were observed as zones of inhibition, categorised as an area of exclusion around the material where no bacterial growth is observed. The zone of inhibition is the diameter of the full

zone given in millimetres. For the vacuum-filtered disk assay, $CuCl_2$ and $CuSO_4$ were also used for comparison with the Cu-containing composite. The application of a common antibiotic, gentamicin, would serve as a baseline for comparison.

Liquid media studies

A loopful of bacterial culture was transferred from a maintained agar plate using a sterile inoculation loop to a 10 mL aliquot of nutrient broth and grown overnight on a shaking incubator at 150 rpm and 30°C. Following overnight growth, the broth was centrifuged at 4000 rpm for 15 min and the pellet washed twice and re-suspended in 10 mL of PBS. For the minimum inhibitory concentration, the optical density of bacterial suspensions was adjusted to 0.07 at 660 nm equating to 10^8 CFU/mL. For the shake flask studies, the optical density of *E. coli* suspensions was adjusted to 0.015 and suspensions of *B. subtilis* to 0.025 at 660 nm, equating to 10^7 CFU/mL. Subsequently, 1 mL of a 1:100 dilution of the bacterial suspension was added to 100 mL of PBS to give a final cell concentration of 10^3 CFU/mL.

Shake flask studies were carried out in 250 mL Erlenmeyer flasks with a final volume of 100 mL PBS. Materials were added to each flask in order to bring them to the desired concentration in ppm (mg/L). After the addition of particulates, flasks were sonicated for 40 min to disperse the materials. Following inoculation with cells, flasks were incubated for up to 24 h at 30°C on an orbital shaking incubator at 150 rpm. Samples of 1 mL were taken at 1.5 h intervals up to 6 h and again at 24 h. Samples were then serially diluted, plated and counted in triplicate.

The minimum inhibitory concentrations (MIC) of $CuCl_2$, $CuSO_4$ and CuNPs were determined using the standard 96-well plate method as described by Andrews (2001). Two-fold dilutions were carried out from an initial concentration of 1000 mg/L. On account of the particulate nature of GO, rGO and Cu-rGO, MIC determinations were carried out for these materials in larger volumes (1 mL) in test tubes. An initial concentration of 1000 mg/L was used and two-fold dilutions were carried out in a series of nine test tubes for each material. A tube containing no material was used as a control for bacterial growth. A series of tubes without bacteria were used as controls for the materials' optical density measurements. Following serial dilution, 50 µL of a suspension of bacteria at an optical density of 0.07 (10^8 CFU/mL) was added to each tube. The tubes were then incubated at 30°C for 24 h. Results were recorded as optical density measurements at 660 nm. Streak plating was carried out from each well/tube on to nutrient agar in order to validate whether or not the organism had been completely inhibited.

Agar slurry analyses of graphene films

Agar slurry (100 mL) was prepared by adding sodium chloride (NaCl) (0.85 g) and bacteriological agar (0.3 g) to 100 mL of DI water. Then, 1 mL of adjusted bacterial culture (optical density 0.07 at 660 nm) was added to 100 mL agar slurry for a final concentration of 10^6 CFU/mL, and 150 µL of inoculated agar slurry was added to 1 × 1 cm squares of GO, rGO and Cu-rGO films and incubated for up to 24 h in a humid environment at 30°C. Following incubation, the slurry was re-suspended in saline solution and the bacteria counted via the pour plate technique (see Figure 2.4).

Scanning electron microscopic analysis of bacterial cells

Disks of each of the materials, GO, rGO and Cu-rGO, prepared via vacuum filtration were placed into 5 mL of nutrient broth inoculated with 1 mL of *E. coli* suspension adjusted to 0.07 optical density in a 6-well cell culture plate, which was then incubated overnight at 30°C. Following incubation, disks were removed from the 6-well plates and the micro-organisms were fixed with 5% glutaraldehyde for 30 min at 4°C and dehydrated stepwise using a gradient of ethanol solutions (50, 60, 70, 80, 90 and 100%) for 10 min each. Following dehydration, microbiological samples were sputter coated with gold using a Quorum 750T (Sussex, UK) for 90 seconds at 20 µA. Samples were viewed using an acceleration voltage of 20 kV and a probe current of 35 mA.

Prototype studies

Technical drawings for the prototypes were created using AutoCAD 2012 and Solid Works 2011 software. The materials used for the manufacture of the flow prototypes were polymethyl methacrylate (PMMA) tubing at 1000 mm (L) × 50 mm (outside diameter) × 40 mm (inside diameter) (Radionics,

Ireland). Support structures were cut from 2 mm thick PMMA sheets using a Zing Laser cutter (Epilogue, USA). Sections were cut using a DWE7491 table saw (Dewalt, Ireland) and internal rebates were cut using a RP0900 router (Makita, Ireland). Internal bonding of films and membranes was performed using an inert polyvinyl siloxane dental glue (Coltene, Ireland). External and structural bonding was done using Bostik clear silicone sealant (Radionics, Ireland). All prototypes were cleaned, sterilised with 70% industrial methylated spirits (IMS) and flushed with 1 L of sterile DI water before microbiological assays were carried out. Either 700 mL or 5 L of sterile saline solution (0.85% NaCl) were inoculated with *E. coli* to a final concentration of 10^2 CFU/mL in separate experimental parameters to examine prototype performance. In the preliminary run, using 700 mL, a Watson-Marlow 114 DV peristaltic pump (Watson-Marlow, Ireland) was used at a flow rate of 22 mL/min to give a ramp-up stage of 30 min. Subsequently, 1 mL samples were taken in triplicate after 30 min, following the ramp-up stage, and at 1 h intervals thereafter up to 6 h using the pour plate technique. For the larger volume examination of 5 L, the same flow rate was employed; however, samples were taken after the initial ramp-up phase and then after each litre eluted until the total volume had passed. Samples of 1 mL were taken at each point and counted in triplicate via pour plates. In addition, to examine the viability of the organisms, 1 mL samples were added to 9 mL of both nutrient and R2A broth and incubated overnight. Following the experiment, each membrane was removed from the prototype, cut into halves and placed into each of R2A broth and nutrient broth to examine the state of the bacteria on the surface.

To examine the removal of cryptosporidium by the prototype, 100 oocysts (provided by City Analysts Ltd, Dublin) of *C. parvum* were added to 10 L of sterile saline solution (0.85% NaCl) to give an inoculum size of 10 oocysts/L. This was passed through the prototype, collected and then passed through a filtramax filtration unit. Microscopic analysis was carried out on the filtrated material by City Analysts Ltd to examine if oocysts were present.

2.2.3 Adsorbent bead preparation

Graphite flakes (acid washed) were obtained from Asbury Carbons (USA). $KMnO_4$, H_2SO_4, H_2O_2, calcium alginate (Ca-Alg), calcium chloride ($CaCl_2$) and sodium hydroxide (NaOH) were purchased from Sigma Aldrich.

An aqueous solution of sodium alginate (Na-Alg) (2 wt%) was prepared by dissolving Na-Alg (5.0 g) in DI water (250 mL) to give a clear, viscous solution. This process was achieved by the stepwise addition of small amounts of Na-Alg powder to DI water at RT while vigorously stirring with a magnetic stirrer.

To prepare the Na-Alg/GO solutions with different GO contents, 5.0, 10.0 or 20.0 g of 1% GO concentrate was dissolved in 50 mL of DI water using ultra-sonication treatment (Wise Clean sonicator, model WUC-A02h, Korea) for 1 h. It was not possible to achieve a stable dispersion of GO above this amount. The aqueous GO solution was then added slowly to the aqueous Na-Alg solution (200 mL, 2.5% wt/wt) under constant and gentle mechanical stirring (IKA Verke, model MST B, Germany) for 30 min at RT giving 250 mL of a light-brown, translucent Na-Alg/GO solution marked as GO5, GO10 or GO20 accordingly.

Ca-Alg beads were prepared using the aqueous Na-Alg solution (2 wt%, 5 g of Ca-Alg per 250 mL DI water) and a syringe pump (pump supplied by KR Analytical Ltd, Cheshire) with a flow rate of 10 mL/min using a 20 mL plastic syringe and a 1 mm needle. As the beads were formed, they were dropped into an aqueous coagulation bath of $CaCl_2$ (6 wt%, 35 g per 500 mL) at RT. The bath was continuously stirred with a magnetic stirrer to prevent bead agglomeration. In order to maintain a constant size and shape of beads, the height of the syringe tip from the electrolyte surface and the rate of dropping were kept constant throughout the bead preparation step. The beads were then left in the coagulation bath for 24 h without any stirring in order to obtain the complete formation of Ca-Alg gel beads. The Ca-Alg gel beads were then collected and washed three times with DI water (300 mL). The resulting Ca-Alg gel beads, which have a uniform spherical shape with an average diameter of 0.46 ± 0.03 cm, are shown in Figure 2.5a.

Ca-Alg/GO beads with different amounts of GO (5 g, 10 g or 20 g GO was dissolved in 50 mL DI water) were prepared using a corresponding aqueous solution of Na-Alg/GO and a syringe pump (pump supplied by KR Analytical Ltd, Cheshire) with a flow rate of 10 mL/min. The solutions were dropped into an aqueous

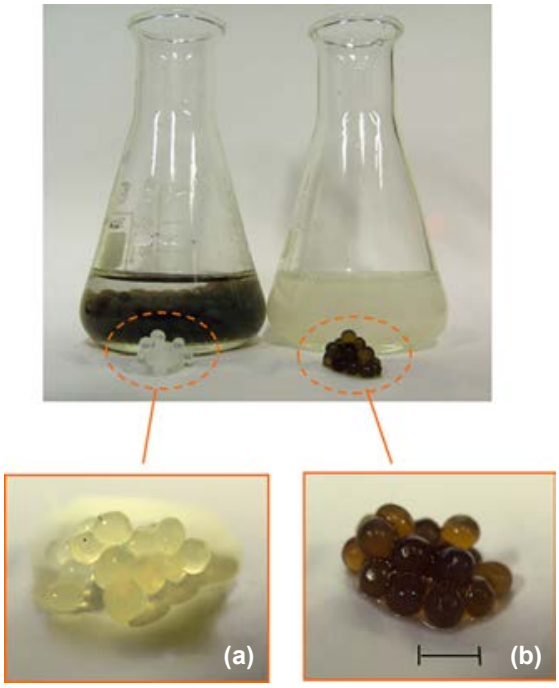

Figure 2.5. Images of (a) Ca-Alg wet gel beads and (b) Ca-Alg/GO wet gel beads. The scale bar is 0.5 cm.

coagulation bath of $CaCl_2$ (6 wt%, 35 g per 500 mL) at RT and the bath was continuously stirred with a magnetic stirrer to prevent bead agglomeration. The beads were then left in the coagulation bath for 24 h without any stirring in order to obtain the complete formation of Ca-Alg/GO gel beads. The Ca-Alg/GO gel beads were then collected and washed three times with DI water (300 mL).

Assuming the complete exchange of the Na^+ with Ca^{2+} ions, the ratio of alginate to GO for the GO5 beads will remain 1:0.01; for the GO10 beads it is 1:0.02 and for the GO20 beads it is 1:0.04. The resulting Ca-Alg/GO gel beads, which have a uniform spherical shape with an average diameter of 0.46 ± 0.02 cm, are shown in Figure 2.5b.

The Ca-Alg and Ca-Alg/GO gel (wet) beads (5.0 g each) obtained were placed into plastic vials and dried in an oven at 50°C to a constant weight (approximately 2 days; Figure 2.6).

The Ca-Alg and Ca-Alg/GO gel beads and the dried beads were activated in a pH 4 solution. The selected beads (5 g for the gel beads or approximately 0.2 g for the dried beads) were placed in a 250 mL conical flask. Subsequently, 0.1 M HCl was slowly added to

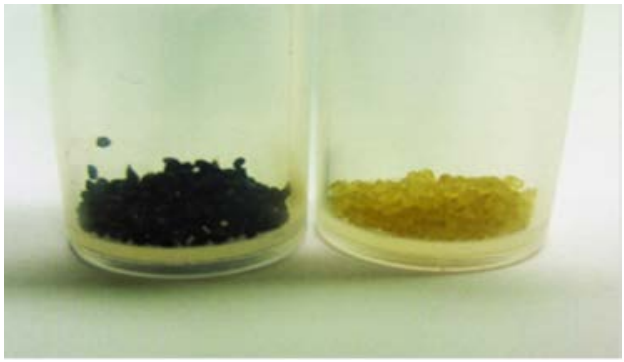

Figure 2.6. Images of Ca-Alg/GO dried beads (left) and Ca-Alg dried beads (right).

200 mL of DI water until the desired pH was achieved, controlled by a JENWAY 3510 pH meter. Of this pH 4 solution, 50 mL was added to the conical flask and placed on an agitator for 2 h at a constant rate to ensure an optimum activation process.

Contaminant solutions with different concentrations [methylene blue (MB), famotidine and diclofenac] were prepared by dissolving the requisite amounts of the contaminant in DI water. Batch adsorption experiments were conducted at RT using 50 mL of each solution and Ca-Alg or Ca-Alg/GO dried beads. Through preliminary experiments it was confirmed that a 120 min incubation was sufficient to attain equilibrium between the adsorbents (dried beads) and adsorbate. After each adsorption experiment, the concentration of the contaminant remaining in each solution was determined using UV-Vis or high-performance liquid chromatography (HPLC).

The adsorption capacity at equilibrium (q_e) was then calculated using Equation 2.1

$$q_e = \frac{(C_0 - C_e)V}{W} \qquad \text{(Equation 2.1)}$$

where C_0 (mg/L) and C_e (mg/L) are the initial and equilibrium concentrations of contaminant, respectively, V is the volume (L) of the solution and W is the dry weight (g) of the beads used.

The appropriate adsorption isotherm (Langmuir, Freundlich, etc.) was found by fitting the models to the experimental data, while kinetic modelling for dynamic adsorption was determined by the fitting of appropriate models (e.g. pseudo-first order, pseudo-second order, etc.) to time series data.

2.2.4 Ultrafiltration membranes

Materials

Polysulfone (PSf) P-3500 was supplied by Solvay Speciality Polymers (Belgium). Expandable graphite flakes with average flake size >500 µm were obtained from Asbury Graphite Mills (USA). Titanium isopropoxide (TTIP; 97%), $KMnO_4$ (99%), H_2O_2 (30% aqueous solution), paraformaldehyde ((HCHO)n), chlorotrimethylsilane ($(CH_3)3SiCl$), tin(IV) chloride ($SnCl_4$), deuterated chloroform ($CDCl_3$), HA, polyvinylpyrrolidone (PVP; 40 kDa), BSA and anhydrous ethanol were procured from Sigma-Aldrich. *N*-methyl-2-pyrrolidone (NMP; 99%), isopropyl alcohol (IPA), NaOH, H_2SO_4 (98%), nitric acid (HNO_3; 68%) chloroform ($CHCl_3$), methanol and HCl (37%) were purchased from VWR Chemicals (Ireland). Lysozyme was obtained from Fluka Chemicals. Trimethylamine ($(CH_3)_3N$), *N*,*N*-dimethylacetamide (DMAc), NMP, diethyl ether $(C_2H_5)_2O$), sodium dihydrogen phosphate (NaH_2PO_4), disodium hydrogen phosphate (Na_2HPO_4) and NaOH were procured from Merck Chemicals. Other chemicals and reagents were commercial grade and used as received. DI water used in this study was produced via a Milli-Q integral system (Merck Millipore, Ireland).

Preparation of quaternised PSf-GO membranes

Quaternised polysulfone (QPSf) was synthesised from chloromethylated PSf (PSf-CH_2Cl) via an *in situ* quaternisation reaction at 40°C. PSf-CH_2Cl was synthesised by a chloromethylation reaction using (HCHO)n, $(CH_3)3SiCl$ and $SnCl_4$ as a catalyst. The typical procedure for the synthesis of PSf-CH_2Cl was as follows: 5 g PSf was dissolved in 250 mL $CHCl_3$ [analytical reagent (AR) grade, stored in the presence of 4 Å molecular sieves] in a round-bottom flask equipped with a reflux condenser and magnetic stirrer. After dissolution of PSf, 3.5 g (115 mmol) of (HCHO)n and 12.5 g (115 mmol) of $(CH_3)_3SiCl$ were alternatively added. Subsequently, 0.4 mL (1.5 mmol) $SnCl_4$ in 10 mL $CHCl_3$ was slowly added to the reaction mixture solution with stirring at 55°C and the reaction was continued for 72 h at 55°C. The resulting mixture solution was then precipitated in 500 mL methanol and the precipitated polymer was collected on filter paper by vacuum filtration. The PSf-CH_2Cl was again dissolved in 50 mL $CHCl_3$ and then precipitated in 250 mL methanol to remove traces of impurities. A white powder was obtained, which was dried in a vacuum oven at 40°C for 12 h. The proton nuclear magnetic resonance (^{1}H-NMR) spectrum for PSf-CH_2Cl was recorded in $CDCl_3$ solvent (Figure 2.7a). The peak at 4.56 ppm corresponds to the CH_2Cl group, and this confirmed the successful synthesis of PSf-CH_2Cl (Figure 2.7b). The degree of chloromethylation of PSf was found to be 45.6%.

In this study, PSf/QPSf and PSf/QPSf/GO hybrid membranes were fabricated by solution casting and the phase inversion method. Predetermined amounts of GO nanosheets were dispersed into NMP by sonication; then, 16 wt% of the dried PSf and QPSf (1:1) was added into the suspension of GO nanosheets in NMP and stirring continued at 50°C until the polymers dissolved completely. The blend solutions were then sonicated for 30 min and left at RT without stirring to remove any trapped air bubbles. The obtained blend solutions containing PSf/QPSf/GO nanosheets were then cast onto a glass plate using a casting knife with a gap height of 250 µm. The proto-membrane film with glass plate was left for 30 s and was subsequently submerged in a drinking water coagulation bath until the membrane peeled off from the glass plate. Membranes of ~125 µm thickness under wet conditions were obtained, which were thoroughly washed with DI water to remove traces of NMP. The base membrane was also fabricated in the same way without GO nanosheets. The compositions of the casting solutions for the fabrication of all membranes are given in Table 2.2.

The fabricated membranes are designated as membrane AG-X (X being the weight per cent (%) of GO nanosheets to total weight of polymers blend, i.e. AG-0, AG-1, AG-2 and AG-5).

Preparation of GO–TiO_2 UF membranes

The synthesis of the GO nanosheets was as described previously. The GO–TiO_2 nanocomposite was synthesised from GO nanosheets and TTIP via *in situ* sol–gel reaction at pH 2. Of the GO nanosheet paste (i.e. 400 mg of GO), 100 g was added to a round-bottom flask containing 80 mL DI water and 120 mL IPA. The resulting mixture, in the round-bottom flask, was placed in a bath sonicator

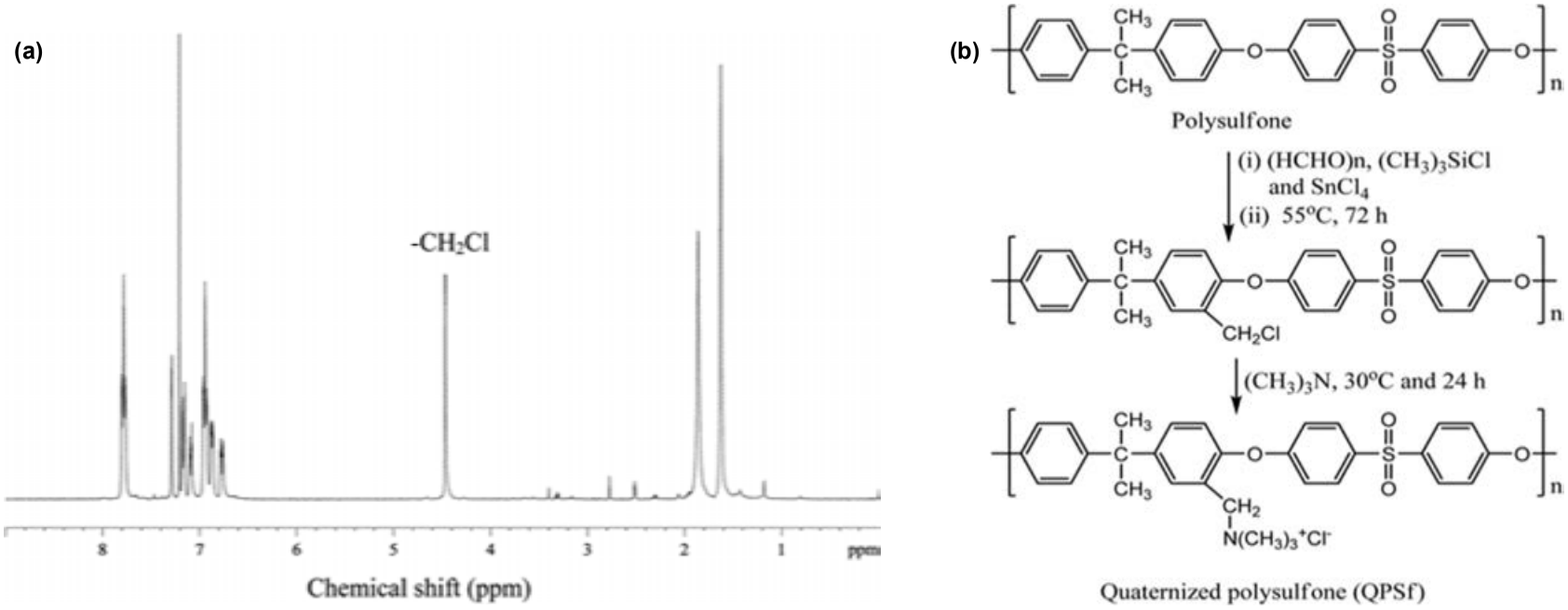

Figure 2.7. (a) The ^{1}H-NMR spectrum for PSf-CH_2Cl in $CDCl_3$; (b) the reaction route for the synthesis of QPSf via chloromethylation and the *in situ* quaternisation reaction using $(CH_3)_3N$.

(40 kHz) for 1 h to obtain an adequate suspension of GO. Then, 0.16 mL of TTIP (40 wt% to the total weight of GO) in 20 mL IPA was added dropwise to the suspension with stirring at RT. The pH of the resulting suspension was adjusted to 2 using 4 M HCl and the reaction mixture solution was continuously stirred overnight at 60°C (Figure 2.8). A light-grey gel was obtained, which was dried at 60°C for 12 h in a vacuum oven and subsequently ground using a pestle and mortar to obtain a fine powder. TiO_2 nanoparticles were also synthesised in the absence of GO nanosheets. The loading amount of TiO_2 in GO–TiO_2 nanocomposite was found to be 30 wt%. Raman spectra for GO–TiO_2 nanocomposite and TiO_2 particles were recorded on a Raman spectrometer (Micro–Raman Horiba Jobin–Yvon LabRam HR800). Transmission electron microscopy (TEM) images of the GO–TiO_2 nanocomposites were also obtained in order to evaluate the morphology. The leaching of TiO_2 nanoparticles from the GO–TiO_2 nanocomposite during sonication was tested by dipping the TEM grid in an adequate dispersion of GO–TiO_2 for 10 min. There were no TiO_2 nanoparticles visible on the TEM grid following sonication, which is an indication that the TiO_2 nanoparticles were stably bound within the nanocomposite.

Hybrid membranes were fabricated from blend solutions of PSf/PVP/GO–TiO_2 nanocomposite in NMP by the NIPS method. The precise amount of GO–TiO_2 was dispersed into NMP solvent and then sonicated in a bath sonicator for 1 h at 40 kHz. After that, 14 wt% PSf and 4 wt% PVP were alternatively dissolved by continuous stirring for 24 h at 50°C. The polymer blend solutions were sonicated again for an additional 30 min and left at RT for removal of the trapped air bubbles. The polymer blend solutions were then spread onto a glass plate using an elcometer with 250 µm gate height. The cast films along with glass plates were left at RT for 30 s, and subsequently immersed in a DI water coagulation bath until the membranes had peeled off. The membranes (~125 µm thickness in wet condition) were again kept in DI water for 24 h to ensure complete removal of PVP and traces of NMP. The membranes were stored in DI water before further use and characterisation. The base membrane was fabricated from a blend solution of PSf and PVP, without nanocomposite.

Table 2.2. The composition of the casting solutions for the fabrication of positively charged hybrid membranes

Membrane	PSf (wt%)	QPSf (wt%)	GO (wt%)[a]	NMP (wt%)
AG-0	8	8	–	84.0
AG-1	8	8	1	83.84
AG-2	8	8	2	83.68
AG-5	8	8	5	83.2

[a]**The percentage of GO is based on the total fraction of PSf and QPSf in the membrane casting solutions.**

Figure 2.8. Schematic reaction route for synthesis of the GO–TiO_2 nanocomposite from GO nanosheets and TTIP via the sol–gel reaction at pH 2 and 60°C.

Preparation of HA solution

A stock solution of HA (1000 ppm) was prepared by dissolving 1 g HA into 100 mL 0.1 M NaOH solution with subsequent addition of 900 mL DI water. The pH of the resulting solution was then immediately adjusted to 7 by adding a few drops of 4 M HCl. This solution was stirred for an additional 4 h at RT and filtered through Whatman 41 filter paper. HA solutions of known concentration (10, 20, 40 and 50 ppm) were prepared from a stock solution of HA after dilution with DI water.

Membrane characterisation

The water uptake (φ), porosity (ε), ion-exchange capacity (IEC), fixed ion concentration (Af), free water (φ_f) and bound water (φ_b) of the membranes were determined. The attenuated total reflection Fourier transform infrared (FTIR) spectrum for membranes was recorded on a Perkin Elmer Spectrum 100 spectrometer. The spectrum was recorded over a wide range from 650 to 4000 cm^{-1} with 32 scans at a resolution of ±4 cm^{-1}. A SurPass Electrokinetic Analyser (Anton Paar GmbH, Austria) was used to measure the outer surface zeta potential (ζ) of the membranes. The outer surface zeta potential of the membranes was calculated using the Helmholtz–Smoluchowsky equation (Equation 2.2).

$$\zeta = \frac{\Delta E_{SP}}{\Delta P} \times \frac{\eta \kappa}{\varepsilon_r \varepsilon_0} \qquad \text{(Equation 2.2)}$$

where $\Delta E_{SP}/\Delta P$ is the change in streaming potential with pressure, η is the electrolyte solution viscosity, κ is the conductivity of electrolyte solution, ε_0 is the permittivity of free space and ε_r is the permittivity of electrolyte solution.

The surface and cross-section morphologies of membranes were observed using a Hitachi S3400N (UK) scanning electron microscope at an acceleration voltage of 20 kV using a secondary electron detector. Membrane samples were flash-frozen using liquid nitrogen and broken to achieve an even cross-section; these were then mounted onto stainless steel stubs and sputter coated with gold (60 s, 40 μA) to create a conductive surface. The water contact angle of membranes was determined using an FTÅ200 contact angle analyser (First Ten Angstroms, Inc., USA) equipped with video capture by a sessile drop method. To minimise the experimental error, the contact angle was measured at five locations for each membrane and the average value was then reported. In addition, the free energy of interaction at the interface between the liquid and the membrane surface (−ΔGSL) was calculated using the Young–Dupre equation (Equation 2.3).

$$-\Delta G_{SL} = (1 + \cos\theta)\gamma^T_L \qquad \text{(Equation 2.3)}$$

where θ is the measured water contact angle and γ^T_L is the total surface tension of water (72.8 mJ m^{-2}).

The tensile strength and percentage elongation at break point of membranes were determined using a Zwick Z005 displacement controlled tensile testing machine (Zwick-Roell, Germany) at a crosshead speed of 2 mm/min.

Membrane performance assessment

Pure water flux measurement

A dead-end stirred UF cell (Amicon 8200; Millipore Co., USA) connected to a N_2 gas cylinder and solution reservoir was used to determine the pure water flux of membranes. Each membrane was initially compacted by filtering DI water for 30 min at 2 bar and then the pressure was released to 1 bar. Thereafter, DI water was passed through the membranes for 1 h at 1 bar applied pressure. The mass of collected permeate was measured on a digital balance (Ohaus Adventure Pro Balance, UK). The pure water flux (J_w; L/m^2 per h) was calculated using Equation 2.4.

$$J_w = \left(\frac{V}{A \times \Delta t} \right) \qquad \text{(Equation 2.4)}$$

where V is the volume of the collected permeate (L), A is the effective membrane area (m^2) and Δt is the permeation time (h).

Antifouling performance

The antifouling ability of membranes was evaluated by conducting adsorption and filtration experiments at known pH and constant applied transmembrane pressure. In this study, BSA was selected as a model protein while HA was selected as a NOM equivalent to evaluate the antifouling ability of membranes. Static adsorption experiments were conducted to determine the adsorbed amount of foulant on the membranes.

Circular pieces of membranes (diameter 2.5 cm) were placed into conical flasks containing a 25 mL solution of BSA (1 g/L) in 10 mmol phosphate buffer or 10 mL HA solution (10 ppm) at pH 7. The conical flasks were then placed on a shaker at RT for 8 or 24 h with a stirring speed of 100 rpm. The concentration of BSA or HA in the supernatant solutions was determined using a Cary 50 Bio UV-Vis spectrophotometer (Varian Inc., USA) at wavelengths of 280 nm or 254 nm, respectively. The adsorbed amount of BSA/HA per unit area of membrane (Q; μg/cm^2) was calculated using Equation 2.5.

$$Q = \left(\frac{C_0 - C}{A} \right)$$

(Equation 2.5)

where C_0 and C are the initial and final concentrations of BSA or HA in solution (μg) and A is the effective membrane area (cm^2). Both sides of the membranes were in contact with foulant solution; the data refer to protein binding at the outer and accessible inner surface of membranes and hence the effective membrane area used was twice the membrane surface area.

In order to evaluate the contribution of reversible fouling, the UF cell was filled with 500 mL BSA (1 g/L) solution of pH 3 or 10 ppm HA solution of pH 7. The filtration of BSA solution was performed for 2 h at 1 bar pressure with a stirring speed of 400 rpm, while HA solution was filtered at 1 bar feed pressure for 8 h with a stirring speed of 400 rpm. The flux of foulant solution (J_p; L/m^2 per h) was determined from the collected permeate over the course of the filtration. The membranes were then removed from the UF cell and thoroughly washed with tap water. The cleaned membranes were replaced in the cell, which was refilled with DI water. The water flux of the cleaned membranes was recorded by passing DI water for 30 min at 1 bar. The flux recovery ratio (FRR; in %) of membranes was determined using Equation 2.6.

$$\text{FRR}\ (\%) = \left(\frac{J_{wp}}{J_w} \right) \times 100$$

Equation 2.6

where J_{wp} is the water flux of the cleaned membrane after filtration of BSA/HA solution and J_w is the initial pure water flux.

The following equations were used to evaluate the fouling mechanism in detail. The total fouling ratio (R_t), reversible fouling ratio (R_r) and irreversible fouling ratio (R_{ir}) were calculated using Equation 2.7.

$$R_t = \left(\frac{J_w - J_p}{J_w} \right),\ R_r = \left(\frac{J_{wp} - J_p}{J_w} \right),\ R_{ir} = \left(\frac{J_w - J_{wp}}{J_w} \right)$$

Equation 2.7

where J_p is the foulant solution flux and the other terms are as described above.

Ultrafiltration experiments

Ultrafiltration of protein [BSA or lysozyme (LYZ)] or HA solution through the membranes was conducted at pH 5, 7 and 11. Subsequently, 250 mL solution of BSA or LYZ (1 g/L) of known pH was filled into the reservoir and then UF experiments were conducted for 1 h at 1 bar. UF of HA solutions using the fabricated membranes was performed at varied concentrations (10, 20, 40 and 50 ppm), pH 7 and 1 bar feed pressure. The reservoir was filled with HA solution of known concentration and fixed pH, and filtration was then carried out at 1 bar feed pressure for 8 h. After the end of the experiments, the HA concentration in the feed and the permeate solutions was determined at 254 nm, while the concentration of BSA or LYZ in the feed and the permeate solutions was determined at a wavelength of 280 nm. The observed transmission of protein (τ_{obs}) through the membranes was calculated using Equation 2.8.

$$\tau_{obs} = \frac{C_p}{C_f}$$

Equation 2.8

where C_p is the concentration of protein (BSA or LYZ) in the permeate solution after filtration and C_f is the concentration of protein in the feed solution before filtration.

The removal efficiency of the membrane for HA was calculated using Equation 2.9.

$$R_{HA}(\%) = \left(\frac{C_{feed,0} - C_{permeate,t}}{C_{feed,0}} \right) \times 100$$

Equation 2.9

where $C_{feed,0}$ is the concentration of HA in the initial feed solution (ppm) and $C_{permeate,t}$ is the concentration

of HA in the permeate solution after the end of filtration (ppm).

2.2.5 Prototype studies

Prototype construction

Technical drawings for the prototypes were created using AutoCAD 2012 and Solid Works 2011 software. The materials used for manufacturing of the flow prototypes were PMMA tubing at 1000 mm (L) × 50mm (outside diameter) × 40 mm (inside diameter) (Radionics, Ireland). Support structures were cut from 2 mm thick PMMA sheets using a Zing Laser cutter (Epilogue, USA). Sections were cut using a DWE7491 table saw (Dewalt, Ireland) and internal rebates were cut using a RP0900 router (Makita, Ireland). Internal bonding of films and membranes was performed using a inert polyvinyl-siloxane dental glue (Coltene, "president plus"). External and structural bonding was done using Bostik clear silicone sealant (Radionics, Ireland).

Bacterial removal by prototype

All prototypes were cleaned, sterilised with 70% IMS and flushed with 1 L of sterile DI water before microbiological assays were carried out. Subsequently, 700 mL or 5 L of sterile saline solution (0.85% NaCl) was inoculated with *E. coli* to a final concentration of 10^2 CFU/mL under separate experimental parameters to examine prototype performance. In the preliminary run, using 700 mL, a Watson-Marlow 114 DV peristaltic pump (Watson-Marlow, Ireland) was used at a flow rate of 22 mL/min to give a ramp-up stage of 30 min. Then, 1 mL samples were taken in triplicate at 30 min, following the ramp-up stage, and at 1 h intervals thereafter up to 6 h and the bacteria counted using the pour plate technique. For the larger volume examination of 5 L, the same flow rate was employed; however, samples were taken after initial ramp-up phase and then after each litre eluted until the total volume had passed. Samples of 1 mL were taken at each point and counted in triplicate via pour plates. In addition, to examine the viability of the organisms, 1 mL samples were added to 9 mL of both nutrient broth and R2A broth and incubated overnight. Following the experiment, each membrane was removed from the prototype, cut into halves and placed into each of R2A broth and nutrient broth to examine the state of the bacteria on the surface.

Removal of cryptosporidium by prototype

To examine the removal of cryptosporidium by the prototype, 100 oocysts (provided by City Analysts Ltd, Dublin) of *C. parvum* were added to 10 L of sterile saline solution (0.85% NaCl) to give an inoculum size of 10 oocysts/L. This was passed through the prototype, collected and passed through a filtramax filtration unit for collection. Microscopic analysis was carried out by City Analysts Ltd for the presence or absence of oocysts following passage through the unit.

3 Results

3.1 Characterisation of Graphene Composites

The graphene materials (GO, rGO and Cu-rGO) were characterised by UV-Vis spectrophotometric analysis (Figure 3.1), TGA (Figure 3.2), SEM analysis (Figures 3.3, 3.4 and 3.5), EDX (Figure 3.6) and FTIR analysis (Figure 3.7)

From the *UV-Vis analysis*, GO shows a characteristic peak at ~230 nm, indicating the successful exfoliation and oxidation of graphite to GO. Subsequent chemical reduction results (rGO) in a characteristic redshift of the absorption peak from 230 to 260 nm, indicative of the loss of oxygen functional groups on the surface of GO and the restoration of the electronic conjugation across the sheets. Cu-rGO displays a much broader band from 260 nm to 400 nm than rGO, indicative of the presence of oxidised CuNPs (Figure 3.1).

Solids of GO, rGO and Cu-rGO were characterised for their thermal stability via *TGA*. GO showed a significant drop in weight at ~200°C and showed a more rapid decline in weight loss than the other two materials with less than 30% remaining at 800°C. rGO showed a mild yet steady decline from 0 to 800°C, losing only 30% weight in total, which suggests a much greater thermal stability compared with that of GO. The GCC showed the greatest thermal stability of the three materials losing only 25% of its total weight up to 800°C (Figure 3.2).

The exfoliation of GO sheets from expanded graphite was confirmed by the presence of lustrous silk-like sheets, which were visible under *SEM analysis*. Under low magnification (×500), large sheets of >100 µm width were visible. Sheets also appeared crumpled in some areas and translucent in others, suggesting a variance in the sheet thickness across the sample. This thin nature of the sheets was confirmed via images captured in transmission electron mode; the sheets were almost transparent, suggestive of their thin nature (Figure 3.3).

The physical characteristics of the rGO sheets were also observed under SEM (Figure 3.4a) to examine changes occurring following chemical reduction. While a sheet-like structure was visible, similar to the observations for GO, the veil-like appearance of low-number sheets was absent unlike the GO sample, suggesting the agglomeration of sheets during the

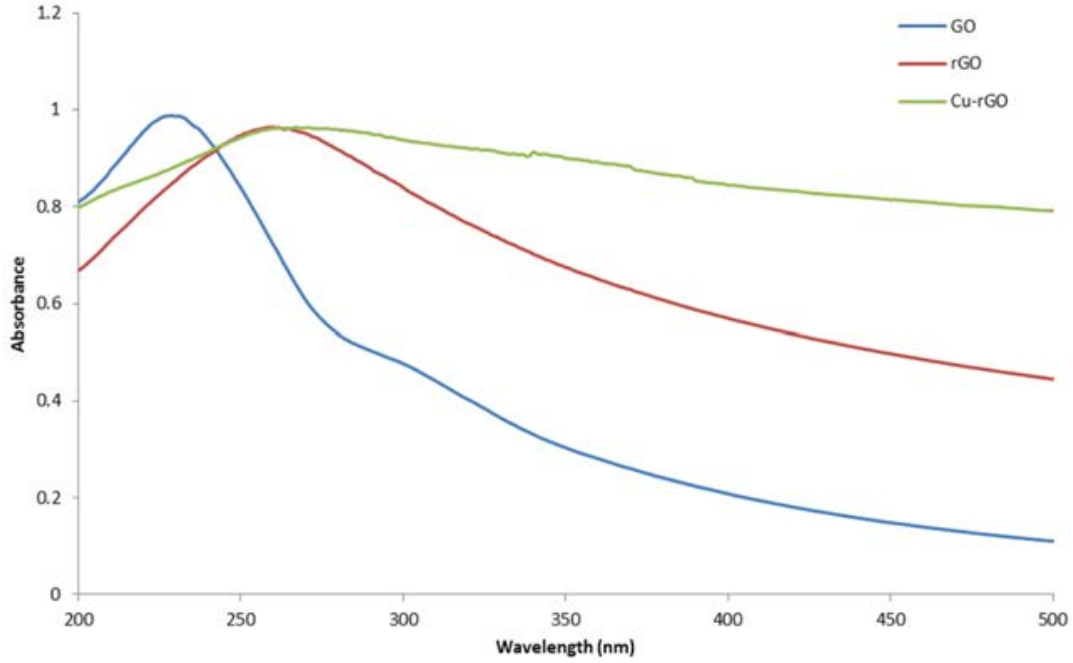

Figure 3.1. UV-Vis spectra of GO, rGO and Cu-rGO.

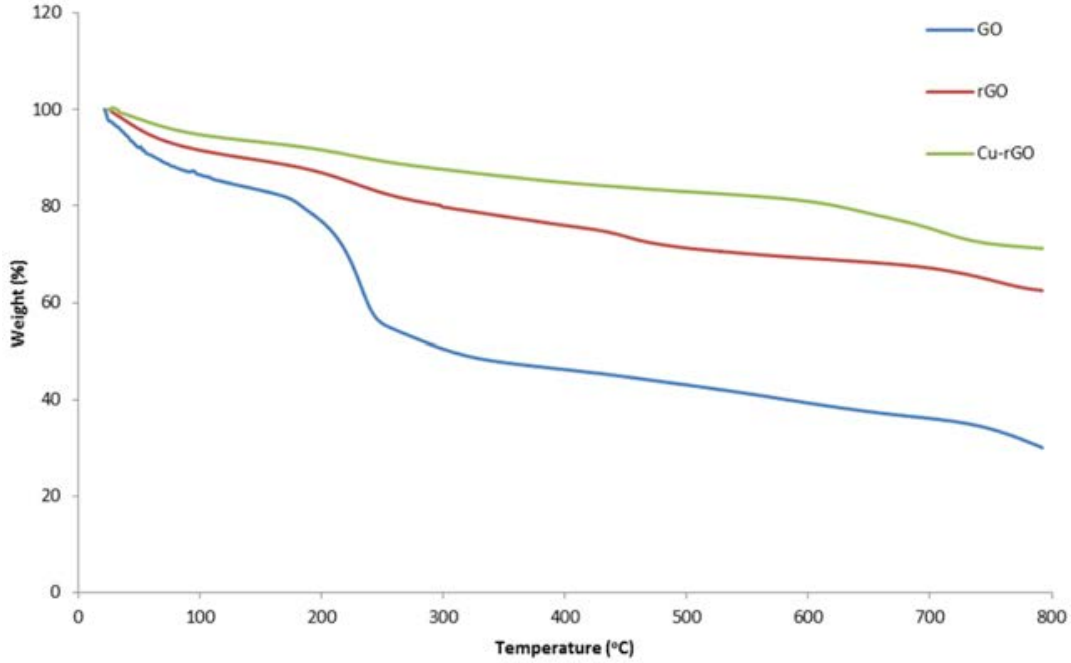

Figure 3.2. TGA carried out on GO, rGO and the GCC (Cu-rGO).

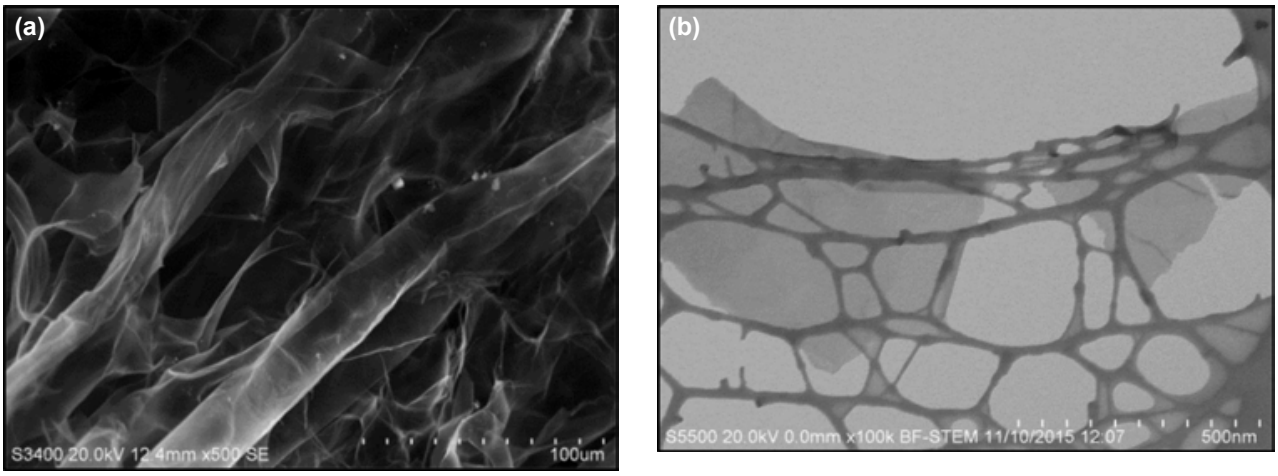

Figure 3.3. Scanning electron micrographs of chemically exfoliated GO sheets at (a) ×500 under secondary electron mode and (b) ×100k under transmission mode on holey carbon substrate.

reduction process. Under transmission electron mode (Figure 3.4b), the rGO sheets appear larger and more opaque than the GO sheets, suggesting that a certain level of sheet agglomeration has occurred following reduction.

Cu-rGO morphology was also examined via SEM analysis and yielded images with a very apparent morphological difference from both the GO and rGO samples. On account of the presence of Cu, the promotion of particulate agglomeration is clearly visible in the Cu-rGO sample. Large agglomerates of sheets can be seen clearly decorated with CuNPs across the surface. Images captured under transmission mode reveal CuNPs agglomerates attached to the graphene sheets, indicative of the attachment of the produced CuNPs during the reduction process (Figure 3.5).

Graphene oxide showed a typical *elemental composition* as seen in Table 3.1 and the EDX spectrum (Figure 3.6). The carbon to oxygen ratio was ~1:1, showing the high level of oxidation of the graphene following chemical exfoliation. There was no residual sulfur, potassium or any other trace elements from the production process, indicating the washing procedure had been performed thoroughly. The

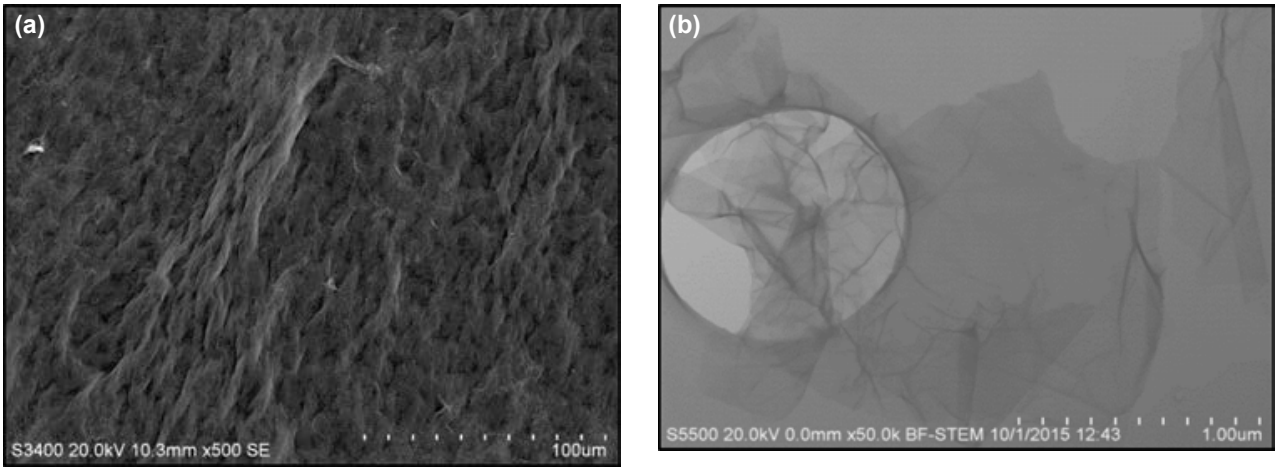

Figure 3.4. Scanning electron micrographs of exfoliated GO sheets following chemical reduction at (a) ×500 magnification under secondary electron mode and (b) ×50k under transmission mode.

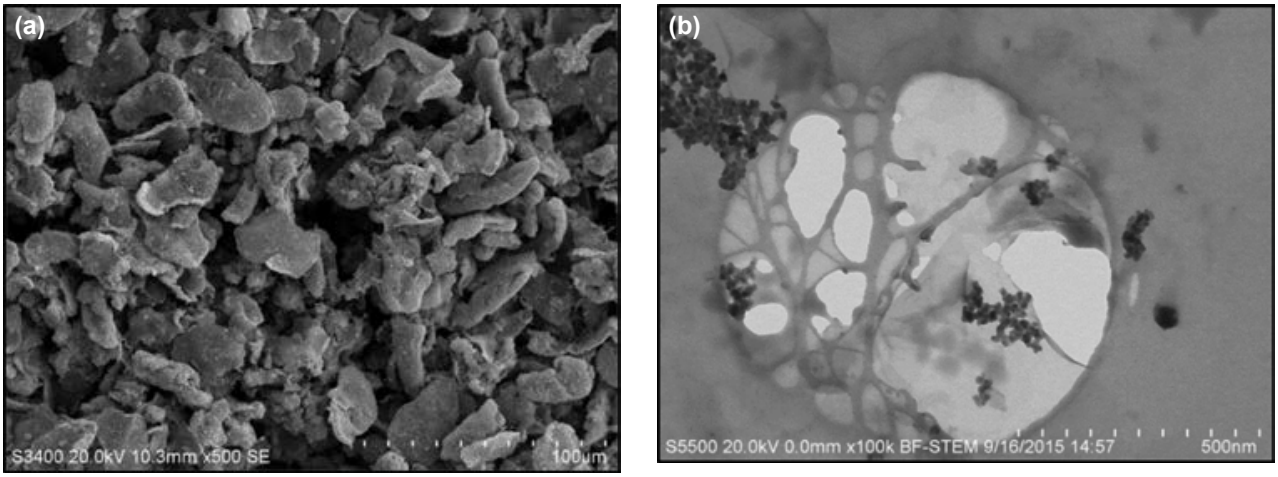

Figure 3.5. Scanning electron micrographs of GCC at (a) ×500 magnification under secondary electron mode and (b) ×100k magnification under transmission mode with CuNPs visible attached to the graphene sheets.

Table 3.1. Average values of EDX analyses taken for the graphene composites and CuNPs

Composite	% Carbon	% Oxygen	% Copper
GO	50.1	46.3	–
rGO	68.68	31.32	–
Cu-rGO	37.16	22.42	40.04
CuNP	–	25.69	74.31

–, not detected.

resulting reduction of GO to rGO is apparent following elemental analysis, as the carbon to oxygen ratio has shifted from 1:1 to 2:1 ratio in favour of carbon. This is a clear indication that the reduction process has been carried out successfully, as the change in the carbon to oxygen ratio is suggestive of the loss of the oxygen-containing functional groups present in the GO. The GCC showed a markedly lower level of oxidation than was observed for GO, indicative of the loss of oxidative groups present on the surface during the reduction process, from 46% in GO to 22% in the Cu-rGO. The average Cu composition was found to be 40% with a variance across the surface depending on the site observed, indicating the inhomogeneity

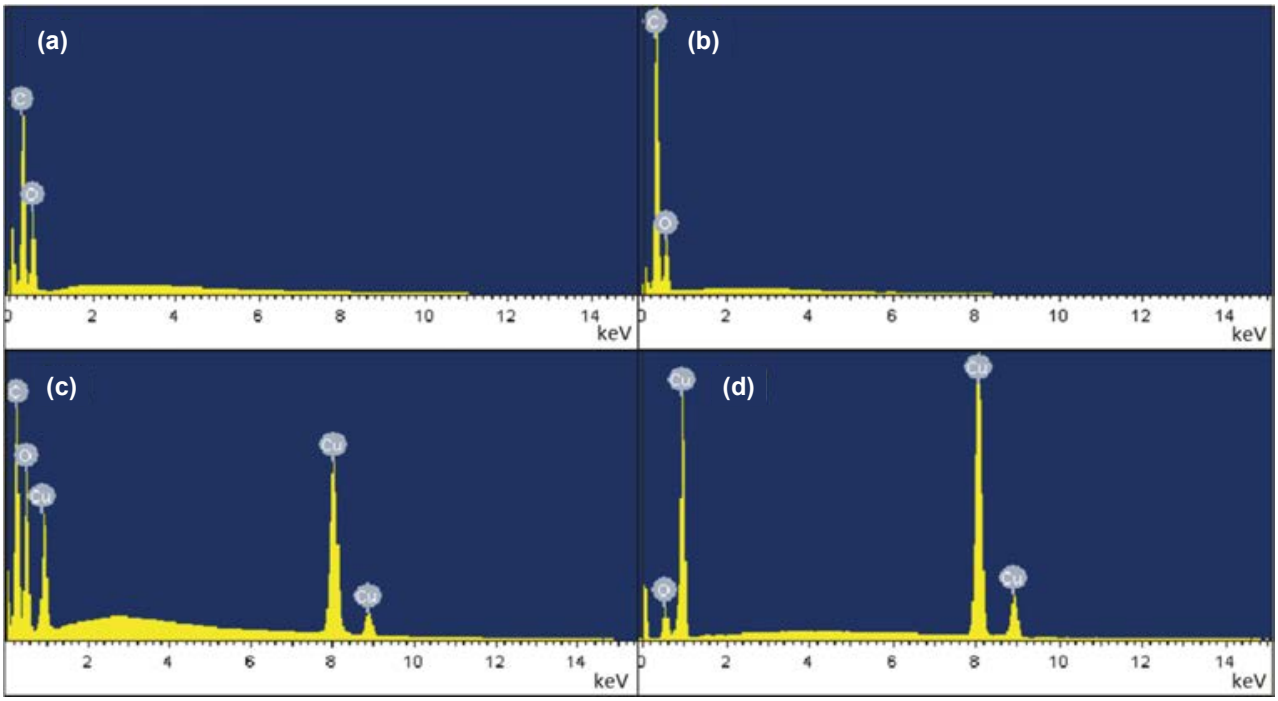

Figure 3.6. EDX spectrum of (a) GO, (b) rGO, (c) the GCC and (d) CuNPs derived from a Cu salt ($CuCl_2$).

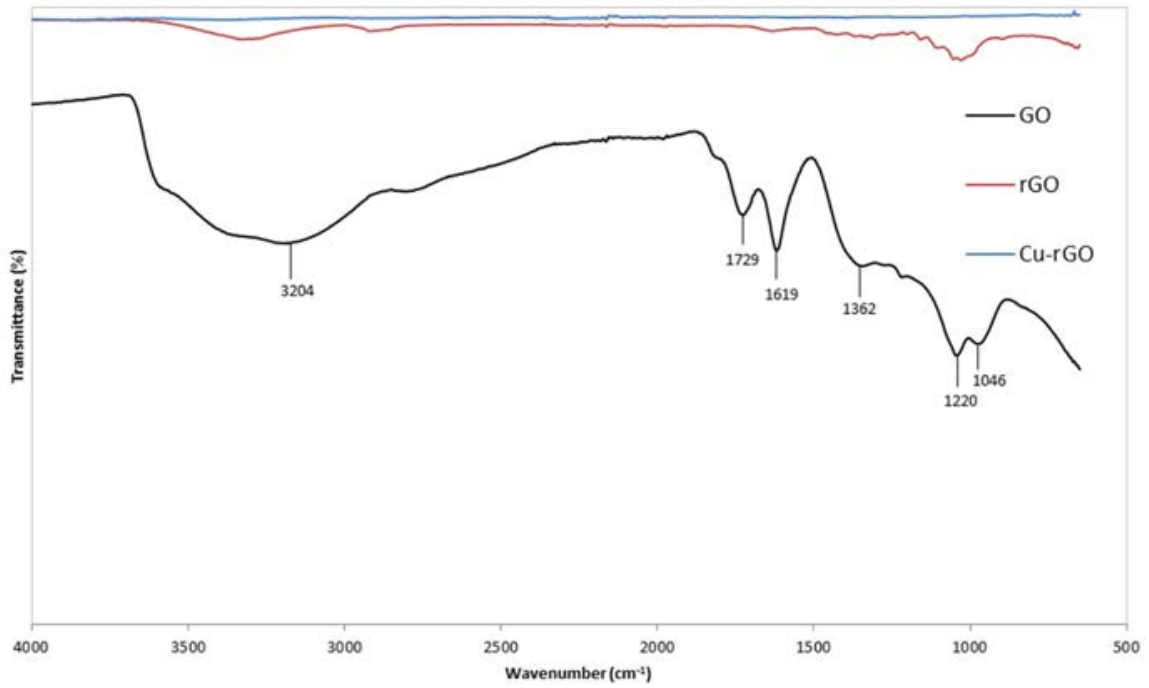

Figure 3.7. FTIR spectrum of GO, rGO and Cu-rGO.

of Cu attachment across the graphene sheets during production. This inhomogeneity can also been seen from the SEM analysis in Figure 3.6.

In addition to the production of the composite, a separate process without the addition of graphene was also performed to examine the effect of the reduction process on the $CuCl_2$ used to produce the composite. The form of Cu present, i.e. Cu metal (Cu), cuprous oxide (Cu_2O), cupric oxide (CuO) or the highest Cu oxide (Cu_2O_3), in the composite is important, as different forms of Cu will possess different levels of antibacterial efficacy. The resulting average values

can be seen in Table 3.1. The average elemental percentage of oxygen present in the compound is 24%.

FTIR analysis was carried out to examine the change in the molecular structure of the graphene materials following reduction of GO to rGO and the production of the Cu composite (Figure 3.7). Adsorption bands for GO are observed at 3204, 1729 and 1046 cm^{-1} and can be attributed to O-H deformation, C=O carbonyl stretching and C-O-C stretching, respectively. The remaining peaks at 1619, 1362 and 1220 cm^{-1} correspond to the carboxyl groups present in the GO. Following reduction to rGO and composite production there is a very notable reduction in these adsorption bands indicating the loss of the functional groups from the graphene materials during the reduction process. The observation of these adsorption bands as well as the change observed following the reduction process are in line with those observed in the literature from previous productions of GCCs (Xu *et al.*, 2009; Chen *et al.*, 2011).

3.2 Determination of Antibacterial Activity of Graphene Composites

3.2.1 Solid media testing

Antibacterial studies were carried out in solid media on both *E.coli* and *B. subtilis* using four approaches (Figure 2.3). There were no observable zones of inhibition from either the well diffusion (Figure 2.3a) or disk diffusion assay (Figure 2.3b) methods. Using the solid exposure method (Figure 2.3c), no response was observed for either organism using GO and rGO, but there were clear zones of inhibition present for the Cu-rGO and the CuNPs. The size of the zones was not measured, as the shape and size of the applied solids varied and results were recorded as a positive or negative response. The final approach, vacuum-filtered disk assay (Figure 2.3d) designed to allow for direct contact between the organisms and the composite, did yield a positive result, with the zones of inhibition of each material shown in Table 3.2.

3.2.2 Shake flask studies

In order to examine the effect of free particles of graphene materials, liquid media studies with agitation were carried out (Figure 2.4). These studies were designed to mimic those in the literature that had reported a kinetic or shear-based antibacterial effect on planktonic bacterial cells. PBS, a saline buffer solution, was used as a non-growth medium. Both *E. coli* and *B. subtilis* were used and challenged with 100 mg/L of each material over a 6 h period along with 24 h sampling.

The results from these experiments are shown in Figure 3.8. There was no statistically significant reduction in the population of *E. coli* cells during the 6 h incubation period with either the GO or rGO. The Cu composite resulted in a reduction of 25% ± 2%, greater than the same concentration of CuNPs, which resulted in 14% ± 3%. In the 6 h period, it was shown that the Cu-containing salts, $CuCl_2$ and $CuSO_4$, had a more acute effect than the particulates, achieving 35% ± 2% and 36% ± 4% reduction in population size, respectively. There was still no statistically significant reduction in population over a 24 h period from the GO or rGO. The results over a 24 h period showed a markedly different trend for the salts and other particulates. The Cu-rGO and CuNPs achieved a reduction in population of 81±1 and 80±3%, respectively. The *B. subtilis* was shown to be more susceptible to the Cu-containing compounds than

Table 3.2. Zones of inhibition for each of the materials employed in the vacuum-filtered disk assay

Zone size (mm)	*E. coli*	*B. subtilis*
Blank	No zone	No zone
GO	No zone	No zone
rGO	No zone	No zone
Cu-rGO	11 mm	14 mm
$CuCl_2$	14 mm	19 mm
$CuSO_4$	10 mm	15 mm
CuNPs	12 mm	16 mm
Gentamycin	19 mm	20 mm

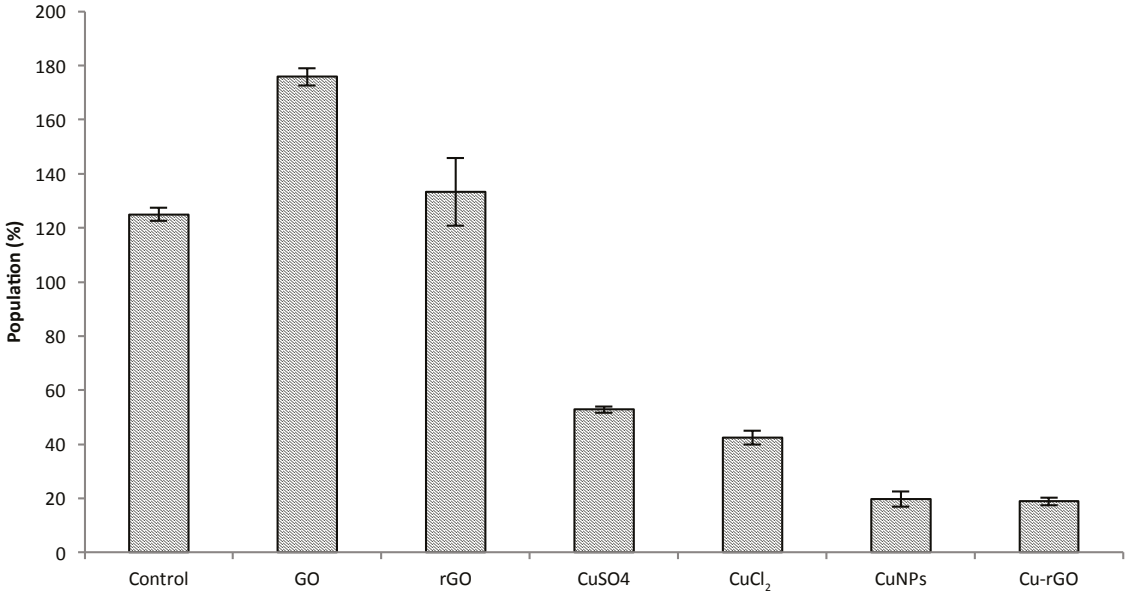

Figure 3.8. *E. coli* exposure to the various materials in PBS following a 24 h period at 100 mg/L.

the *E. coli*, however, with total loss of cell viability occurring in 6 h with all of the materials. Most notable is that the Cu-rGO is performing at a comparable rate with the stand-alone nanoparticles at the same concentration while only containing 40% Cu. This would suggest that in saline solution and with agitation, the GCC is enhancing the activity of the CuNPs present on the surface.

3.2.3 Minimum inhibitory concentration evaluation

In order to examine the dose-dependent response of both organisms in liquid media, as well as to establish the minimum concentration required to inhibit all bacterial growth, an MIC determination was carried out in nutrient broth. Concentrations of up to 1000 mg/L were tested as these are the upper limits found within previous reports for the antibacterial testing of graphene materials. Neither of the stand-alone graphene materials, GO and rGO, showed any inhibition of either of the organisms up to 1000 mg/L. A concentration of 1000 mg/L of Cu-rGO was required to totally inhibit the growth of both organisms (Figure 3.9), which was the highest concentration needed of any material tested. Considering the Cu load of the graphene composite at 40%, it is not surprising that this concentration was required. The 1000 mg/L of composite is equal to 400 mg/L of CuNPs, the observed MIC for the nanoparticles without graphene material. Unlike the shake flask scenario, which includes agitation in a low-growth medium, the MIC evaluation is stationary and in a rich-growth media. These two exposure scenarios are very different and this may explain the different responses the organisms present to the different materials in each case. The Cu salts, which showed lower MIC values of 400 mg for each organism, are most likely outperforming the composite on account of their greater level of water solubility is enhancing contact with the bacteria (Figures 3.10 and 3.11).

3.2.4 SEM analysis of cell morphology

In order to verify the observed results described in section 3.2.1, the morphological profile of *E. coli* following exposure to vacuum-filtered disks was examined under SEM. *E. coli* can be seen to be numerous across the surface of GO (Figure 3.12) and rGO (Figure 3.13) and appear unperturbed by contact with the surface, having intact membranes and standing proud of the surface, suggesting that the surface of each material does not possess innate antimicrobial activity when in direct contact with micro-organisms. *E. coli* exposed to the surface of Cu-rGO (Figure 3.14), however, show clear membrane damage, looking deflated and conforming to the surface of the material rather than standing proud of it, indicating that the addition of Cu to the material results in the contact killing of organisms on the surface.

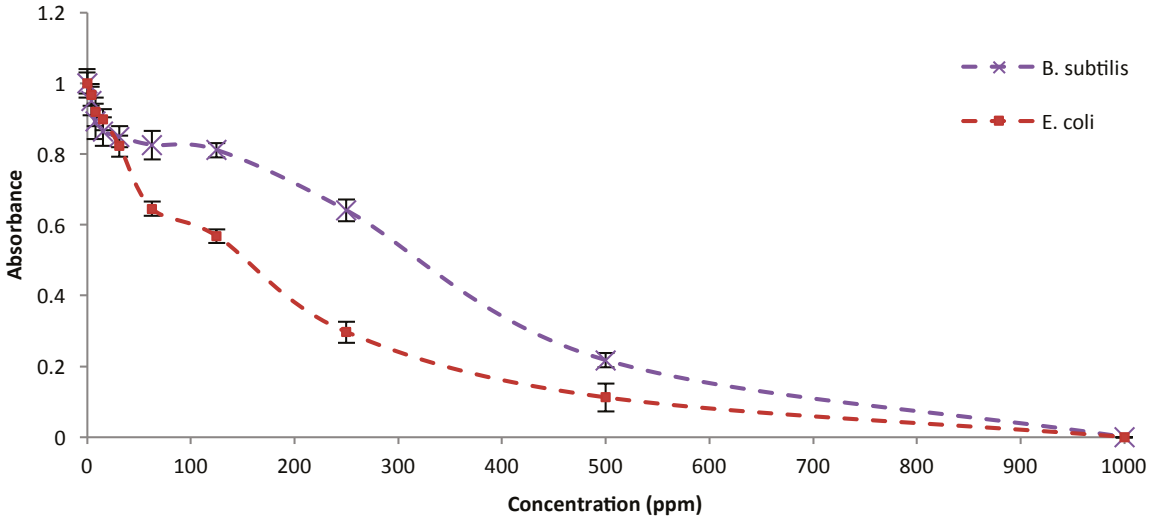

Figure 3.9. Determination of the MIC values for each organism, *E. coli* and *B. subtilis*, for Cu-rGO.

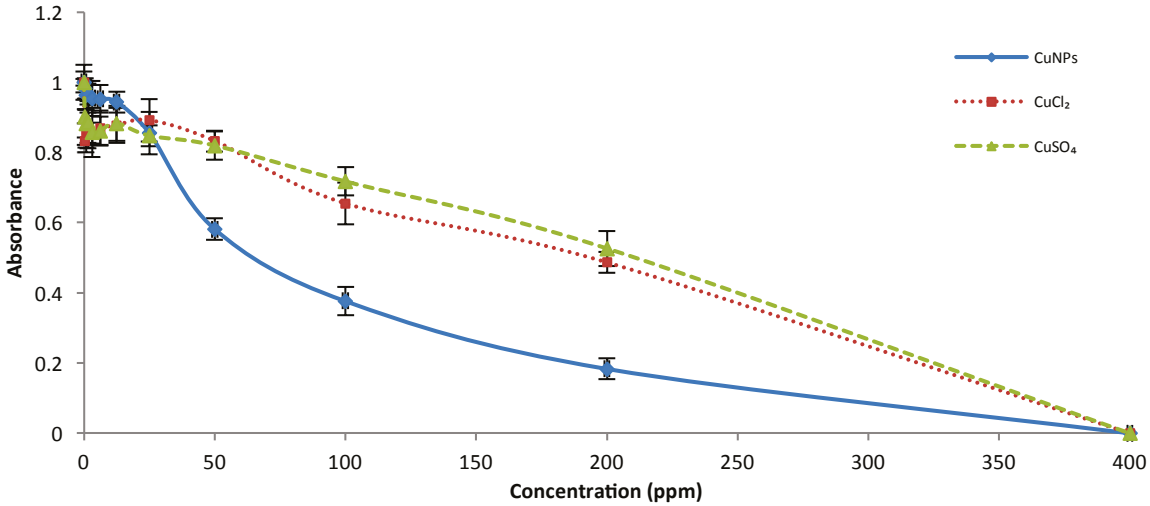

Figure 3.10. Determination of MIC values for *E. coli* for each of the Cu-containing compounds via the broth microdilution method: CuNPs, $CuCl_2$ and $CuSO_4$.

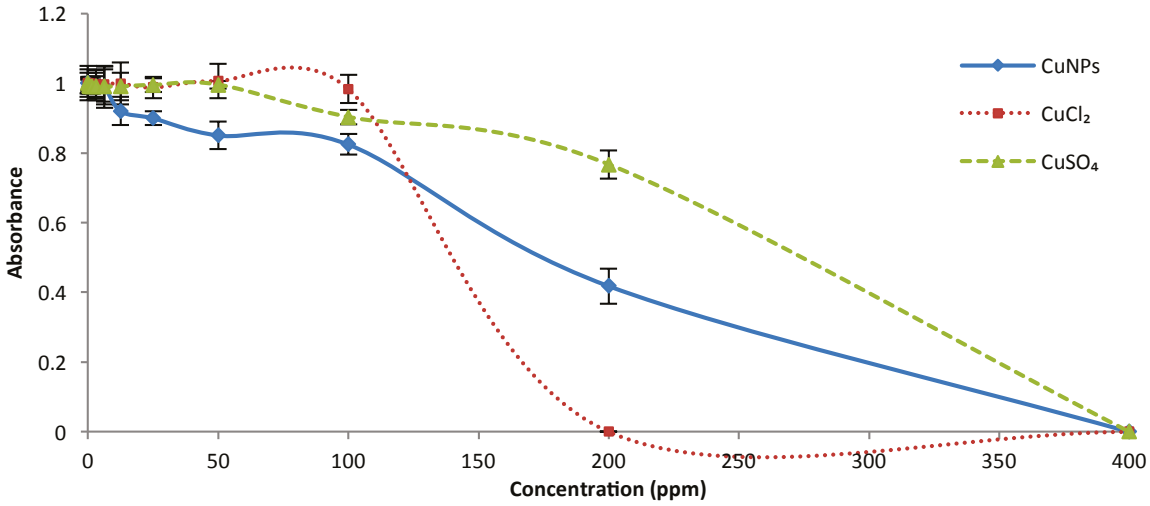

Figure 3.11. Determination of MIC values for *B. subtilis* for each of the Cu-containing compounds via the broth microdilution method: CuNPs, $CuCl_2$ and $CuSO_4$.

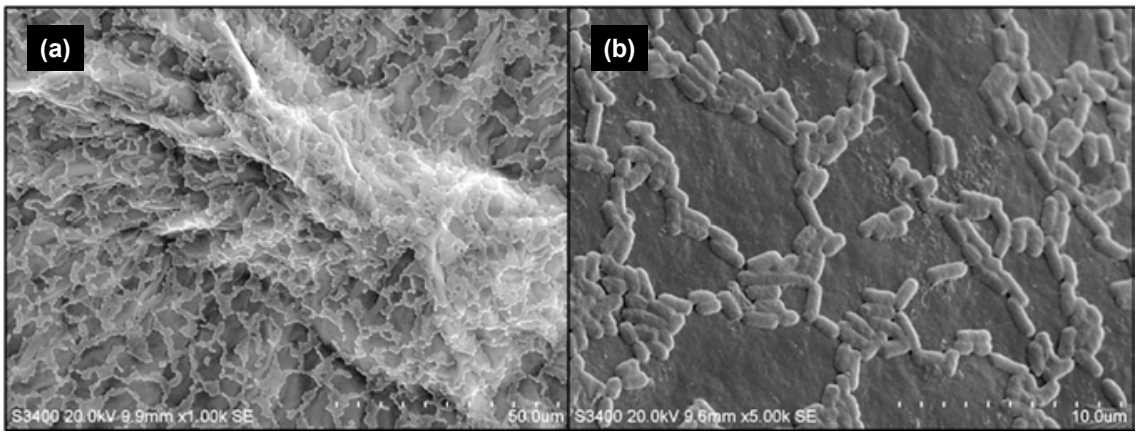

Figure 3.12. *E. coli* exposure to the surface of GO at (a) ×1000 magnification and (b) ×5000 magnification.

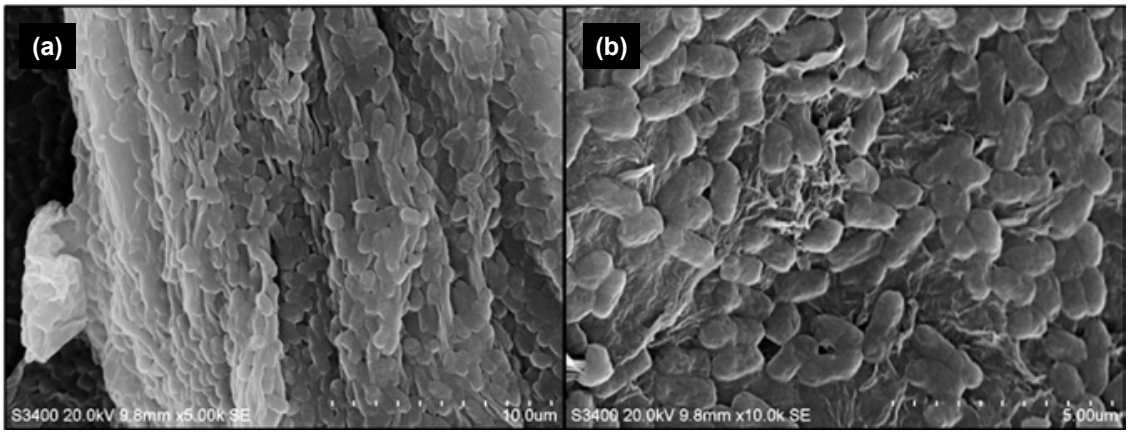

Figure 3.13. *E. coli* exposure to the surface of rGO at (a) ×5000 magnification and (b) ×10,000 magnification.

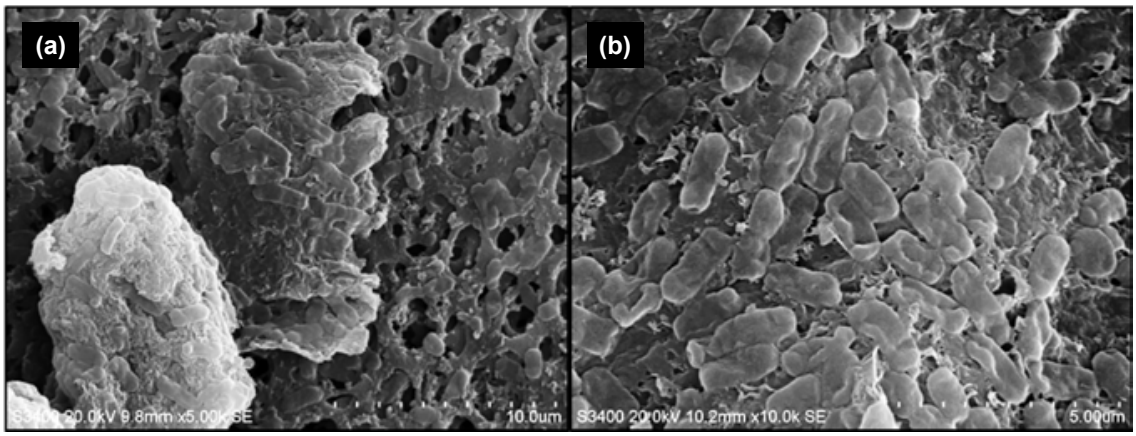

Figure 3.14. *E. coli* exposure to the surface of Cu-rGO at (a) ×5000 magnification and (b) ×10,000 magnification.

3.3 Pharmaceutical Removal

3.3.1 Graphene-impregnated beads

One approach for the integration of graphene into a drinking water system that was examined in this project was to sequester the graphene particles into a support material. To this end, GO-PSf beads were produced and their adsorptive capabilities were assessed. The beads were examined under SEM to ascertain the availability of graphene within the structure. Not only were the beads porous, but the graphene sheets (Figure 3.15) were freely available within the porous structure and clearly visible compared with the pure PSf bead.

Once the PSf beads were made with GO concentrations of up to 1 wt%, they were tested in the field for removal of some anions/cations from water obtained at the discharge point of a WWTP that discharged into the Slaney River. Despite excellent distribution of GO around the pores inside the PSf beads (Figure 3.15b), no significant reduction in concentration of anions/cations was observed after 24 h. This is probably because the hydrophobic nature of PSf prevented penetration of water into the beads and active adsorption of anions/cations onto GO was not possible. It was therefore decided to change the substrate to Ca-Alg, which has been reported to have a very high affinity for the chelation of various metal ions and cationic dyes (Yang *et al.,* 2012). The porous structure of ionotropic alginates is an attractive platform for attachment of GO for the adsorption of toxic metals and pharmaceuticals from wastewater. GO-impregnated Ca-Alg beads (Figure 3.16) were prepared and subjected to drying and acid activation at pH 4, and their performance was assessed using MB, diclofenac and famotidine as model pollutants. Preliminary experimentation suggested that dried activated beads showed the most promise in terms of adsorption capacity.

The effects of GO content, adsorbent dose, pH, temperature and pollutant concentration were investigated for all matrices. In all cases, the higher the GO content, the better the bead performance.

Methylene blue

The pH was not found to significantly affect the bead performance over the range pH 7–12 and therefore subsequent experimentation was carried out at pH 7. Decreasing temperature was seen to improve alginate bead performance; however, it had little impact on the highest GO loading (Figure 3.17).

The Langmuir isotherm (Equation 3.1) was found to fit the system well (Table 3.3).

$$\frac{C_e}{q_{eq}} = \frac{C_e}{q_{max}} + \frac{1}{q_{max} k_L} \qquad \text{Equation 3.1}$$

where C_e is the equilibrium concentration of the solution (mg/L), q_{eq} is the amount adsorbed at equilibrium (mg/g), q_{max} is the maximum adsorption capacity (mg/g) and k_L is a Langmuir constant related to the affinity of the binding sites and energy of adsorption (L/g).

This is similar to results for adsorption of MB onto graphene found previously; however, the maximum adsorption capacity found here is excellent (1334.2 mg/g) in comparison with previously published

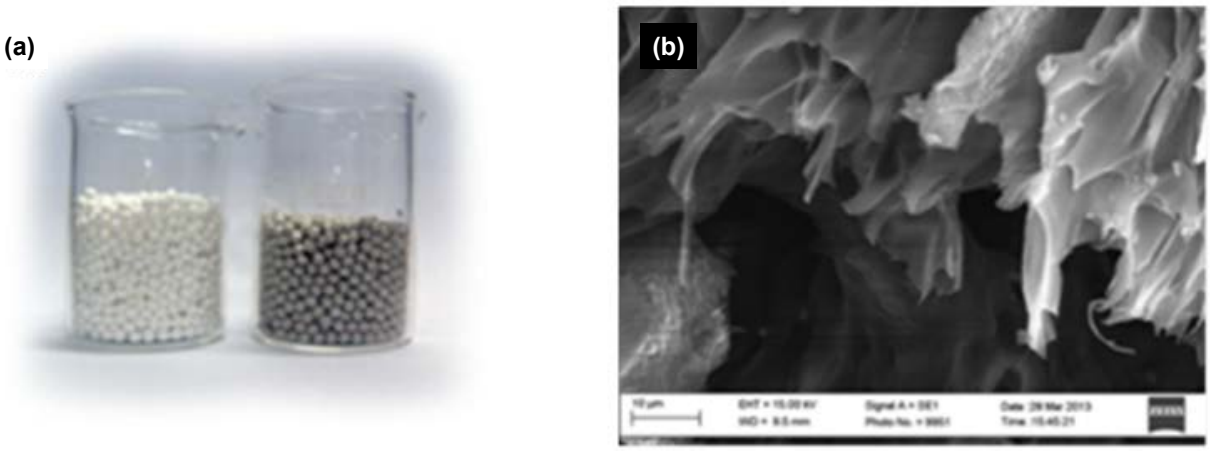

Figure 3.15. (a) PSf and GO-PSf beads and (b) SEM of GO-PSf beads.

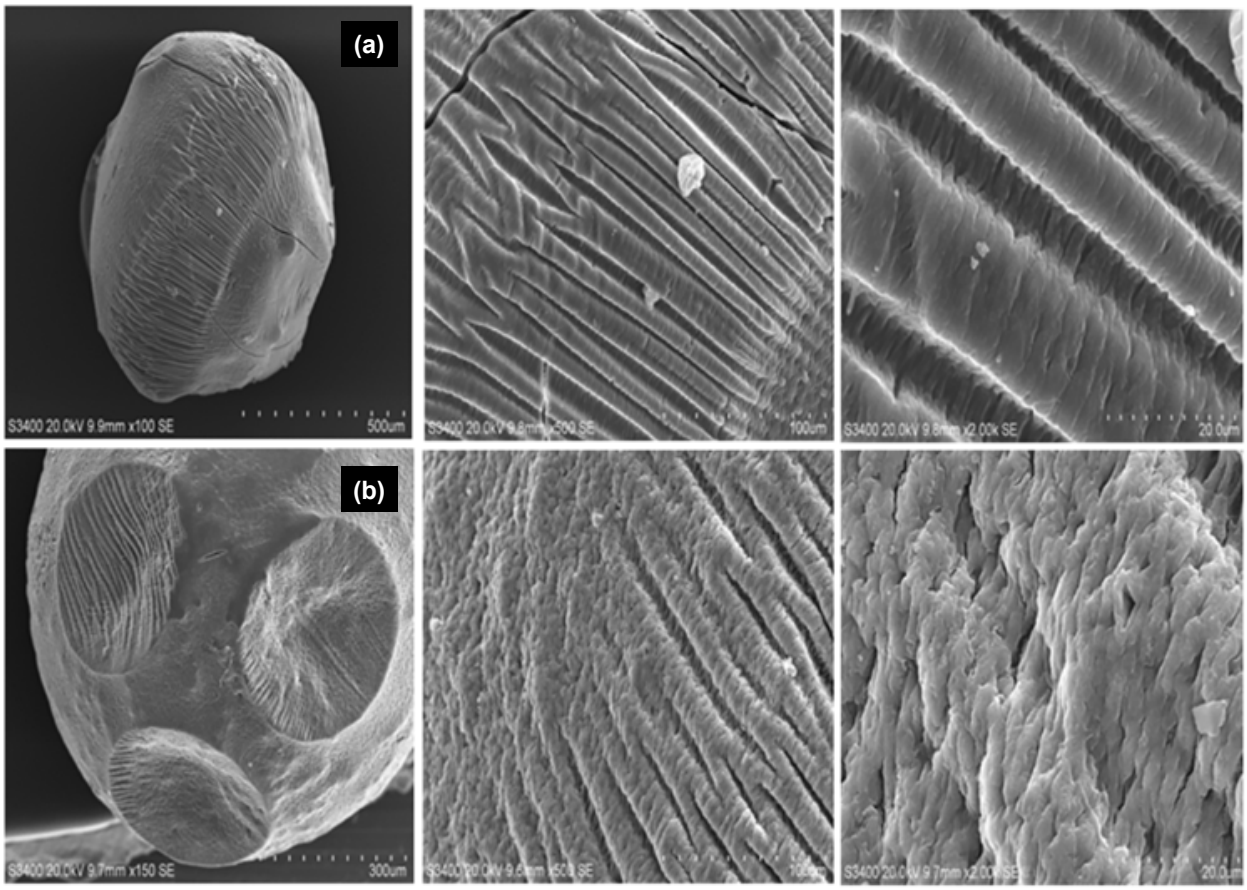

Figure 3.16. SEM images for (a) alginate and (b) alginate-GO beads.

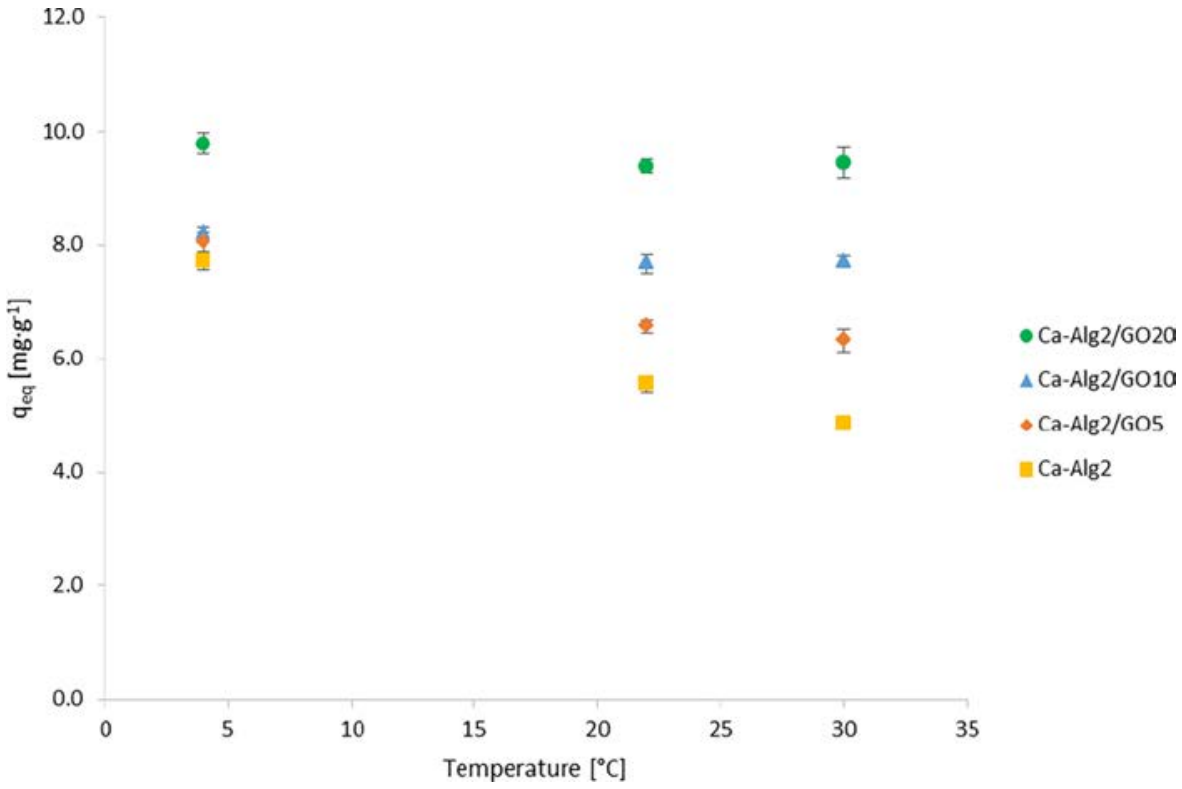

Figure 3.17. Effect of temperature on MB removal.

Table 3.3. Langmuir coefficients for MB adsorption

Bead type	Ca-Alg	GO5	GO10	GO20
q_{max} (mg/g)	1063.9	1153.2	1212.3	1334.2
K_L	85.56	88.93	84.21	76.21
R^2	0.939	0.930	0.923	0.923

results of 153.85 mg/g for graphene (Liu *et al.*, 2012b), approximately 400 mg/g for activated carbon (Kumar and Sivanesan, 2006), 580 mg/g for activated carbon produced from steam-activated bituminous coal (El Qada *et al.*, 2006) and 315 mg/g for activated carbon produced from walnut shells (Yang and Qiu, 2010). The control results (alginate beads) also yield a high maximum adsorption capacity, indicating that the drying/pH activation strategy works well.

Pseudo-first order kinetics were found to fit the experimental data well, with R^2 values of >0.99 for all bead types.

Desorption was also examined using 0.1 M HCl and 1 M NaCl to investigate the robustness of the beads and the potential for continued reuse. Desorption was possible in all cases, with 70% desorption seen under acidic conditions (Figure 3.18). Bead swelling or damage was not observed during desorption, indicating the potential for long-term bead reuse.

Diclofenac

The pH was found to significantly affect the performance of the beads for removal of diclofenac, with removal possible only below pH 3 (Figure 3.19). This is probably because the dissociation constant of diclofenac (p*K*a) is 4; thus, diclofenac is ionised only below this pH. Limited removal of diclofenac at neutral pH is to be expected, which may limit its applicability in standard water treatment. However, 80% removal of diclofenac at pH 3 (from a starting concentration of 10 mg/L) shows promise where targeted removal of this problem contaminant is necessary.

A decrease in temperature was seen to improve the adsorption of diclofenac at pH 7 (Figure 3.20). Pseudo-first order kinetics were again found to be the best fit to the experimental data (Table 3.4).

Limited acid desorption of up to 30% was achieved (Figure 3.21), indicating that further optimisation work is needed to allow reuse of the beads.

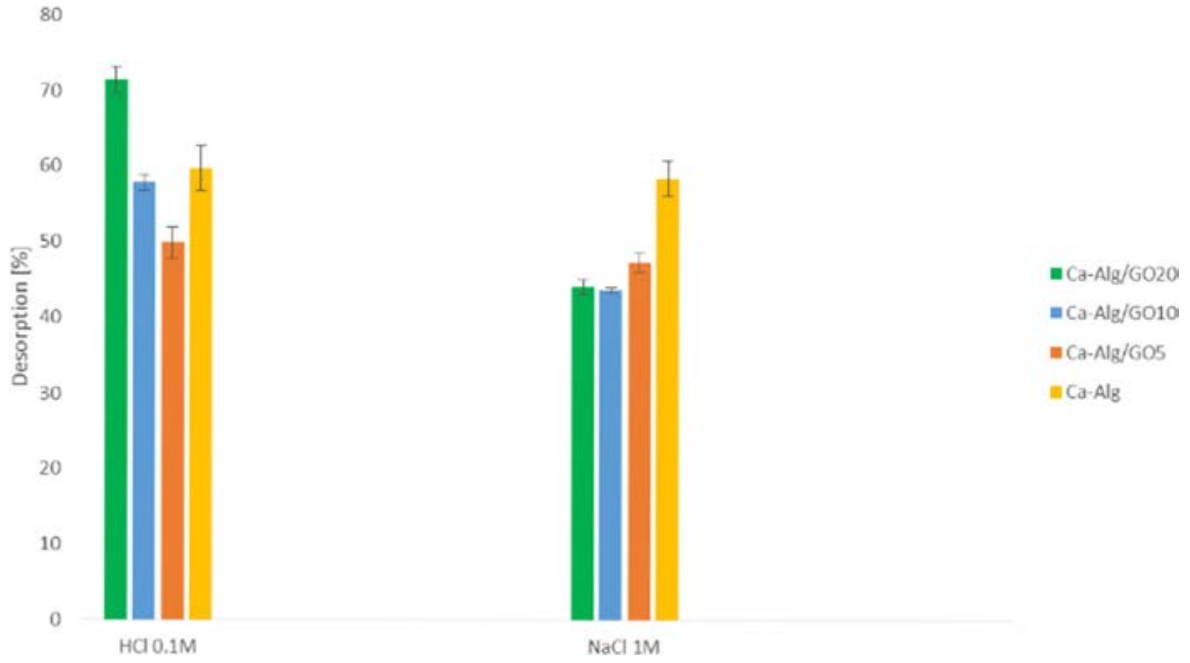

Figure 3.18. Desorption with 0.1 M HCl and 1 M NaCl.

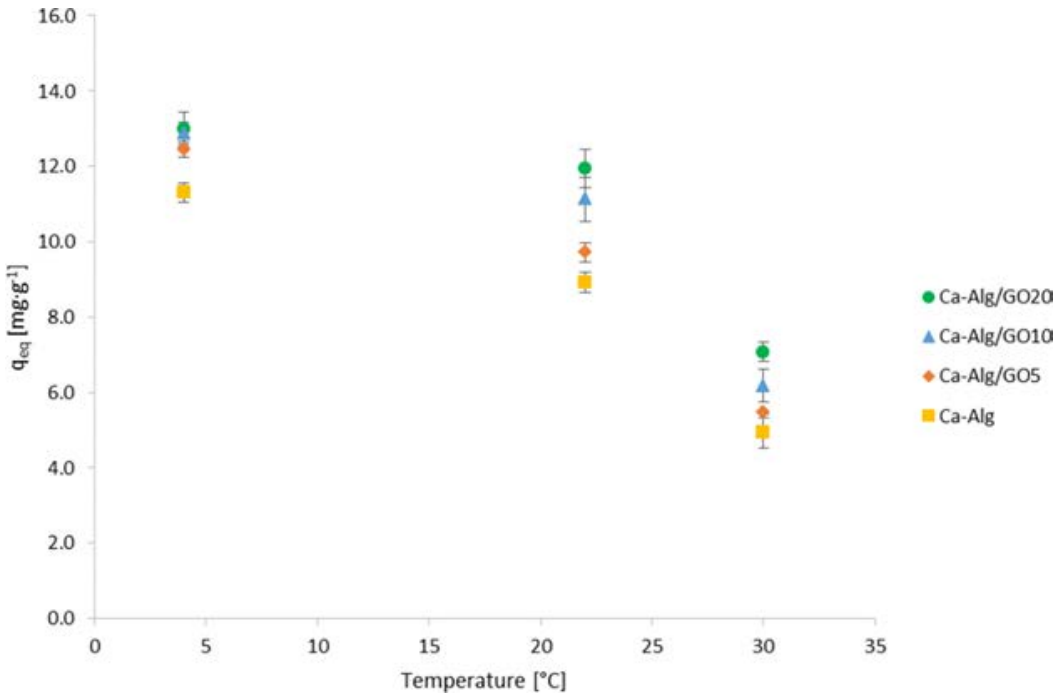

Figure 3.19. Effect of pH on diclofenac removal.

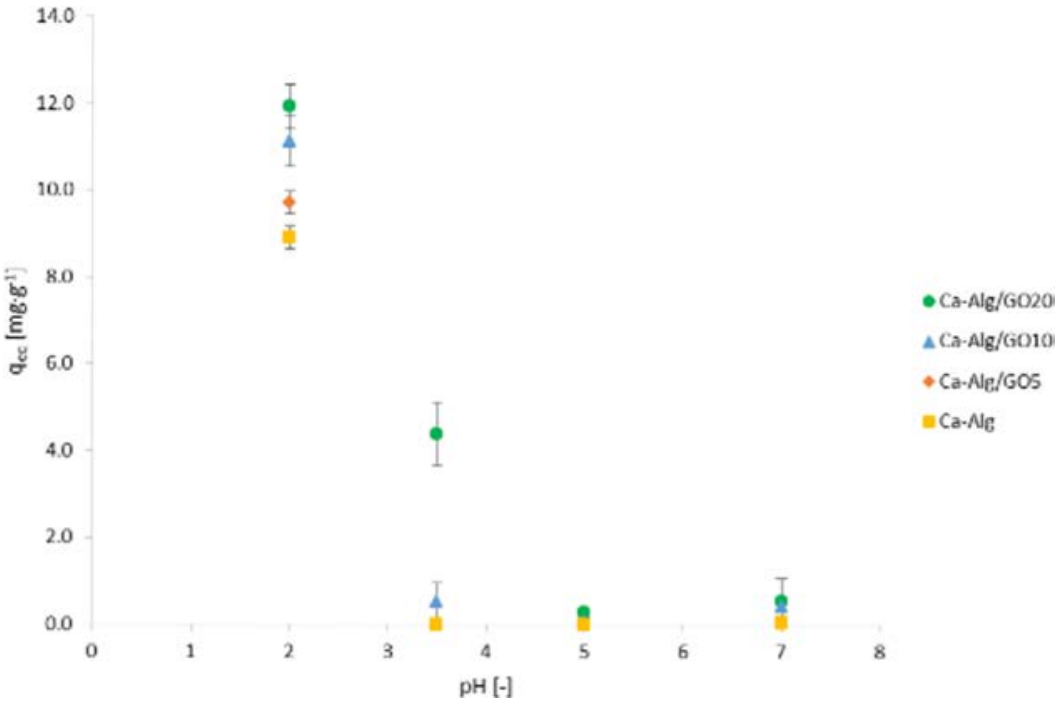

Figure 3.20. Effect of temperature on diclofenac adsorption.

Table 3.4. Pseudo-first order kinetics for diclofenac adsorption

	Ca	GO5	GO10	GO20	Units
R^2	0.97456	0.982	0.98653	0.98791	–
q_{eq}	3.697	4.283	4.742	4.256	mg/g
k_1	2.420E–03	1.590E–03	1.900E–03	1.780E–03	per min

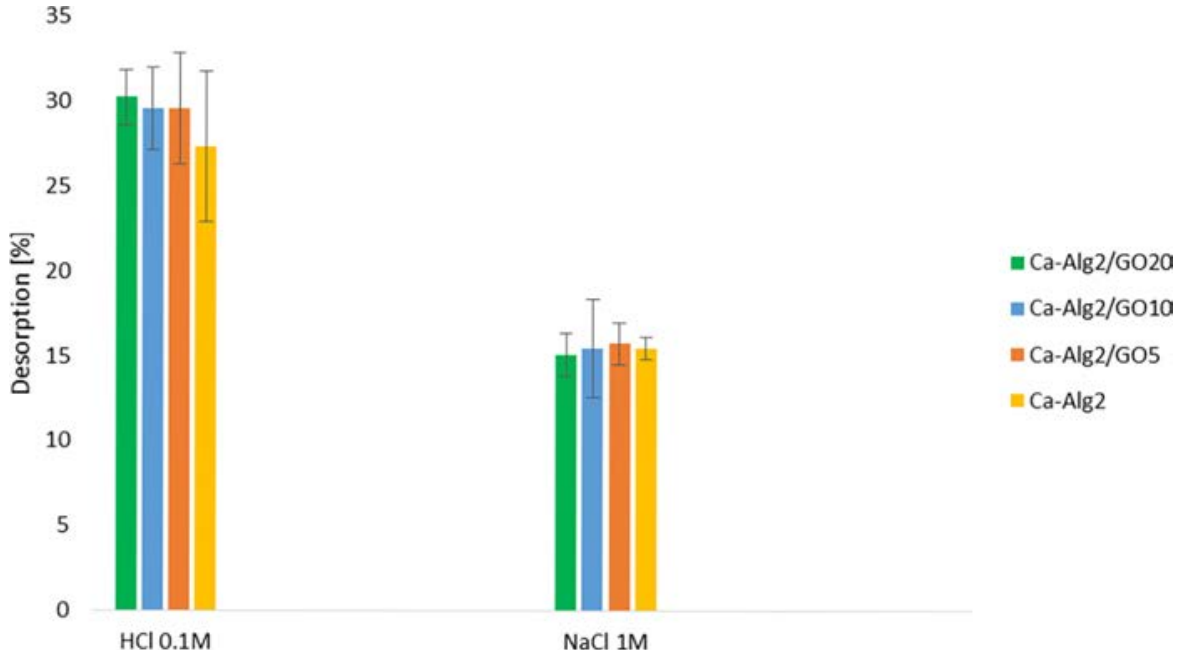

Figure 3.21. Desorption of diclofenac.

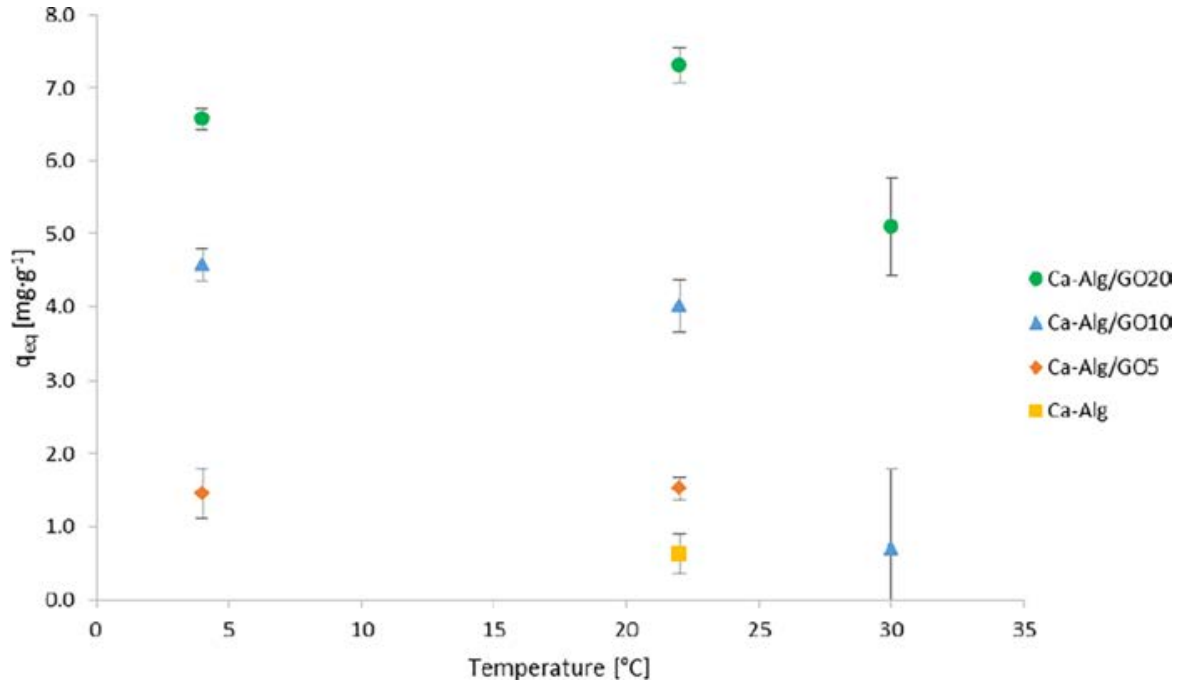

Figure 3.22. Effect of pH on famotidine adsorption.

Famotidine

pH was not seen to significantly impact on the removal of famotidine (Figure 3.22), while elevated temperatures adversely affected removal (Figure 3.23). This was particularly the case for beads containing low/no GO, where very little removal was seen at 30°C. The Langmuir isotherm was again found to describe the system well (Table 3.5). The pseudo-second order model was found to fit the kinetics of the process best (Table 3.6).

Desorption on the basis of ionic strength adjustment was found to work best (Figure 3.24); however, again, only limited desorption was achieved, indicating that further optimisation is necessary.

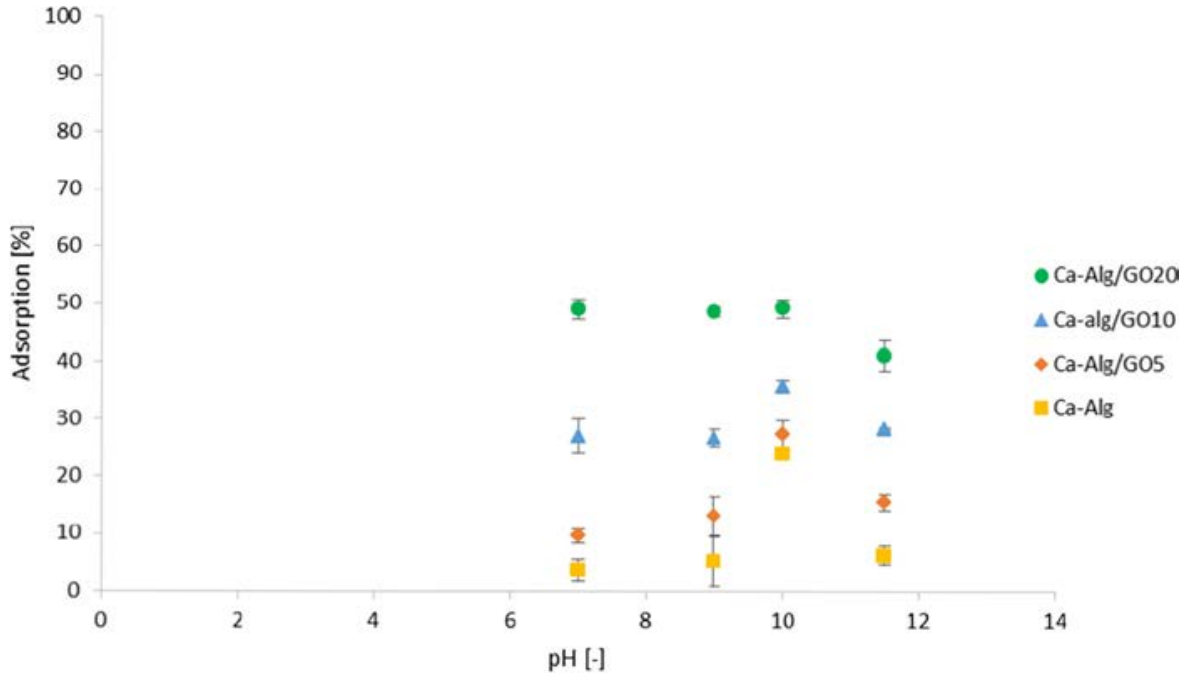

Figure 3.23. Effect of temperature on famotidine adsorption.

Table 3.5. Langmuir isotherm parameters for famotidine adsorption

Langmuir	Ca	GO5	GO10	GO20
q_{max} (mg/g)	28.96	31.69	33.57	35.50
K_L	123.25	85.39	57.02	23.10

Table 3.6. Pseudo-second order kinetic parameters for famotidine adsorption

	Ca	GO5	GO10	GO20	Units
R^2	0.99404	0.98806	0.99687	0.99598	–
q_{eq}	2.927	4.148	6.064	8.496	mg/g
k_2	4.577E–03	2.889E–03	2.446E–03	1.359E–03	g/min per mg

3.3.2 Performance of immobilised composites

Free particles and free-standing films of GO, rGO and Cu-rGO were examined for the adsorption of famotidine, MB and diclofenac. In addition, the adsorptive potential of Cu-rGO-impregnated glass fibre membranes was also investigated.

Diclofenac was shown to preferentially adsorb to graphene-containing materials at pH <3 as per section 3.3.1.2; however, this pH is unrealistic for application in water treatment. Therefore, investigations were performed at pH 7. There was no significant removal of diclofenac by any of the materials tested, as expected. For the adsorption of *famotidine*, the rGO performed best when free particles were used and achieved ~5% higher removal across the concentration range than GO. The Cu-rGO showed a lower adsorptive potential than the other two materials, which can be attributed to the proportion of Cu present, and this offers no advantage in terms of removal (Figure 3.25).

Most notable in the adsorption by the three materials in film format is the significant decrease in capacity. Compared with the free particles that had capacity in the 200–300 mg/g range, the films had significantly reduced adsorption with GO showing the highest at 113 mg/g at the highest initial concentration of 3.2 mg/mL. Another interesting observation is that the GO had a much higher performance than the other two materials (Figure 3.26). This is most likely due to the instability of the GO film and its tendency towards

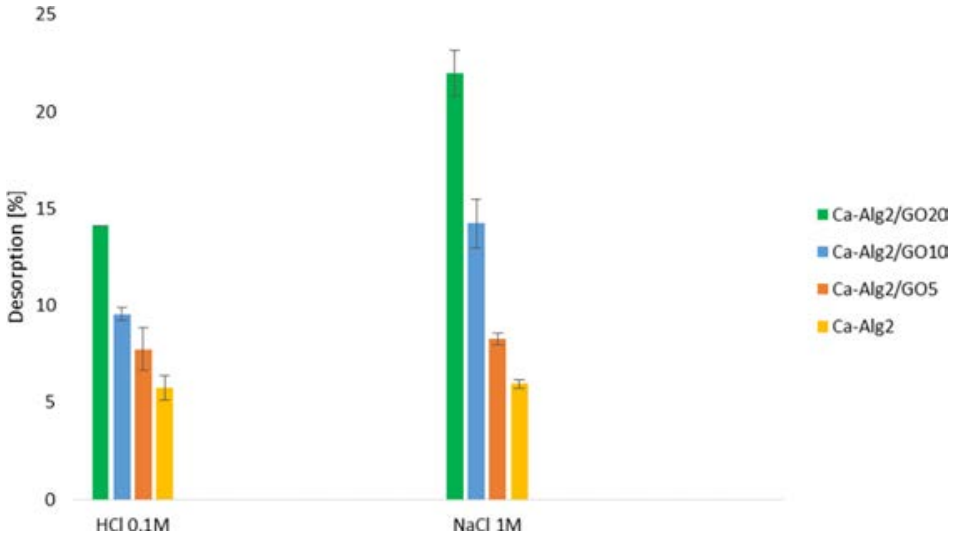

Figure 3.24. Desorption of famotidine.

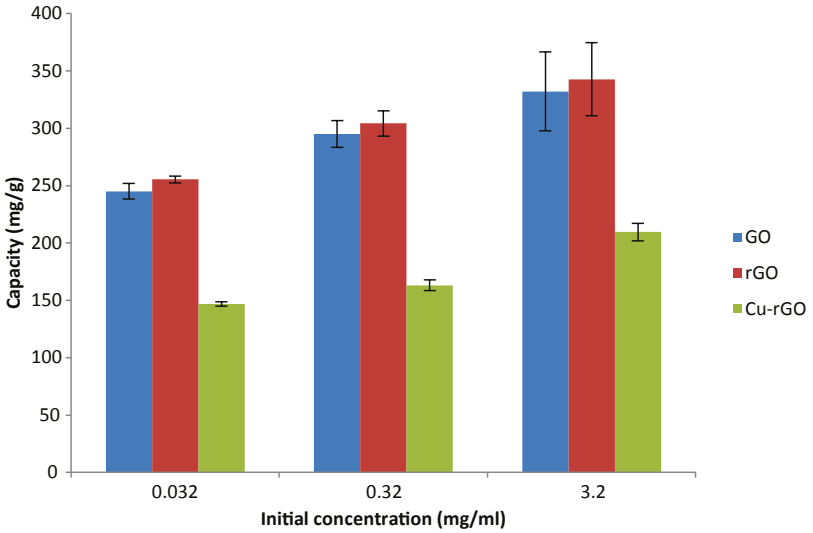

Figure 3.25. Adsorption of famotidine by free particles of GO, rGO and Cu-rGO at various concentrations.

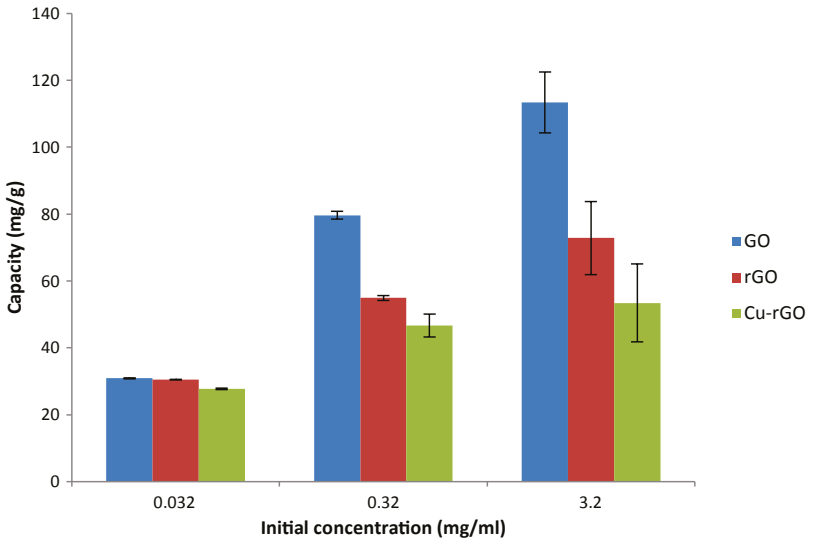

Figure 3.26. Famotidine adsorption by films of GO, rGO and Cu-rGO at various concentrations.

expansion in water. This is due to the presence of the high number of oxidative groups on the surface of the GO compared with the rGO and the composite. The GO film was seen to "puff up" when put into solution. This most likely resulted in a higher overall surface area and therefore an increase in adsorption capacity. This, however, significantly compromises the structural stability of the GO, making it unsuitable, as the film will fray and particles will enter the solution, which, in a water treatment scenario, would require removal at a later stage. The impregnated membranes, having a diameter of 40 mm compared with the 15 mm of the films, had a much higher adsorption capacity. Alhough this was lower than that of the free particles, on account of the attachment of the particles to the surface, the removal of famotidine was still significant, at 183.62 mg/g at a concentration of 3.2 mg/mL, compared with that of the films (Figure 3.27).

Compared with the adsorption of famotidine, the potential for *MB* removal is far greater. The free particles of GO, rGO and Cu-rGO showed loading capacities of 739, 661 and 605 mg/g, respectively, at the highest concentration studied: 0.48mg/mL. The GO showed the highest adsorptive potential of the three in this format (Figure 3.28). Alhough the Cu-rGO showed the lowest adsorption, again most likely due to the presence of the Cu, the relative ratio compared with the loss of adsorptive capacity was lower than that seen with the famotidine, with almost total removal at the lowest concentration and >80% removal at

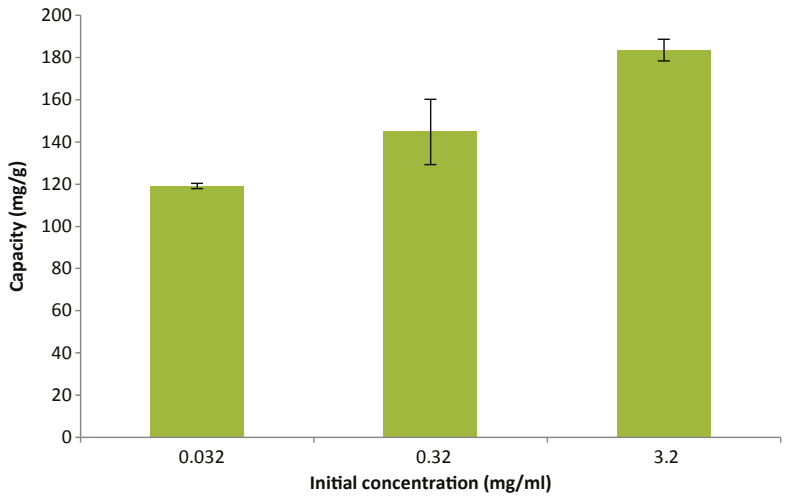

Figure 3.27. Famotidine adsorption by Cu-rGO-impregnated membranes (10 mg Cu-rGO per membrane).

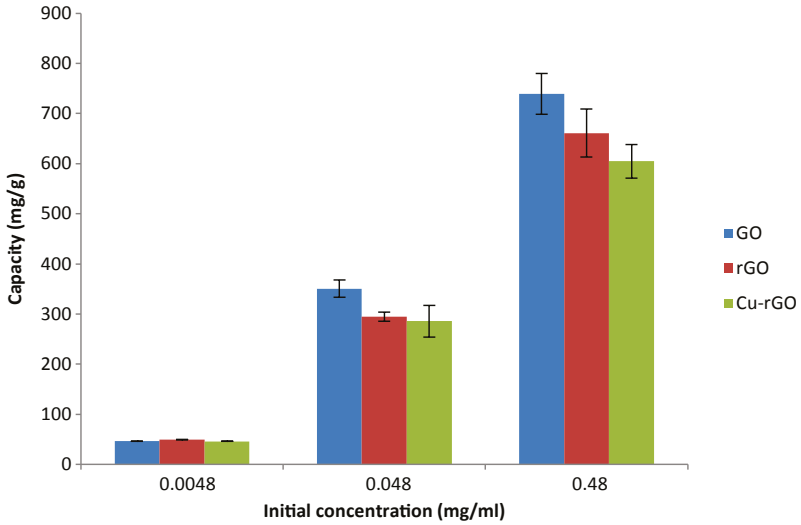

Figure 3.28. MB removal by free particles of GO, rGO and Cu-rGO.

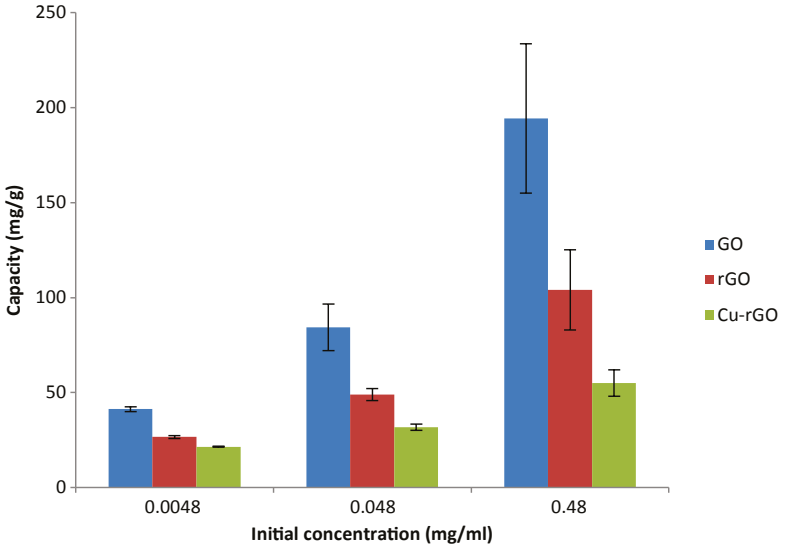

Figure 3.29. MB removal by 10 mg films of GO, rGO and Cu-rGO.

the intermediate concentration of 0.048 mg/mL. This may indicate that graphene materials have a higher tendency towards the removal of dyes such as MB.

The adsorption of MB by the various films showed a similar trend to that of the famotidine. The overall adsorption in all cases was reduced compared with the free particles, again due to the loss of relative surface area during the formation of the films. The GO once again showed the highest potential for removal at 194 mg/g at the highest concentration (Figure 3.29). This is, again, likely to be the result of the water solubility and the expansion of the GO in solution resulting in structural instability and an increase in available surface area.

Finally, the MB removal by the Cu-rGO-impregnated membranes showed a marked increase compared with the films, which at the highest concentration of MB showed a loading capacity of 482 mg/g (Figure 3.29). This is significantly higher than 55 mg/g as shown by the Cu-rGO film at the same concentration (Figure 3.30). This highlights the importance of the format in which the material is used. While the composite films may be robust and usable, there is a resultant loss of adsorptive potential due to the loss in surface area. The impregnated membranes offer a higher adsorptive potential than the films while placing the Cu-rGO onto a robust substrate. The larger diameter and relative porosity of the membrane allows for more contact of the Cu-rGO present with the solution and a higher overall adsorptive capacity.

While the adsorption capacity for MB exhibited by the Cu-rGO membranes is not as good as the adsorption capacity of the GO-Alg beads, the famotidine adsorption capacity is improved. In addition, the antibacterial efficacy of the impregnated Cu-rGO is key to the system functioning as intended. It is clear that a combined approach to the integration of these technologies (adsorption, antimicrobial and filtration) has the potential to offer a neat solution to providing clean drinking water.

3.3.3 Membrane separations

As was previously reported, GO colloids could be effectively removed from water by microfiltration, and pH did not have a notable influence on GO removal from the aquatic environment. Furthermore, GO is an effective absorbent and could aid in removal of

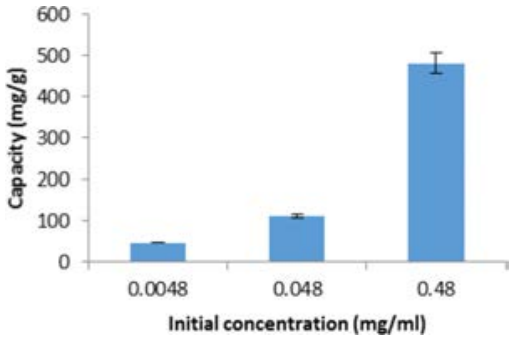

Figure 3.30. MB adsorption by Cu-rGO-impregnated membranes at various concentrations.

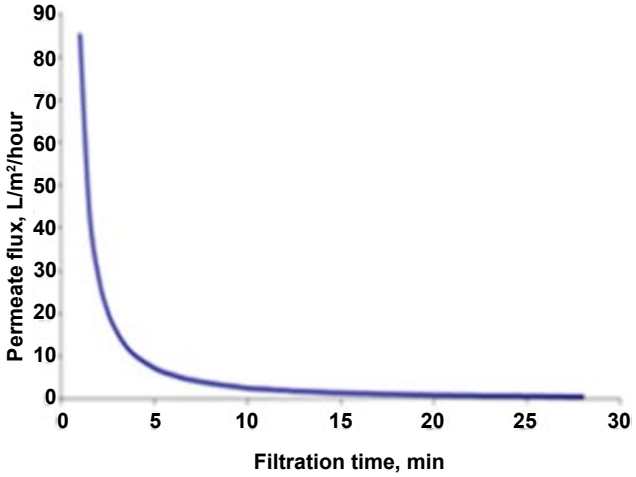

Figure 3.31. Permeate flux decline during GO microfiltration.

some pharmaceuticals via π–π interaction, cation–π bonding or the aggregation effect (Ghadim *et al*., 2013), and we have demonstrated the effectiveness of removal of diclofenac with GO from water solutions by microfiltration through a ceramic membrane. However, during filtration of GO for GO–diclofenac mixtures, severe flux decline was observed within 10 min (Figure 3.31), leading to a loss of productivity of purified water.

The use of NF membranes for the removal of pharmaceuticals shows great promise and is discussed in detail in the introduction to this report. Typically, porous membranes such as UF membranes are used as the support layer for NF membranes and enhancement in flux of this layer is heavily implicated in governing water transport through NF membranes. In addition, given the adsorptive nature of the GO-Cu composite rig developed, pre-treatment is likely to be advantageous. Therefore, the development of filtration strategies focused on UF-type membranes.

Low-fouling, novel positively charged hybrid UF membranes with adjustable charge density were fabricated from blends of PSf and QPSf in combination with varied fractions of GO nanosheets by a NIPS method (Kumar *et al.*, 2015). FTIR spectroscopy in the attenuated total reflection mode, SEM, outer surface zeta potential and contact angle studies were conducted to characterise the morphologies of hybrid membranes, namely their structures, charge and surface properties. Results confirmed the fabrication of porous, hydrophilic and positively charged membranes. The water permeabilities (flux) and antifouling ability of membranes with protein solutions were dependent on the fraction of quaternary ammonium groups and GO nanosheets in the membrane matrix.

The flux was found to be quite dependent on the substructure, where straight and slightly large finger-like macrovoids were observed when 1 to 2 wt% GO nanosheets to total weight of polymer blend (PSf/QPSf) was added (AG-1 and AG-2). On the other hand, the finger-like macrovoids in the membrane AG-5 were suppressed with further increases in the fraction of GO nanosheets to 5 wt% (Figure 3.32).

The antifouling ability of the membranes was improved after the incorporation of GO nanosheets, on account of the substantial increase in negative surface charge and hydrophilicity induced. In addition, the irreversible protein fouling of membranes was substantially decreased with an increasing fraction of GO nanosheets (%), leading to enhancement in the FRR, where simple flushing with water restored the membrane flux easily (Figure 3.33).

The presence of various functional groups on the surface of GO means that inorganic metallic oxides can be anchored to the GO by sol–gel or other chemical reduction methods (Pant *et al.,* 2012) and then used in the manufacture of membranes to improve their performance in filtration applications. As mentioned previously, incorporation of TiO_2 can lead to a better dispersion of GO with the membrane matrix, leading to improved membrane properties. GO−TiO_2 nanocomposite was synthesised by *in situ* sol−gel reaction at pH 2 using a GO nanosheets suspension and a TTiP precursor (Kumar *et al.*, 2016). The synthesised GO−TiO_2 nanocomposite was explored as a filler to fabricate improved antifouling novel hybrid UF membranes for removal of HA from aqueous solutions. Membranes were fabricated from polymer blend solutions containing PSf and GO−TiO_2 with varied loading amounts (0–5 wt%, denoted MG-0 to MG-5) by the NIPS method. Contact angle, atomic force microscopy, SEM, FTIR spectroscopy and outer surface zeta potential studies were conducted in order to characterise the membranes in terms of roughness, structure, surface properties and charge. The porous hydrophilic hybrid membranes were shown to have an asymmetric structure with improved surface roughness (Figure 3.34).

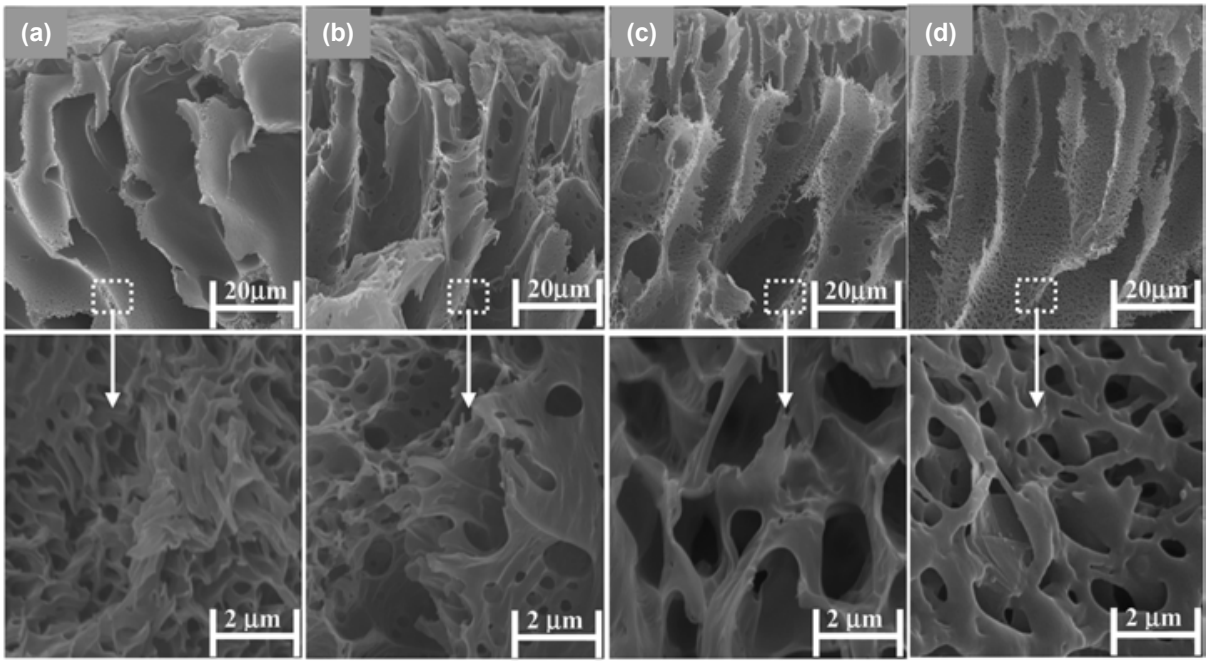

Figure 3.32. Cross-section SEM images at high and low resolution for positively charged hybrid membranes prepared with varied fractions of GO nanosheets; (a) AG-0, (b) AG-1, (c) AG-2 and (d) AG-5.

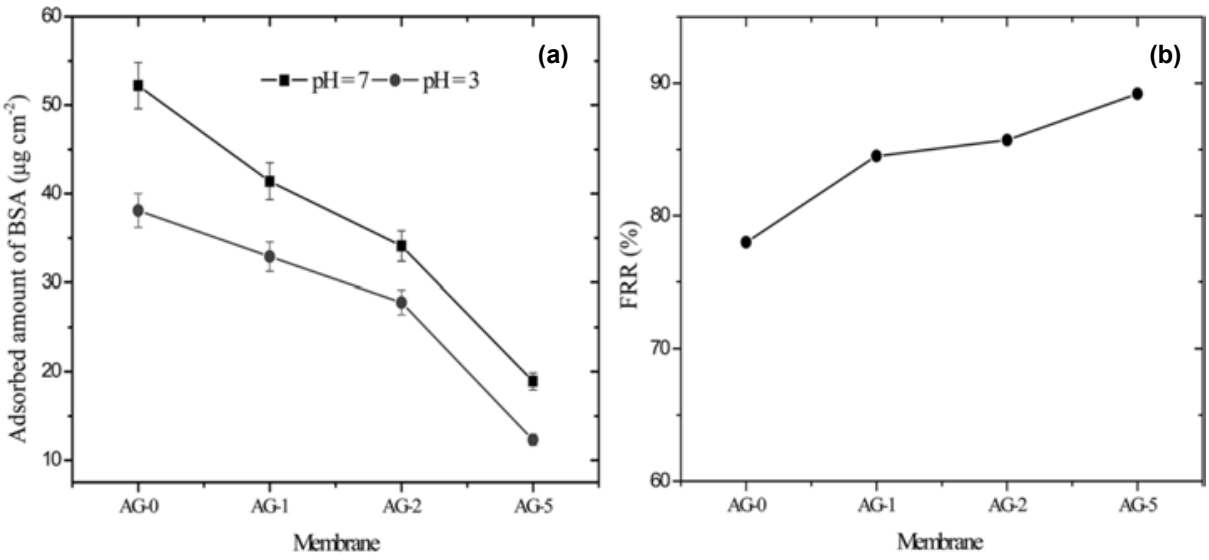

Figure 3.33. (a) Adsorbed amount of BSA on positively charged hybrid membranes at pH 3 and 7, and (b) FRR values for membranes after UF of 500 mL BSA (1 g/L) solution at pH 3.

The water permeability and antifouling capacity of hybrid membranes with 10 ppm HA solution were dependent on the loading amount of GO–TiO_2. The incorporation of the GO–TiO_2 nanocomposite was found to improve the antifouling characteristics of the membranes when challenged with HA solutions. Irreversible HA fouling was substantially reduced with increased loading of the GO−TiO_2 nanocomposite (wt%). The lowest irreversible fouling ratio (3.2%) was obtained for the membrane containing 5 wt% nanocomposite (MG-5; Figure 3.35).

Ultrafiltration of HA solutions of varied concentrations using hybrid membranes was studied at pH 7 and 1 bar feed pressure. The removal efficiency of hybrid membranes for HA was controlled by the membrane surface charge concentration, porosity and HA

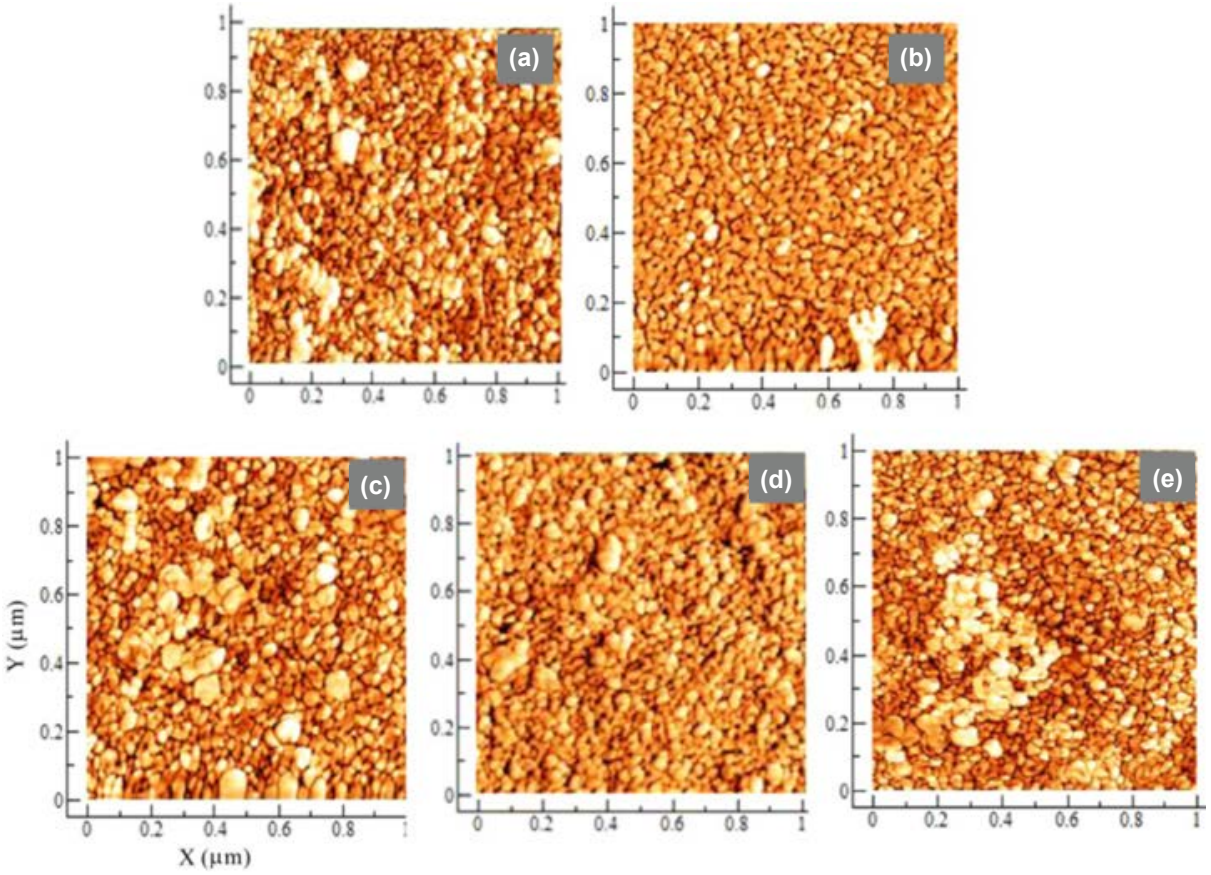

Figure 3.34. Two-dimensional atomic force microscopy images for hybrid membranes: (a) MG-0, (b) MG-1, (c) MG-2, (d) MG-3 and (e) MG-5.

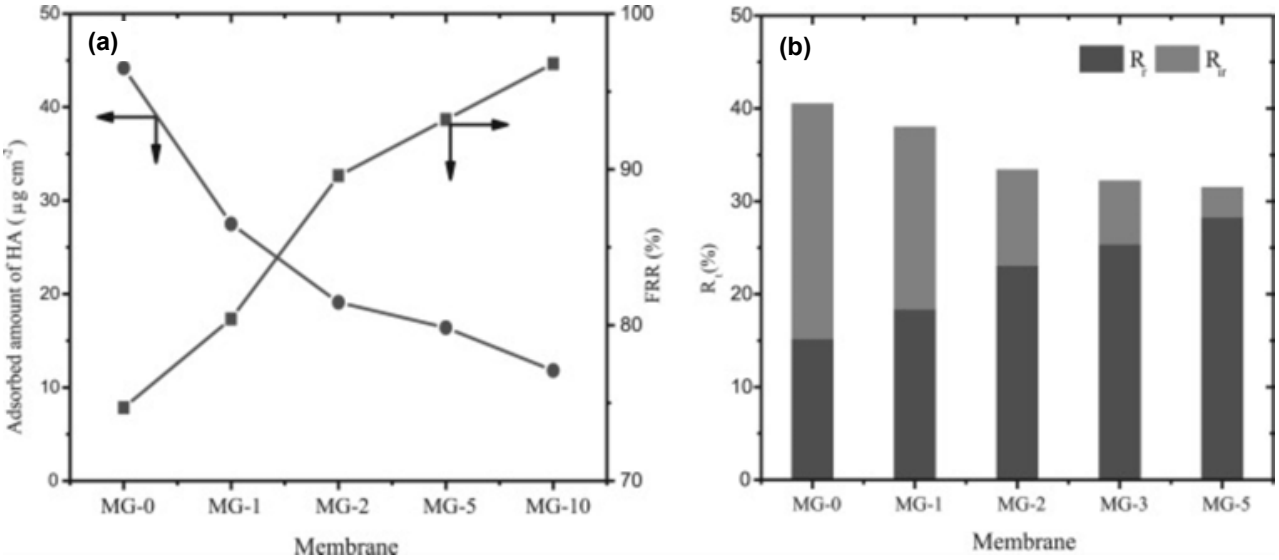

Figure 3.35. (a) Adsorbed amount of HA at pH 7 and FRR values of water permeability for hybrid membranes after 8 h UF of 10 ppm HA solution at pH 7 with subsequent cleaning with 0.05 M NaOH and (b) the summary of R_t, R_r and R_{ir}.

exclusion. The membrane MG-5 had the highest HA removal efficiency for 10 ppm HA solution at pH 7 (Figure 3.36).

The novel preparation method used in this work has led to a J_w that is significantly higher than that of GO–TiO_2 membranes previously described in the literature using a surface-coated-type membrane (60 L/m^2 per h) (Gao *et al.*, 2013). It also corresponds well with the reported data for similar types of commercial or modified polymer (PSf) UF membranes (Molina *et al.*, 2014).

The potential for fouling of the GO-Cu flow-through rig with pollutants such as NOM is reasonably high, with the possibility of flux reduction and fouling of adsorptive surfaces, leading to a loss in efficacy. Therefore, the impact of a UF pre-treatment step was investigated by challenging the system with a model water-containing HA as a NOM equivalent and MB as a model pollutant.

It was found that it was possible to remove around 50% of MB alone (from a starting concentration of 1 mg/L, with a crossflow rate of 5.5 L/min and an applied pressure of 2 bar); however, the presence of NOM significantly enhanced the removal, with 93–98% MB removal seen for concentrations ranging from 100 to 1000 µg/L, with >98% removal of 10 mg/L HA. Membrane fouling was not observed over a 1 h operation period, with fluxes maintained at 70–80 L/m^2 per h.

While it is expected that the combination of UF pre-treatment and GO-Cu rig will affect acceptable removal of PPCPs, commercially available NF membranes were assessed for removal of diclofenac, a non-steroidal anti-inflammatory drug used for pain relief, with a molecular weight of 296 Da. Batch NF of 12 L of model polluted water was performed, with a starting concentration of 5 ppm and crossflow velocity of 2 L/min. Excellent rejection of approximately 98% was observed over a 3 h operation period (Figure 3.37), at pressures ranging from 7.5 bar to 12.5 bar. It was observed that the optimum pressure for energy consumption while retaining diclofenac was the lower pressure of 7.5 bar, with reasonably good flux (clean water productivity) of approximately 11.5 L/m^2 per h, which did not decline significantly over the 3 h period of filtration. It should be noted, however, that for continued productivity of clean water using NF, water pre-treatment is essential, as the presence of foulant material, such as HAs, typically found in drinking water sources can impact strongly on the permeate flux. It is envisaged that the application of NF where required (for example in the event of a large-scale PPCP pollution event) would be possible in sequence after UF and GO-Cu treatment to polish the treated water and ensure acceptable levels of difficulty in removing PPCPs.

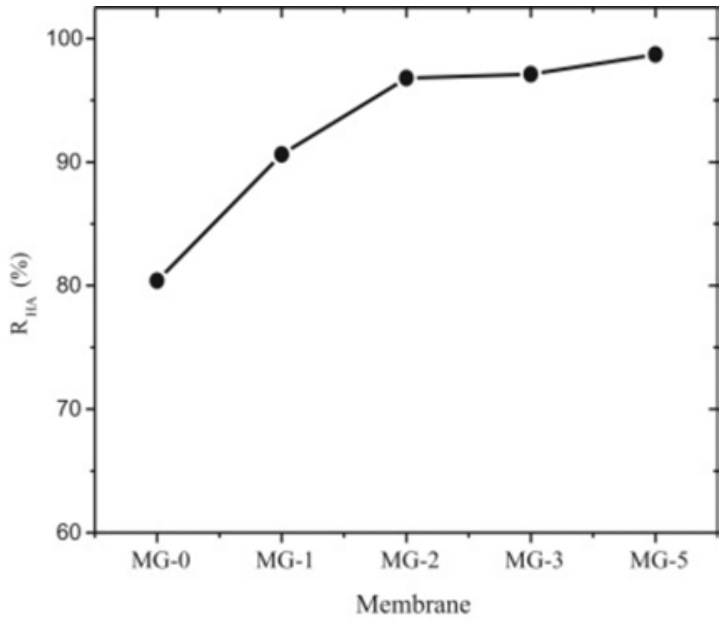

Figure 3.36. Rejection of HA (10 ppm) by hybrid membranes with varied amount of GO–TiO_2 nanocomposite (wt%) at pH 7, 1 bar feed pressure and 400 rpm.

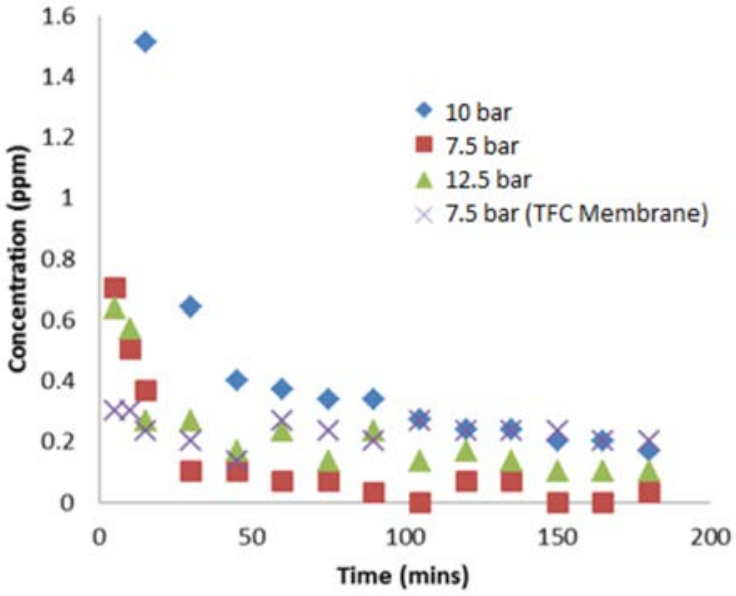

Figure 3.37. Nanofiltration of diclofenac.

3.4 Prototype Studies

3.4.1 Short-term test of prototype

In order to examine the antibacterial efficacy of the free-standing graphene-composite films, antibacterial evaluation was carried out via an agar slurry method for determining the antibacterial activity of incorporated agents. The films performed well against both *E. coli* and *B. subtilis* as examples of Gram-negative and Gram-positive organisms at a concentration of 10^5 cells/cm^2, with total loss of viability occurring at 40 min and >80% reduction in viability occurring at 30 min (Figure 3.38). There was no observable antibacterial effect from either GO or rGO. These composite films would then be incorporated into the unit prototype.

Initial tests were carried out using version 1 of the prototype (Figure 3.39), which incorporated four free-standing composite films and four chambers. The initial test showed a relatively low impact on the bacterial population with only 32% removed from 700 mL after 6 h of continuous flow, and 58% being removed after 24 h of exposure. This low level of inhibition, compared with the agar slurry evaluation, can be attributed to the lack of direct contact between the bacteria and the unit. Therefore, the incorporation of composite-impregnated membranes was carried out to investigate their effectiveness compared with the films. This incorporation of the impregnated membranes proved far more effective, removing >99% of the population within 6 h. This is most likely because of the larger surface area as well as the added filtration performance of the membranes. Control experiments incorporating non-impregnated membranes, however, showed a 64% reduction within 6 h and no bacteria present after 24 h showing that the membranes alone resulted in the majority of the removal. However, the incorporation of the graphene improved the performance compared with the membrane alone (Figure 3.40).

In order to increase the immediate effectiveness of the prototype, a new design was created (version 2), which incorporated up to nine composite-impregnated membranes (Figure 3.41). The rationale was that increasing the number of membranes would result in total removal of the bacteria from the start-up phase. This was to prove correct, as the prototype resulted in total removal with no bacteria present in the filtrate within 1 h. The control experiment, however, resulted in the same level of removal with no bacteria present after 1 h. The focus then moved towards the state of the bacteria following exposure to the incorporated and control membranes as well as the performance of the unit at higher volumes.

In order to examine the effect that exposure to the unit had on the state of the bacteria, a viability test was also carried out. Five litres of inoculated solution at 10^2 CFU/mL of *E. coli* were passed through the

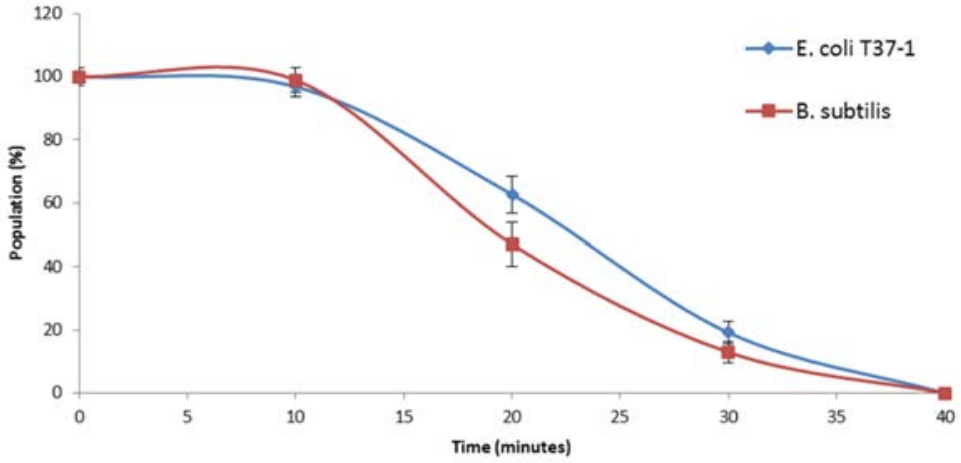

Figure 3.38. Antibacterial activity of the composite films as surfaces against *E. coli* (blue) and *B. subtilis* (red).

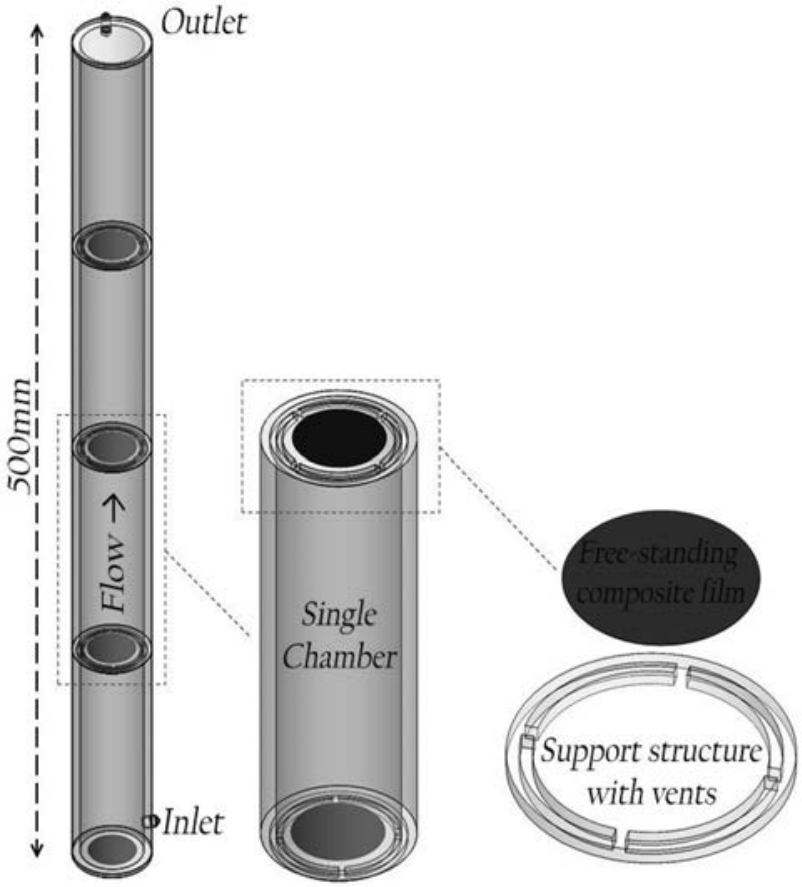

Figure 3.39. Version 1 of the prototype with four chambers and four support structures to incorporate the free-standing graphene films in a flow-through system.

units. There were a small number of organisms (~3–4) present following the initial start-up phase; however, there were no bacteria present following flow-through of both the impregnated and the control unit, indicating that the bacteria were being retained. In order to examine the viability of the organisms present on the surface, membranes were removed from each unit following testing, cut into halves and each half added to two separate broths: R2A or nutrient broth. The control unit showed growth in both the R2A broth and

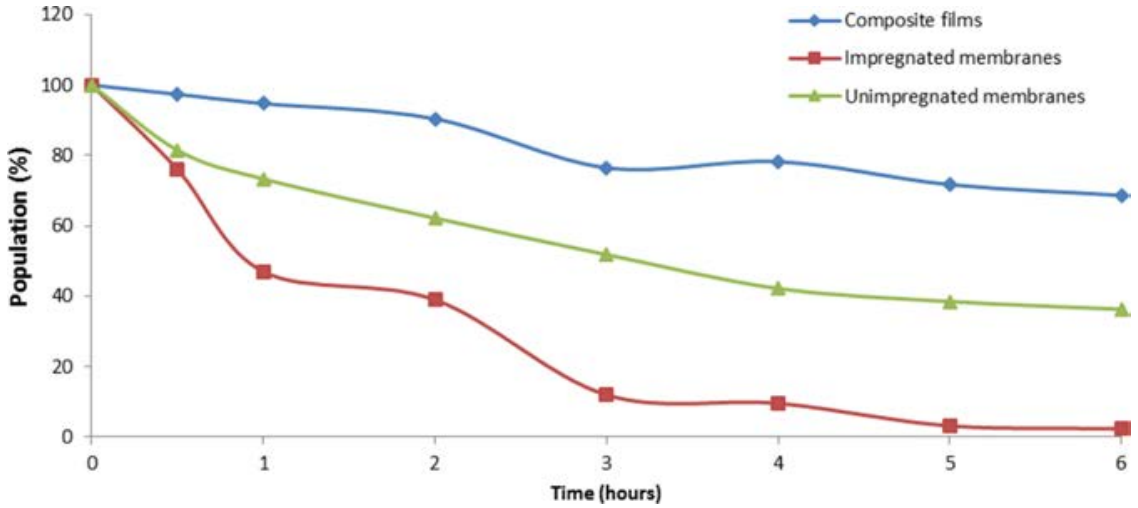

Figure 3.40. Bacterial removal by each of the initial prototype tests; the four composite films, unimpregnated glass fibre membranes and composite-impregnated glass fibre membranes.

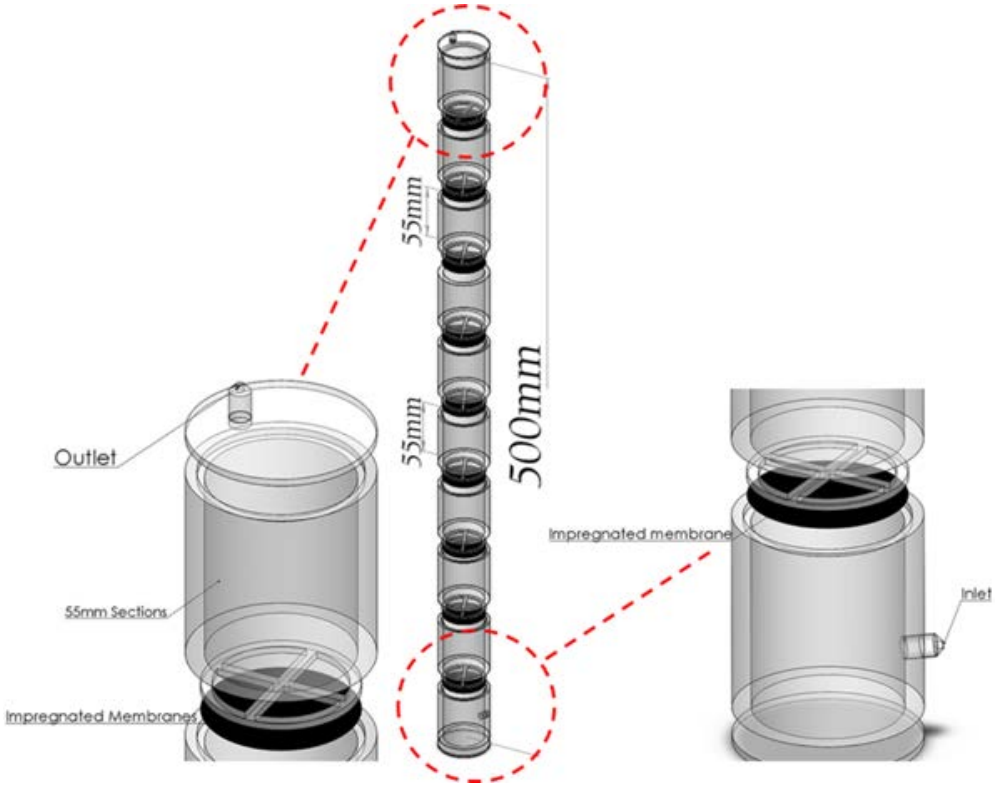

Figure 3.41. Version 2 of the prototype, which incorporated nine composite-impregnated membranes.

the nutrient broth for all of the membranes, indicating that while the bacteria are being retained within the prototype, they are still viable. The unit incorporating the composite-impregnated membranes, however, showed growth only within the nutrient and R2A broths for the first membrane. This suggests that contact with the impregnated membranes results in not only retention, but also loss of viability of the organism. The growth on the first membrane would suggest that the greater level of retention occurs at the earlier stages within the prototype and may result in saturation of the composite (Table 3.7).

To investigate the response of the prototype to cryptosporidium, the unit was challenged with 10 L of sterile saline (0.85%) containing 10 oocysts/L. The 10 L volume was then passed through the filtramax

Table 3.7. Viability of bacteria attached to both control membranes (with no composite) and the composite-impregnated membranes following unit testing; ✓ indicates growth and ✗ indicates no growth

Number of membranes	Control membranes		Composite membranes	
	R2A	NB	R2A	NB
1	✓	✓	✓	✓
2	✓	✓	✗	✗
3	✓	✓	✗	✗
4	✓	✓	✗	✗
5	✓	✓	✗	✗
6	✓	✓	✗	✗
7	✓	✓	✗	✗
8	✓	✓	✗	✗
9	✓	✓	✗	✗

NB, nutrient broth.

Table 3.8. The physical characteristics of each of the four water types including turbidity, pH and colour

	Karst spring	Treated river water	Granite water	Peaty water
Turbidity (AU)	0	0	0.002	0.006
pH	7.35	7.22	9.6	6.99
Colour	Clear	Clear	Pale yellow	Yellow

filtration unit and, following microscopic analysis by City Analysts Ltd, no oocysts were detected.

Finally, four different water types were used to examine if the source of water would impact the performance of the prototype unit. The four water types employed were: karst, treated river water, granite source and peaty water. Five litres of each water type were provided by TE Laboratories and each volume was pre-filtered using Whatman No 6 filter paper with a 3 µm particle retention size. Pre-filtering was performed using a vacuum filter to remove any large particles or detritus. pH and turbidity readings were also taken following pre-filtering for each water type. Turbidity was examined using UV-Vis spectroscopy at 660 nm. Samples were spiked with *E. coli* to a concentration of 10^2 CFU/mL and passed through a prototype unit containing nine GCC-coated glass fibre membranes at a flow rate of 22 mL/min. Total flow time was ~4 h in each case and samples were taken as 1 mL pour plates in triplicate every hour. Each of the water samples was shown to be free of large particles or detritus, with all samples having turbidity readings under 0.01 attenuation units (AU) (Table 3.8), with no obvious dirt visible by eye. pH readings showed that the karst, treated river and peaty water all had pH values close to 7 and that the granite water had a more basic pH of 9.6. During flow-through testing, no bacteria were found in the permeate for any of the four water samples indicating that all the organisms were retained within the unit. This would suggest that none of the water types used had any impact on the operation of the unit in terms of its bacterial retention compared with the saline solution used previously. However, if higher concentrations of *E. coli* had been employed, it is possible that this would have proven a greater challenge to the system and that bacteria could have been released and growth may have occurred. Following flow-through testing, the membranes were removed from the prototypes and added to wells of nutrient broth. These were then incubated and examined for the presence/absence of growth. There was no growth in any of the nutrient broth wells following the addition of the membranes, indicating that the organisms retained on the surface were inactivated by the composite coating. This finding is independent of the retention of the bacteria onto the membrane, as the coating was shown to act as a bactericide to higher concentrations of *E. coli* (Figure 3.38).

3.4.2 Long-term testing of prototype

The purpose of the long-term testing of the prototype was to test the robustness of the prototype over an extended period of time, e.g. weeks to months. The prototype was challenged at two flow rates, 22 mL/min and 90 mL/min, which was considered the maximum flow rate possible for the prototype as designed. However, in the course of testing the prototype, the first membrane failed at 13 h at the lower flow rate and within 10 h at the higher flow rate, with all nine membranes failing within 23 h and 15 h at the lower and higher flow rates, respectively. These tests show that failure of the prototype was due to the membranes bursting, rather than any failure due to poor retention of the pollutants (Figure 3.42). While the lower flow rate does improve the lifespan of the unit, the support structure employed requires a redesign to more evenly distribute the pressure across the membranes in order to avoid rupture. A modification to better facilitate the distribution of pressure across the membrane is to use a more porous or "holey" design, similar to a Büchner funnel (Figure 3.43).

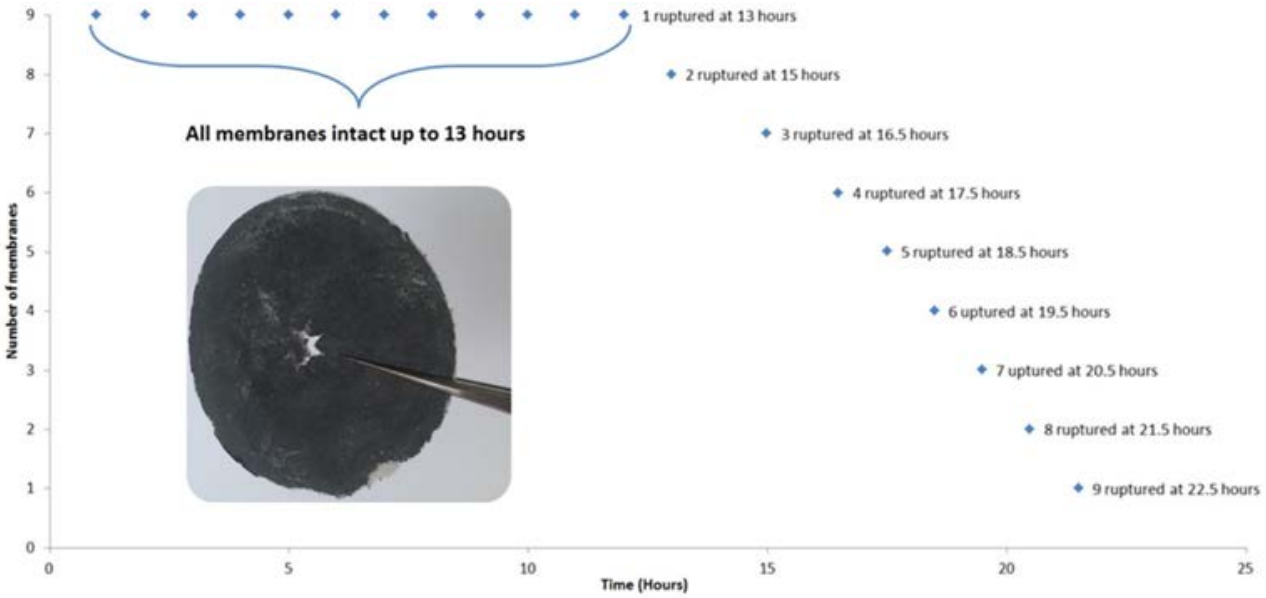

Figure 3.42. Graphical representation of membrane failure over time within the unit during long-term testing (flow rate 22 mL/min).

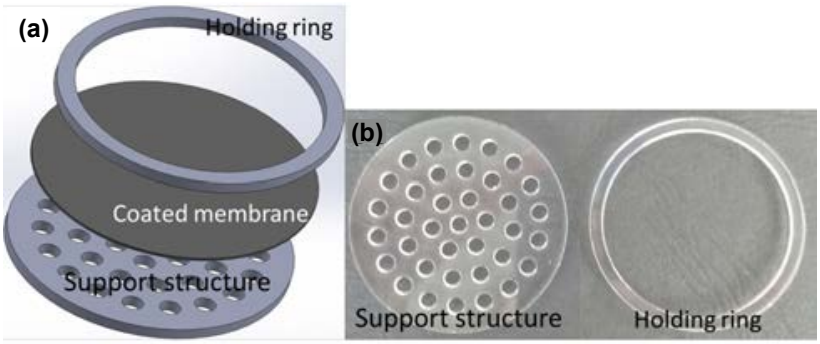

Figure 3.43. Proposed redesign of the support structure: (a) a "holey" support structure would be placed on top of the membrane and the membrane fixed in place with a holding ring to better facilitate a more even distribution of pressure across the membrane during flow-through testing; (b) the proposed design cut from PMMA.

3.4.3 Life cycle inventory and energy balance

The life cycle assessment (LCA) format adopted for the study adheres to the framework presented in the ISO 14040 series of standards (ISO, 2006; Lecouls, 1999) and references guidelines on the standards published by Guinée *et al*. (2001). The LCA software used is GaBi 6.0. The GaBi database provided by Thinkstep (formerly PE International) contains inventory data for upstream and downstream processes.

Goal and scope

The *goal* of this life cycle inventory (LCI) and energy balance was to assess the environmental impact associated with the production and use of the GCC water purification system. The *scope* of the study is shown in Table 3.9. The type of LCA is a stand-alone audit. A comparative assessment requires LCI or life cycle impact assessment (LCIA) data for competing systems, the data for which are not available.

The *boundaries* of the system extend from cradle to grave. All available life cycle inventory for material and energy production are included. The 2013 Irish electrical grid-mix is used in the study (43% natural gas, 27.1% hard coal, 14.8% heavy fuel oil, 8.3% peat, with the remainder a mix of biomass, wind and hydro).

In this study, the selection of the most appropriate *functional unit* was not straightforward. The volume of water treated would provide a good basis for comparative assessment, but it does not provide any information on the system's removal efficiency. However, the contaminant concentrations used in the study were magnitudes above the values that could be expected to be found in a water supply, and the reported removal efficiencies during testing were 100%. Furthermore, as noted in section 3.4.2 of this report, physical bursting of membranes occurred long before any decrease in pollutant removal capacity was observed. Strengthening the supporting membrane substrate may increase the volume of water that can be treated before failure occurs; however, the choice of substrate material may have a negative (or positive) influence on the LCIA. Therefore, because the use of the GCC is the novelty in this research, it has been decided that the most appropriate functional unit should relate the reported removal capacities to the production of the membranes. The reported maximum removal capacities are 0.482 g MB/g GCC and 0.184 g famotidine/g GCC, which equates to 1 mg MB/2.07 mg GCC and 1 mg famotidine/5.44 mg GCC. Hence, two functional units were used for the study: 1 mg MB removed and 1 mg of famotidine removed.

Table 3.9. LCA model scope

Item	Details
LCA type	Stand-alone audit
Audience	Scientific
Scale	Laboratory test
Time range of data	2012–2017

Inventory analysis

The material and energy inventory is presented in Table 3.10. Several substitutions have been made where LCI data were unavailable. $KMnO_4$ production impact assessment is limited to aggregated CO_2, SO_2 and NO_x emissions data provided by US EPA (2016). $CuCl_2$ and silicon oil production LCI were unavailable and have been accounted for with datasets that include Cu and silicon resource depletion accounting and the resources used during raw material acquisition. The equivalent global warming potential (GWP) associated with PMMA production is relatively high at 3.75 kg CO_2/kg PMMA resin. However, the quantity used in the construction of the unit is small. PMMA has a long lifetime and is assumed to be 100% recyclable. Assuming a unit lifetime of 10 years and an average flow rate of 10 L/day through the system, the quantity of PMMA required per functional unit is 13 mg. The quantity of nitrocellulose used in the production of PMMA is unknown, but is assumed to be small enough for its contribution to be negligible. The ascorbic acid production LCI was not available. The life cycle material and energy flow used in this study is shown in Figure 3.44.

Energy use is divided into three phases (Table 3.11). Phases 1 and 2 are the construction phase energy use. Phase 1 is the electricity used during the Hummers process and includes graphite expansion, stirring and centrifugation. Phase 2 is the energy used during the GCC preparation and includes sonication, stirring and oven drying. Phase 3 is the use-phase electricity consumption. The energy used during the construction phase is the dominant energy sink at

Table 3.10. System material and energy inputs

Parameter	Quantity per 40 mg GCC	Quantity per unit construction	Quantity per mg MB	Quantity per mg famotidine
Inputs				
Graphite (g)	2	4.5	0.104	0.273
$KMnO_4$ (g)	10	22.5	0.519	1.364
H_2SO_4 (mL)	250	562.5	12.967	34.078
H_2O_2 (mL)	150	337.5	7.780	20.446
DI water (L)	4.5	10.13	0.234	0.615
HCl (L)	1	2.25	0.052	0.137
$CuCl_2$ (mL)	150	337.5	7.780	20.446
Silicon oil (mL)	500	1125	25.934	68.155
Ascorbic acid (mL)	20	45	1.037	2.725
Nitrocellulose	unknown	unknown	unknown	unknown
PMMA (g)	N/A	500	0.013	0.034
Electricity (kWh)	51	114.75	2.654	6.975

114.75 kWh/unit construction or 2.645 kWh/mg MB removed. The energy consumed during the unit's use phase accounts for less than 1% of the total energy at 0.009 kWh/L treated water (Figure 3.45). The energy data presented here are laboratory scale system values. It is assumed that system scale-up, or mass production, would result in significant energy scale economies.

Life cycle impact assessment

The Institute for Environmental Science (CML; Leiden University) 10 November 2001 LCIA methodology was chosen for the study. The impact categories included in the methodology are presented in Table 3.12. A general observation in the LCIA was that the impact from energy use dominated all impact category profiles and in some cases accounted for over 90% of the total output. The GWP profile presented in Figure 3.46 typically reflects the general trend throughout all impact categories. As stated previously, it is assumed that energy economies of scale will reduce the energy input and improve the environmental profile. Notwithstanding the large impact from energy production, H_2SO_4 and H_2O_2 production account for the greatest percentage of impact in most categories.

The LCIA results for both functional units are presented with and without the energy input in Figure 3.47. The total impacts in each category are presented in Table 3.13. The LCIA profiles without energy are presented in Appendix 2. It was determined that presenting the LCIA profiles with energy is of no benefit because they generally appear as per Figure 3.46. Both sets of LCIA results were normalised with Western European normalisation factors (2001–2013). Western European normalisation factors are the aggregated quantity of a substance for the region of Western Europe. The presented normalised values are ratios of the system's substance output to the aggregated quantity of that substance (Jolliet *et al.*, 2003). For example, the aggregated GWP output for Western Europe between 2001 and 2013 was 4.89×10^{12} kg CO_2 equivalent. The GWP with the MB functional unit (including energy) is 1.54 kg CO_2 equivalent (Table 3.13). Therefore, the normalised value for GWP is 1.54 kg CO_2/4.89×10^{12} kg CO_2 = 3.14×10^{-13} kg CO_2.

Conclusions of LCIA and energy usage study and limitations

- The Hummers process used in the preparation of GO accounts for the greatest percentage of overall potential impact regardless of inclusion or omission of prototype production energy consumption values, and efforts to reduce environmental impact should focus on this stage of production. H_2O_2 and H_2SO_4 production in particular were found to account for the greater percentage of impact in most impact categories. The production of graphite and HCl accounted for smaller but not insignificant levels of potential

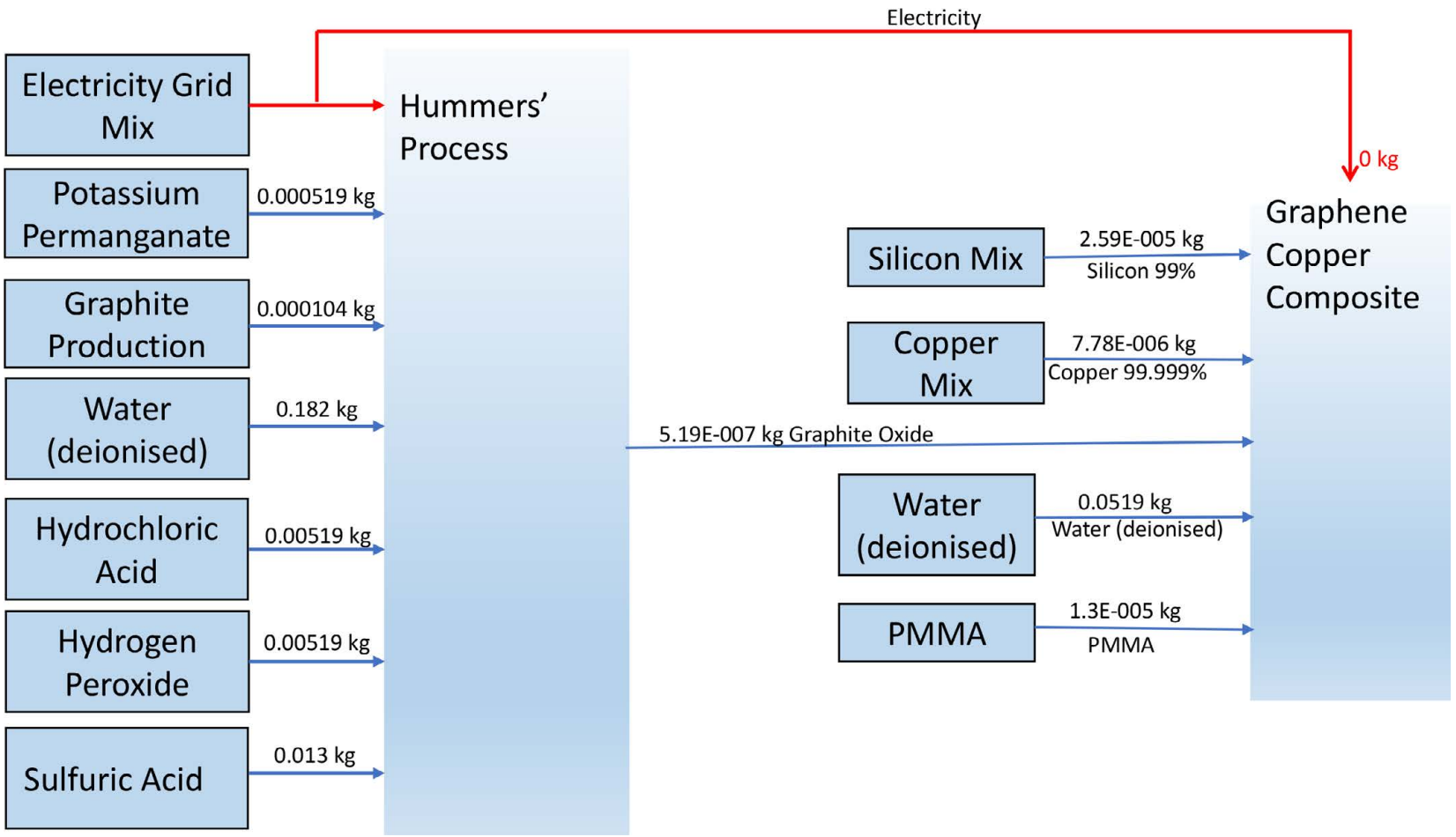

Figure 3.44. Life cycle material and energy flow schematic.

Table 3.11. Energy use arising from construction, preparation and use of prototype

Energy sink	Specific quantity (40 mg GCC)	kWh/40 mg GCC	kWh/unit construction	kWh/mg MB removed	kWh/mg famotidine removed
Phase 1 – graphite oxide production					
Graphite expansion	700W × 0.004167 h	0.029	0.066	0.002	0.00524
Stirring	620W × 24 h	14.880	33.480	0.772	2.02264
Centrifugation	5kW × 4 h	20.000	45.000	1.037	2.71694
Phase 2 – GCC preparation					
Sonication	340W × 1 h	0.340	0.765	0.018	0.04716
Stirring	620W × 24 h	14.880	33.480	0.772	2.02264
Drying oven	550W × 1 h	0.550	1.238	0.029	0.07598
Sonication	340 W × 1 h	0.340	0.765	0.018	0.04716
Phase 3 – use phase					
Pumping	(24 W × 0.38 h)/L			0.009	0.009
Total		51.000	114.750	2.657	6.96134

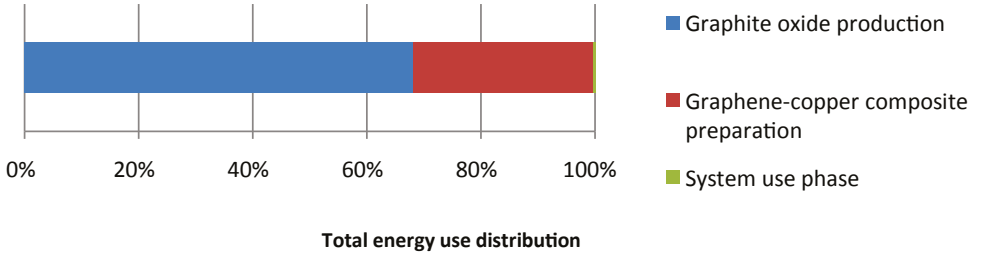

Figure 3.45. System energy use.

Table 3.12. CML 2001 LCIA categories

Impact category	Abbreviation	Units
Global warming potential	GWP	kg CO_2 equiv.
Acidification potential	AP	kg SO_2 equiv.
Eutrophication potential	EP	kg PO_4^{3-} equiv.
Ozone depletion potential	ODP, steady state	kg R11 equiv.[a]
Photochemical oxidation potential	PCOP	kg C_2H_6 equiv.
Ecotoxicity		kg $C_6H_4Cl_2$ equiv.
Freshwater aquatic	FAETP inf.	
Terrestrial	TETP inf.	
Marine aquatic	MAETP inf.	
Human toxicity potential	HTP inf.	kg $C_6H_4Cl_2$ equiv.
Abiotic depletion elements	ADPe	kg Sb equiv.
Abiotic depletion fossil	ADPf	MJ

[a]**The refrigerant R11 is a chlorofluorocarbon.**

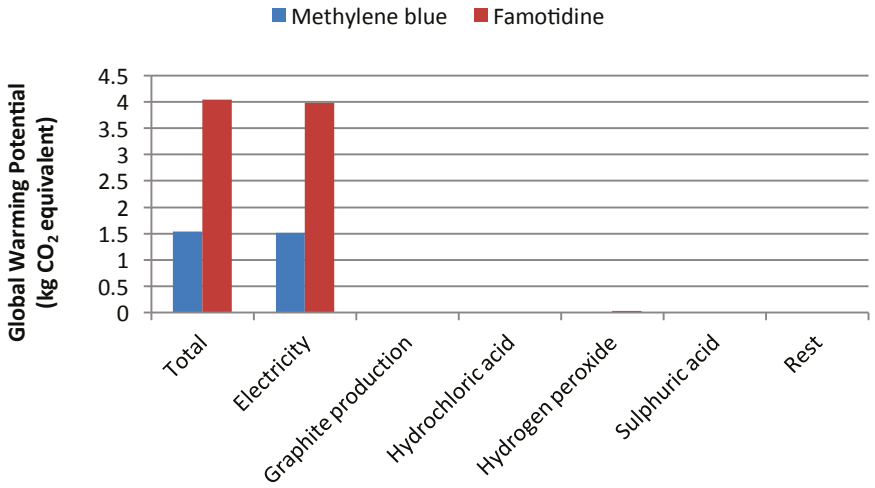

Figure 3.46. Global warming potential.

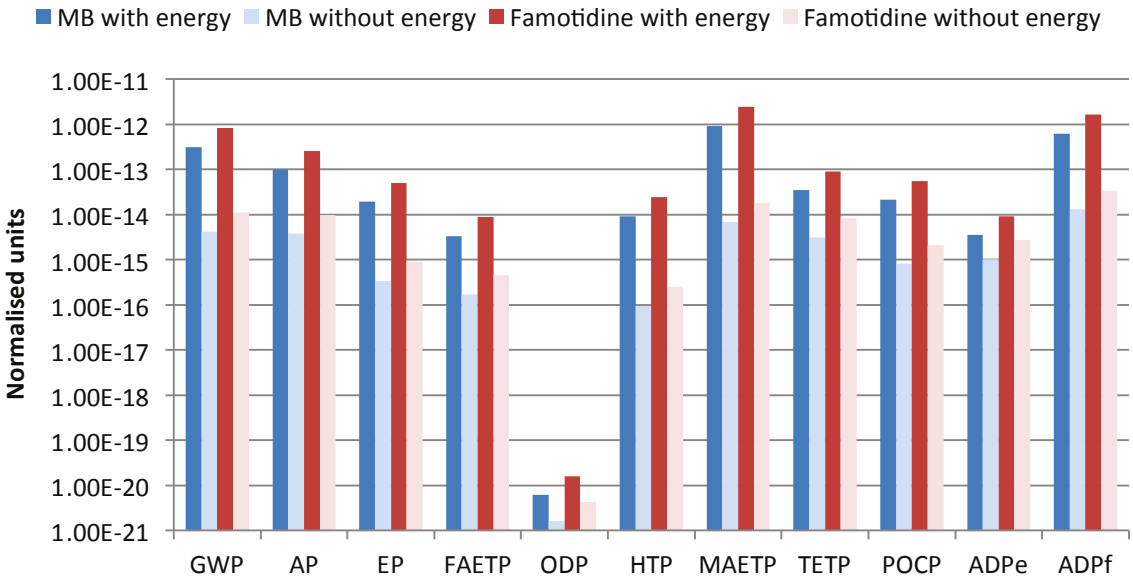

Figure 3.47. LCIA with and without energy input (categories as defined in Table 3.12).

Table 3.13. Impact category potentials with and without energy

Impact category[a]	Units	MB – potential including energy	Famotidine – potential including energy	MB – potential excluding energy	Famotidine – potential excluding energy
GWP	kg CO_2 equiv.	1.54	4.04	2.05×10^{-2}	5.4×10^{-2}
AP	kg SO_2 equiv.	2.69×10^{-3}	7.07×10^{-3}	1.02×10^{-4}	2.69×10^{-4}
EP	kg PO_4^{3-} equiv	2.46×10^{-4}	6.47×10^{-4}	4.34×10^{-6}	1.14×10^{-5}
FAETP	kg $C_6H_4Cl_2$ equiv.	1.68×10^{-3}	4.41×10^{-3}	8.64×10^{-5}	2.27×10^{-4}
ODP	kg R11 equiv.	5.33×10^{-13}	1.40×10^{-12}	1.43×10^{-13}	3.76×10^{-13}
HTP	kg $C_6H_4Cl_2$ equiv.	6.99×10^{-2}	1.84×10^{-1}	7.16×10^{-4}	1.88×10^{-3}
TETP	kg $C_6H_4Cl_2$ equiv.	1.62×10^{-3}	4.26×10^{-3}	1.48×10^{-4}	3.88×10^{-4}
MAETP	kg $C_6H_4Cl_2$ equiv.	103	271	7.78×10^{-1}	2.05
PCOP	kg C_2H_6 equiv.	1.74×10^{-4}	4.58×10^{-4}	6.66×10^{-6}	1.75×10^{-5}
ADPe	kg Sb equiv.	2.88×10^{-7}	7.57×10^{-7}	8.48×10^{-8}	2.23×10^{-7}
ADPf	MJ	19.2	50.5	3.97×10^{-1}	1.04

[a]**Categories as defined in Table 3.12.**

impact. The $KMnO_4$ production LCI was limited to inorganic emissions to air. It is reasonable to assume that inclusion of the full LCI of this substance will increase the potentials of other categories.

- The energy used in the production of the GCC membrane is the dominant system flow and accounts for the greatest percentage of the overall impact potential in all categories. It is reasonable to assume that the energy used in prototype development can be significantly reduced with the appropriate manufacturing process. Furthermore, it would be prudent to attain a more current electrical grid mix for Ireland, as investment in more renewable sources of energy are being introduced to the national grid. The impact from energy use is as much a function of the grid mix as the amount of energy being consumed.
- Input data substitutions made for $CuCl_2$ and silicone oil may not reflect the full impact of these flows. The aggregated data for Cu production accounts only for Cu ore acquisition and refinement. It is likely that additional processing stages for the production of $CuCl_2$ will increase the magnitude of impact in several impact categories. Similarly, the silicon input accounts only for ore mining, beneficiation and refinement, and further processing stages are required to produce silicon oil, which will require additional inputs of material and energy.
- The GCC system testing was carried out using single contaminant solutions of MB and famotidine. It is possible that water sources may contain pre-existing quantities of both contaminants and, in this case, further testing could be required to assess the system's removal capacities with solutions containing both contaminants together. However, it was demonstrated that the system could remove 100% of both contaminants separately at concentrations far above what would be expected from a water source. Therefore, it is conceivable that the membrane lifetime operating within an average range of concentrations for both contaminants may be limited by the strength of the membrane support structure and not by a decrease in contaminant removal capacity. A life cycle assessment based on a flow rate functional unit rather than substance mass removal may produce different results.
- Future work should include an assessment of the process to recycle the membrane materials. This will determine if there are any net gains that could improve the system's life cycle profile.

4 Conclusions

1. Both graphene and graphene composites were successfully produced and characterised for incorporation into a water treatment prototype (section 3.1). These materials were immobilised through a variety of methods, including membrane incorporation (section 3.3.3), as alginate bead composites (section 3.3.1) and as free-standing films and filter coatings (section 3.4).
2. An environmental *E. coli* strain was isolated for examination of the antibacterial properties of the graphene materials and used throughout the project (section 2.2.2). Neither graphene nor GO were found to possess antibacterial activity against *E. coli* or *B. subtilis* despite reports within the literature to the contrary (section 3.2). Therefore, the addition of Cu to form a composite was necessary to add antibacterial functionality. Antibacterial activity was examined in solid media (section 3.2.1), liquid growth media (section 3.2.3) and non-growth liquid media (section 3.2.2), and through surface evaluation (section 3.4.1). The Cu composite exhibited antibacterial activity comparable to that of stand-alone CuNPs in solid and non-growth liquid media, indicating a synergistic effect (sections 3.2.1 and 3.2.2). In growth media, however, this synergistic effect was absent, which was attributed to aggregation of the particles in suspension (section 3.2.3). Microscopic examination showed that membrane damage occurred in bacteria exposed to the composite and that this was the most likely mechanism of antibacterial action (section 3.2.4).
3. Therefore, the Cu composite was chosen for incorporation into a water treatment prototype. Free-standing composite films were incorporated into an initial prototype with little bacterial removal and composite-coated glass fibre membranes were chosen as a more ideal method of immobilisation. The final prototype incorporated nine GCC-coated membranes. A two-log reduction in *E. coli* was obtained within 30 min. Analysis following treatment showed the bacteria on the surface of the membranes were non-culturable in nutrient and minimal growth media indicating a loss of bacterial viability. The prototype was also found to remove cryptosporidium at a concentration of 10 oocysts/L (section 3.4.1). The composite-coated membranes were shown to remove MB and famotidine up to 99% at concentrations of 4.8 mg/L and 32 mg/L, respectively. Diclofenac removal was found to be negligible on account of the low pH requirement (pH <3) for removal to occur (section 3.3.2).
4. In addition, acid-activated alginate–GO adsorptive beads were fabricated, which exhibited strong potential for use in the removal of organic pollutants (section 3.3.1). The beads were challenged with MB, diclofenac and famotidine, and were found to show excellent performance for MB removal (with adsorption capacities of over 1300 mg/g – higher than any reported previously in the literature for other adsorbents). However, they were less successful for the removal of pharmaceuticals, with limited removal of diclofenac, except at pH <3, and performance no better than commercially available activated carbons. Positively and negatively charged UF membranes were fabricated using GO and GO–TiO_2 composites (section 3.3.3). The membranes were found to have enhanced antifouling properties, with concomitant improvement in the clean water flux, and were found to be effective in the removal of NOM. The overall system, which incorporates a preliminary UF step followed by the prototype, is effective in the adsorption of small organic molecules and the removal and inactivation of micro-organisms.
5. The first membrane was shown to fail at a flow rate of 22 mL/min after 13 h and at a flow rate of 90 mL/min within 10 h, with all nine membranes failing within 23 h and 15 h at the lower and higher flow rates, respectively. These tests show that failure of the prototype was due to membrane bursting, rather than any failure due to poor retention of the pollutants (Figure 3.42). While the lower flow rate does increase the lifespan of the unit, the support structure employed requires a redesign to more evenly distribute the pressure

across the membranes in order to avoid rupture. A modification to better facilitate the distribution of pressure across the membrane is to use a more porous or “holey” design, similar to a Büchner funnel (Figure 3.43).

6. Testing of the prototype with four different waters (karst, treated river water, granite source and peaty water) showed that none of the water types used had any impact on the operation of the unit in terms of its bacterial retention compared with the saline solution used as the synthetic water.
7. The LCI and energy balance study showed that the largest contributor to the overall environmental impact of the prototype, regardless of inclusion or omission of the prototype itself, was the Hummers process used to make the GCC.

5 Recommendations

1. Liquid-phase exfoliation for the production of graphene, which is employed here, makes use of concentrated acids, strong oxidisers and high temperatures, which contribute heavily to the overall environmental impact of the final product (section 2.2.1). Consideration should be given to the exploration of less energy-intensive and "greener" approaches to graphene production, which have an environmental end-point in mind. It is recommended that alternative methods of production be investigated, as the available literature on GCCs specifically is limited and offers the potential for development of numerous novel production methods.
2. Particular consideration should be given to evaluating the antibacterial efficacy of the composite against a suite of different micro-organisms. Despite the observed antibacterial activity against *E. coli* and *B. subtilis*, the material may perform differently when exposed to different micro-organisms (section 3.2). While cryptosporidium removal by the prototype was investigated, the viability of the oocysts following exposure was not examined (section 3.4.1). The state of the organisms would ideally be analysed as was done with the bacteria. Other organisms such as fungi, which may also be pathogenic, would ideally be investigated to establish a thorough understanding of the material's potential to inactivate many different pathogenic organisms.
3. As the composite can be easily dispersed in water, it is recommended that the use of other substrates be investigated for immobilisation (section 2.2.1). While glass fibre membranes were coated in this case, the potential for the use of cheaper, more porous or more durable substrates presents options for more numerous configurations than those presented within this project. The opportunity presented by a material that can be readily coated onto surfaces, such as the composite produced here, is that it would allow prototypes of very different designs from those explored here to be produced.
4. A high flux UF step is useful in removal of NOM prior to advanced treatment such as that outlined in this report (section 3.3.3). It is recommended that this be included prior to implementation of advanced treatment options as part of best available technology for integrated systems.
5. The inclusion of a UF pre-treatment step allows for the removal of some fractions of PPCP contamination via adsorption onto NOM, which is removed by UF. In addition, the UF pre-treatment protects subsequent adsorption-based steps from competitive adsorption from foulants. A UF pre-treatment is essential prior to NF or RO membrane filtration.
6. The targeted, complete removal of PPCPs such as pharmaceuticals can be achieved using the correct combination of UF, adsorption and NF membranes, with membrane choice tailored to pollutant characteristics (section 3.3.1). This could be advantageous in the event of a stand-alone pollution event and the technology outlined in this project can be upgraded easily to incorporate a post-NF step. It is recommended that, if regulatory limits for PPCPs are made more stringent, monitoring should be employed on water sources to capture stand-alone pollution events, triggering the temporary installation of an NF post-treatment step. It is not recommended that NF be included on a permanent basis, as the energy–economics balance of the technology would then not be favourable on account of the loss of clean water productivity associated with NF.
7. The redesigned prototype, similar to a Büchner funnel, where the pressure across the membranes is more evenly distributed to avoid rupture (Figure 3.43), should be tested.

References

Adams, C., Wang, Y., Loftin, K. and Meyer, M., 2002. Removal of antibiotics from surface and distilled water in conventional water treatment processes. *Journal of Environmental Engineering* 128: 253–260.

Akhavan, O. and Ghaderi, E., 2010. Toxicity of graphene and graphene oxide nanowalls against bacteria. *ACS Nano* 4: 5731–5736.

Akhavan, O., Ghaderi, E. and Esfandiar, A., 2011. Wrapping bacteria by graphene nanosheets for isolation from environment, reactivation by sonication, and inactivation by near-infrared irradiation. *The Journal of Physical Chemistry B* 115: 6279–6288.

Andrews, J.M., 2001. JAC Determination of minimum inhibitory concentrations. *Journal of Antimicrobial Chemotherapy* 48: 5–16.

ASTM Standard E2180–07, 2012. *Standard Test Method for Determining the Activity of Incorporated Antimicrobial Agent(s) In Polymeric or Hydrophobic Materials*. ASTM International, West Conshohocken, PA.

Azaïs, A., Mendret, J., Gassara, S., Petit, E., Deratani, A. and Brosillon, S., 2014. Nanofiltration for wastewater reuse: counteractive effects of fouling and matrice on the rejection of pharmaceutical active compounds. *Separation and Purification Technology* 133: 313–327.

Baker, R.W., 2004. *Membrane Technology and Applications*. 2nd edn. Wiley, West Sussex.

Bao, Q., Zhang, D. and Qi, P., 2011. Synthesis and characterization of silver nanoparticle and graphene oxide nanosheet composites as a bactericidal agent for water disinfection. *Journal of Colloid and Interface Science* 360: 463–470.

Barron, L., Purcell, M., Havel, J., Thomas, K., Tobin, J. and Paull, B., 2009. *Occurrence and Fate of Pharmaceuticals and Personal Care Products within Sewage Sludge and Sludge-Enriched Soils*. STRIVE Report 34. Environmental Protection Agency, Johnstown Castle, Ireland.

Bellona, C. and Drewes, J.E., 2005. The role of membrane surface charge and solute physico-chemical properties in the rejection of organic acids by NF membranes. *Journal of Membrane Science* 249: 227–234.

Bellona, C., Drewes, J.E., Xu, P. and Amy, G., 2004. Factors affecting the rejection of organic solutes during NF/RO treatment – a literature review. *Water Research* 38: 2795–2809.

Benitez, F.J., Aceor, J.L., Real, F.J., Roldan, G. and Rodrguez, E., 2011. Ultrafiltration and nanofiltration membranes applied to the removal of the pharmaceuticals amoxicillin, naproxen, metoprolol and phenacetin from water. *Journal of Chemical Technology & Biotechnology* 86: 858–866.

Berger, C., Song, Z., Li, X., Wu, X., Brown, N., Naud, C., Mayou, D., Li, T., Hass, J., Marchenkov, A., Conrad, E.H., First, P.N. and de Heer, W., 2006. Electronic confinement and coherence in patterned epitaxial graphene. *Science* 312 (5777): 1191–1196.

Braeken, L., Ramaekers, R. and Zhang, Y., 2005. Influence of hydrophobicity on retention in nanofiltration of aqueous solutions containing organic compounds. *Journal of Membrane Science* 252: 195–203.

Burba, P., Geltenpoth, H. and Nolte, J., 2005. Ultrafiltration behavior of selected pharmaceuticals on natural and synthetic membranes in the presence of humic-rich hydrocolloids. *Analytical and Bioanalytical Chemistry* 382: 1934–1941.

Chaabane, T., Zaidi, S., Darchen, A. and Maachi, R., 2013. Treatment of pharmaceutical effluent by electrocoagulation coupled to nanofiltration. *Desalination and Water Treatment* 51: 4987–4997.

Chang, E.E., Liang, C.H., Huang, C.P. and Chiang, P.C., 2012. A simplified method for elucidating the effect of size exclusion on nanofiltration membranes. *Separation and Purification Technology* 85: 1–7.

Chen, Q., Zhang, L. and Chen, G., 2011. Facile preparation of graphene–copper nanoparticle composite by *in situ* chemical reduction for electrochemical sensing of carbohydrates. *Analytical Chemistry* 84: 171–178.

Cheng, L.C., Jiang, X., Wang, J., Chen, C. and Liu, R.S., 2013. Nano-bio effects: interaction of nanomaterials with cells. *Nanoscale* 5: 3547–3569.

Cheryan, M., 1998. *Ultrafiltration and Microfiltration Handbook*. 2nd edn. CRC Press, Boca Raton, FL.

Chua, C.K. and Pumera, M., 2013. Reduction of graphene oxide with substituted borohydrides. *Journal of Materials Chemistry A* 1: 1892–1898.

Contreras, A.E., Kim, A. and Li, Q., 2009. Combined fouling of nanofiltration membranes: mechanisms and effect of organic matter. *Journal of Membrane Science* 327: 87–95.

Darvishmanesh, S., Buekenhoudt, A., Degreve, J. and Van der Burggen, B., 2009. Coupled series–parallel resistance model for transport of solvent through inorganic nanofiltration membranes. *Separation and Purification Technology* 70: 46–52.

Das, M.R., Sarma, R.K., Borah, S.C., Kumari, R., Saikia, R., Deshmukh, A.B. and Boukherroub, R., 2013. The synthesis of citrate-modified silver nanoparticles in an aqueous suspension of graphene oxide nanosheets and their antibacterial activity. *Colloids and Surfaces B Biointerfaces* 105: 128–136.

Derakhsheshpoor, R., Homayoonfal, M., Akbari, A. and Mehrnia, M., 2013. Amoxicillin separation from pharmaceutical wastewater by high permeability polysulfone nanofiltration membrane. *Journal of Environmental Health Science and Engineering* 11: 9.

Doris, Y., Ni Eidhin, C., Roche, M., Page, D., Devaney, D. and Loughnane, A., 2015. *Drinking Water Report 2014*. Environmental Protection Agency, Johnstown Castle, Ireland.

El Qada, E.N., Allen, S.J. and Walker, G.M., 2006. Adsorption of methylene blue onto activated carbon produced from steam activated bituminous coal: a study of equilibrium adsorption isotherm. *Chemical Engineering Journal* 124: 103–110.

Esmaeili, A. and Entezari, M.H., 2015. Cubic Ag/AgBr–graphene oxide nanocomposite: sono-synthesis and use as a solar photocatalyst for the degradation of DCF as a pharmaceutical pollutant. *RSC Advances* 5: 97027–97035.

Evgenidou, E.N., Konstantinou, I.K. and Lambropoulou, D.A., 2015. Occurrence and removal of transformation products of PPCPs and illicit drugs in wastewaters: a review. *Science of the Total Environment* 505: 905–926.

Feng, G., Chu, H. and Dong, B., 2014. Characterizing dissolved organic matter fouling of nanofiltration membranes and evaluating effects of naproxen retention. *Desalination and Water Treatment* 56(11): 1–13.

Feng, B., Xu, K. and Huang, A., 2016. Covalent synthesis of three-dimensional graphene oxide framework (GOF) membrane for seawater desalination. *Desalination* 394: 123–130.

Foley, G., 2013. *Membrane Filtration: a Problem Solving Approach with MATLAB®*. 1st edn. Cambridge University Press, Cambridge.

Ganesh, B.M., Isloor, A.M. and Ismail, A.F., 2013. Enhanced hydrophilicity and salt rejection study of graphene oxide-polysulfone mixed matrix membrane. *Desalination* 313: 199–207.

Ganiyu, S.O., van Hullebusch, E.D., Cretin, M., Esposito, G. and Oturan, M.A., 2015. Coupling of membrane filtration and advanced oxidation processes for removal of pharmaceutical residues: a critical review. *Separation and Purification Technology* 156: 891–914.

Gao, P., Liu, Z., Tai, M., Sun, D.D. and Ng W., 2013. Multifunctional graphene oxide–TiO_2 microsphere hierarchical membrane for clean water production. *Applied Catalysis B: Environmental* 138–139: 17–25.

Garcia, F., Ciceron, D., Saboni, A. and Alexandrova S., 2006. Nitrate ions elimination from drinking water by nanofiltration: membrane choice. *Separation and Purification Technology* 52: 196–200.

Ghadim, E.E., Manouchehri, F., Soleimani, G., Hosseini, H., Kimiagar, S. and Nafisi. S., 2013. Equilibrium, kinetic and thermodynamic studies. *PLoS One* 8(11):e79254.

Gholamvand, Z., 2016. Development of Novel Integrated Photocatalytic Adsorbents (IPCAs) for Organics Removal from Water & Wastewater. PhD Thesis. Dublin City University, Dublin.

Giannakis, S., Polo López, M., Spuhler, D., Sánchez Pérezc, J., Fernández Ibáñez, P. and Pulgarina, C., 2016. Solar disinfection is an augmentable, in situ-generated photo-Fenton reaction – Part 2: a review of the applications for drinking water and wastewater disinfection. *Applied Catalysis B: Environmental* 198: 431–446

Gibs, J., Stackelberg, P.E., Furlong, E.T, Meyer, M., Zaugg, S.D. and Lippincott, R.L., 2007. Persistence of pharmaceuticals and other organic compounds in chlorinated drinking water as a function of time. *Science of the Total Environment* 373: 240–249.

Gómez, M.J., Herrera, S., Sole, D., Garcia-Calvo, E. and Fernandez-Alba, A.R., 2012. Spatio-temporal evaluation of organic contaminants and their transformation products along a river basin affected by urban, agricultural and industrial pollution. *Science of the Total Environment 4*20: 134–145.

Graphene Flagship, 2016. Graphene Flagship. Available online: www.graphene-flagship.eu (accessed 31 August 2016).

Guinée, J.B., Gorrée, M., Huppes, G., Klein, R., De Koning, A. et al., 2001. Impact assessment. In Guinee, J.B. (ed.), *Handbook on Life Cycle Assessment – Operational Guide to the ISO Standards Vol. 7*. Kluwer Academic Publishers, Netherlands, pp. 525–634.

Heo, J., Flora, J., Nam-Guk, H. and Yoon, Y., 2012. Removal of bisphenol A and 17β-estradiol in single walled carbon nanotubes–ultrafiltration (SWNTs–UF) membrane systems. *Separation and Purification Technology* 90: 39–52.

Her, N., Amy, G., Chung, J., Yoon, J. and Yoon, Y., 2008. Characterizing dissolved organic matter and evaluating associated nanofiltration membrane fouling. *Chemosphere* 70(3): 495–502.

Hu, M. and Mi, B., 2013. Enabling graphene oxide nanosheets as water separation membranes. *Environmental Science and Technology* 47: 3715–3723.

Hu, W., Peng, C., Luo, W., Lv, M., Li, X., Li, D., Huang, Q. and Fan, C., 2010. Graphene-based antibacterial paper. *ACS Nano* 4: 4317–4323.

Huang, H., Song, Z., Wei, N., Shi, L., Mao, Y., Ying, Y., Sun, L., Xu, Z. and Peng, X., 2013. Ultrafast viscous water flow through nanostrand-channelled graphene oxide membranes. *Nature Communications* 4: 2979.

Hui, L., Piao, J.G., Auletta, J., Hu, K., Zhu, Y., Meyer, T., Liu, H. and Yang, L., 2014. Availability of the basal planes of graphene oxide determines whether it is antibacterial. *ACS Applied Materials & Interfaces* 6: 13183–13190.

Hummers Jr, W.S. and Offeman, R.E., 1958. Preparation of graphitic oxide. *Journal of the American Chemical Society* 80(6): 1339.

ISO (International Organization for Standardization), 2006. ISO 14040: Environmental Management – Life Cycle Assessment – Principle and Framework. ISO. Available online: https://www.iso.org/standard/37456.html (accessed 1 October 2017).

Jia, G., Wang, H., Yan, L., Wang, X., Pei, R., Yan, T., Zhao, Y. and Guo, X., 2005. Cytotoxicity of carbon nanomaterials: single-wall nanotube, multi-wall nanotube, and fullerene. *Environmental Science & Technology* 39: 1378–1383.

Jiravova, J., Barton Tomankova, K., Harvanova, M., Malina, L., Malohlava, J., Luhova, L., Panacek, A., Manisova, B. and Kolarova, H., 2016. The effect of silver nanoparticles and silver ions on mammalian and plant cells in vitro. *Food and Chemical Toxicology* 96: 50–61.

Jolliet, O., Margni, M., Charles, R., Humbert, S., Payet, J., Rebitzer, G. and Rosenbaum, R., 2003. IMPACT 2002: a new life cycle impact assessment methodology. *The International Journal of Life Cycle Assessment* 8(6): 324.

Kang, S. and Mauter, M.S., 2009. Microbial cytotoxicity of carbon-based nanomaterials: implications for river water and wastewater effluent. *Environmental Science and Technology* 43: 2648–2653.

Kang, S., Herzberg, M., Rodrigues, D.F. and Elimelech, M., 2008. Antibacterial effects of carbon nanotubes: size does matter! *Langmuir* : *ACS Journal of Surfaces and Colloids* 24: 6409–6413.

Kemp, K.C., Seema, H., Saleh, M., Le, N.H., Mahesh, K., Chandra, V. and Kim, K.S., 2013. Environmental applications using graphene composites: water remediation and gas adsorption. *Nanoscale* 5: 3149–3171.

Kim, T.U., Drewes, J.E., Summers, R.S. and Amy, G., 2007. Solute transport model for trace organic neutral and charged compounds through nanofiltration and reverse osmosis membranes. *Water Research* 41: 3977–3988.

Kosutic, K., 2000. Porosity of some commercial reverse osmosis and nanofiltration polyamide thin-film composite membranes. *Journal of Membrane Science* 168: 101–108.

Kosutic, K., Furac, L., Sipos, L. and Kunst, B., 2005. Removal of arsenic and pesticides from drinking water by nanofiltration membranes. *Separation and Purification Technology* 42: 137–144.

Krishnamoorthy, K., Veerapandian, M., Zhang, L.H., Yun, K. and Kim, S.J., 2012. Antibacterial efficiency of graphene nanosheets against pathogenic bacteria via lipid peroxidation. *The Journal of Physical Chemistry C* 116: 17280–17287.

Kumar, K. and Sivanesan, S., 2006. Equilibrium data, isotherm parameters and process design for partial and complete isotherm of methylene blue onto activated carbon. *Journal of Hazardous Materials* 134: 237–244.

Kumar, M., McGlade, D., Ulbricht, M. and Lawler, J., 2015. Quaternized polysulfone and graphene oxide nanosheet derived low fouling novel positively charged hybrid ultrafiltration membranes for protein separation. *RSC Advances* 5: 51208–51219.

Kumar, M., Gholamvand, Z., Morrissey, A., Nolan, K., Ulbricht, M. and Lawler, J., 2016. Preparation and characterization of low fouling novel hybrid ultrafiltration membranes based on the blends of GO−TiO_2 nanocomposite and polysulfone for humic acid removal. *Journal of Membrane Science* 506: 38–49.

Lacey, C., McMahon, G., Bones, J., Barron, L., Morrissey, A. and Tobin, J.M., 2008. An LC-MS method for the determination of pharmaceutical compounds in wastewater treatment plant influent and effluent samples. *Talanta* 75: 1089–1097.

Lacey, C., Basha, S., Morrissey, A. and Tobin, J.M., 2012. Occurrence of pharmaceutical compounds in wastewater process streams in Dublin, Ireland. *Environmental Monitoring and Assessment* 184: 1049–1062.

Lecouls, H., 1999. ISO 14043: Environmental management – lifecycle assessment – life cycle interpretation. *International Journal of Life Cycle Assessment:* 245–254.

Liu, S., Zeng, T.H., Hofmann, M., Burcombe, E., We, J., Jiang, R., Kong, J. and Chen, Y., 2011. Antibacterial activity of graphite, graphite oxide, graphene oxide, and reduced graphene oxide: membrane and oxidative stress. *ACS Nano* 5: 6971–6980.

Liu, S., Hu, M., Zeng, T.H., Wu, R., Jiang, R., Wel, J., Wang, L., Kong, J. and Chen, Y., 2012a. Lateral dimension-dependent antibacterial activity of graphene oxide sheets. *Langmuir: the ACS Journal of Surfaces and Colloids* 28: 12364–12372.

Liu, T., Li, Y., Du, Q., Sun, J., Jiao, Y., Yang, G., Wang, Z., Xia, Y., Zhang, W., Wang, K., Zhu, H. and Wu, D., 2012b. Adsorption of methylene blue from aqueous solution by graphene. *Colloids and Surfaces B: Biointerfaces* 90: 197–203.

Luo, Y., Guo, W., Ngo, H.H., Nghiem, L.D. and Hai, F.I., 2014. A review on the occurrence of micropollutants in the aquatic environment and their fate and removal during wastewater treatment. *Science of the Total Environment* 473–474: 619–641.

Ma, J., Zhang, J., Xiong, Z., Yong, Y. and Zhao, X.S., 2011. Preparation, characterization and antibacterial properties of silver-modified graphene oxide. *Journal of Materials Chemistry* 21: 3350.

McEneff, G., Schmidt, W. and Quinn, B., 2015. *Pharmaceuticals in the Aquatic Environment: A Short Summary of Current Knowledge and the Potential Impacts on Aquatic Biota and Humans*. Environmental Protection Agency, Johnstown Castle, Ireland.

Maliyekkal, S.M., Sreeprasad, T.S., Krishnan, D., Kouser, S., Mishra, A.K., Waghmare, U.V. and Pradeep, T., 2013. Graphene: a reusable substrate for unprecedented adsorption of pesticides. *Small* 9: 273–283.

Mangadlao, J.D., Santos, C.M., Felipe, M.J.L., de Leon, A.C.C., Rodrigues, D.F. and Advincula, R.C., 2015. On the antibacterial mechanism of graphene oxide (GO) Langmuir–Blodgett films. *Chemical Communications* 51: 2886–2889.

Mi, B., 2014. Materials science. Graphene oxide membranes for ionic and molecular sieving. *Science* 343(6172): 740–742.

Molina, S., Carretero, P., Teli, S.B., Campa, J., Lozano, Á.E. and Abajo, J., 2014. Hydrophilic porous asymmetric ultrafiltration membranes of aramid-g-PEO copolymers. *Journal of Membrane Science* 454: 233–242.

Narbaitz, R.M., Rana, D., Dang, H. and Yang, P., 2013. Pharmaceutical and personal care products removal from drinking water by modified cellulose acetate membrane: field testing. *Chemical Engineering Journal* 225: 848–856.

Nazarpour, S. and Waite, S.R., 2016. *Graphene Technology: From Laboratory to Fabrication*. 1st edn. Wiley-VCH, Weinheim, Germany.

Nghiem, L.D. and Hawkes, S., 2007. Effects of membrane fouling on the nanofiltration of pharmaceutically active compounds (PhACs): mechanisms and role of membrane pore size. *Separation and Purification Technology* 57: 176–184.

Nghiem, L.D., Schäfer, A.I. and Elimelech, M., 2005. Pharmaceutical retention mechanisms by nanofiltration membranes. *Environmental Science & Technology* 39: 7698–7705.

Nghiem, L.D., Coleman, P.J. and Espendiller, C., 2010. Mechanisms underlying the effects of membrane fouling on the nanofiltration of trace organic contaminants. *Desalination* 250(2): 682–687.

Nguyen, V.H., Kim, B.K., Jo, Y.L. and Shim, J.J., 2012. Preparation and antibacterial activity of silver nanoparticles-decorated graphene composites. *The Journal of Supercritical Fluids* 72: 28–35.

Nicolosi, V., Chhowalla, M., Kanatzidis, M.G., Strano, M.S. and Coleman, J.N., 2013. Liquid exfoliation of layered materials. *Science* 340(6139): 1226419.

Nicolopoulou-Stamati, P., Hens, L. and Sasco, A.J., 2015. Cosmetics as endocrine disruptors: are they a health risk? *Reviews in Endocrine and Metabolic Disorders* 16: 373–383.

Novoselov K. and Neto, A.C., 2012. Two-dimensional crystals-based heterostructures: materials with tailored properties. *Physica Scripta* T146: 014006.

Novoselov K.S., Geim A.K., Morozov S.V., Jiang D., Zhang Y., Dubonos S.V., Grigorieva I.V. and Firsov A.A., 2004. Electric field effect in atomically thin carbon films. *Science* 306: 666–669.

O'Dea, M. and Duffy, N. 2011. *Industrial Applications of Membrane Technology in Ireland: A Review*. Environmental Protection Agency, Johnstown Castle, Ireland.

Pant, H.R., Park, C.H., Tijing, L.D., Amarjargal, A., Lee, D.H. and Kim, C.S., 2012. Bimodal fiber diameter distributed graphene oxide/nylon-6 composite nanofibrous mats via electrospinning. *Colloids and Surfaces A: Physicochemical and Engineering Aspects* 407: 121–125.

Park, S. and Ruoff, R.S., 2009. Chemical methods for the production of graphenes. *Nature Nanotechnology* 4: 217–224.

Peter-Varbanets, M., Margot, J., Traber, J. and Pronk, W., 2011. Mechanisms of membrane fouling during ultra-low pressure ultrafiltration. *Journal of Membrane Science* 377: 42–53.

Plumlee, M.H., Stanford, B.D., Debroux, J.F., Hopkins, D.C. and Snyder, S.A., 2014. Costs of advanced treatment in water reclamation. *Ozone: Science & Engineering* 36: 485–495.

Praskova, E., Plhalova, L., Chromcova, L., Stepanova, S., Bedaova, I., Blahova, J., Hostovsky, M., Skoric, M., Marsalek, P., Voslarova, E. and Svobodova, Z., 2014. Effects of subchronic exposure of diclofenac on growth, histopathological changes, and oxidative stress in zebrafish (*Danio rerio*). *The Scientific World Journal* 2014: 645737.

Putri, L.K, Lling-Lling Tan, L.L., Ong, W.J., Chang, W.S. and Chai, S.P., 2016. Graphene oxide: exploiting its unique properties toward visible-light-driven photocatalysis. *Applied Materials Today* 4: 9–16.

Quinn, B., McEneff, G. and Schmidt, W., 2015. *Pharmaceuticals in the Irish Aquatic Environment: The Assessment and Potential Human Impact of Exposure to Pharmaceuticals on Marine and Freshwater Bivalves*. Environmental Protection Agency, Johnstown Castle, Ireland.

Radjenović, J., Petrovic, M., Ventura, F. and Barcelo, D., 2008. Rejection of pharmaceuticals in nanofiltration and reverse osmosis membrane drinking water treatment. *Water Research* 42: 3601–3610.

Rana, D., Scheier, B., Narbaitz, R.M., Matsuura, T., Tabe, S., Jasim, S.Y. and Khulbe, K., 2012. Comparison of cellulose acetate (CA) membrane and novel CA membranes containing surface modifying macromolecules to remove pharmaceutical and personal care product micropollutants from drinking water. *Journal of Membrane Science* 409–410: 346–354.

Ruiz, O.N., Fernando, K.A., Wang, B., Brown, N.A., Luo, P.G., McNamara, N.D., Vangsness, M., Sun, Y.P. and Bunker, C.E., 2011. Graphene oxide: a nonspecific enhancer of cellular growth. *ACS Nano* 5(10): 8100–8107.

Safarpour, M., Khataee, A. and Vatanpour, V., 2015. Thin film nanocomposite reverse osmosis membrane modified by reduced graphene oxide/TiO_2 with improved desalination performance. *Journal of Membrane Science* 489: 43–54.

Shannon, M.A., Bohn, P.W., Eelech, M., Georgiadis, J.G., Marinas, B.J. and Mayes, A.M., 2008. Science and technology for water purification in the coming decades. *Nature* 452(7185): 301–310.

Sharma, B.K. and Ahn, J.H., 2013. Graphene based field effect transistors: efforts made towards flexible electronics. *Solid-State Electronics* 89: 177–188.

Shen, J., Shi, M., Li, N., Yan, B., Ma, H., Hu, Y. and Ye, M., 2010. Facile synthesis and application of Ag-chemically converted graphene nanocomposite. *Nano Research* 3: 339–349.

Siegrist, H. and Joss, H., 2012. Review on the fate of organic micropollutants in wastewater treatment and water reuse with membranes. *Water Science & Technology* 66: 1369–1376.

Simon, A., Price, W.E. and Nghiem, L.D., 2013. Changes in surface properties and separation efficiency of a nanofiltration membrane after repeated fouling and chemical cleaning cycles. *Separation and Purification Technology* 113: 42–50.

Snyder, S.A., Westerhoff, P., Yoon, Y. and Sedlak, D.L., 2003. Pharmaceuticals, personal care products, and endocrine disruptors in water: implications for the water industry. *Environmental Engineering Science* 20: 449–469.

Song, B., Zhang, C., Zeng, G., Gong, J., Chang, Y. and Jiang, Y., 2016. Antibacterial properties and mechanism of graphene oxide-silver nanocomposites as bactericidal agents for water disinfection. *Archives of Biochemistry and Biophysics* 604: 167–176.

Speltini, A., Sturini, M., Maraschi, F. and Profumo, A., 2016. Recent trends in the application of the newest carbonaceous materials for magnetic solid-phase extraction of environmental pollutants. *Trends in Environmental Analytical Chemistry* 10: 11–23.

Steinle-Darling, E., Litwiller, E. and Reinhard, M., 2010. Effects of sorption on the rejection of trace organic contaminants during nanofiltration. *Environmental Science & Technology* 44: 2592–2598.

Sun, P., Zhu, M., Wang, K., Zhong, M., Wei, J., Wu, D., Xu, Z. and Zhu, H., 2013. Selective ion penetration of graphene oxide membranes. *ACS Nano* 7: 428–437.

Sweeney, M.F., Hasan, N., Soto, A.M. and Sonnenschein, C., 2015. Environmental endocrine disruptors: effects on the human male reproductive system. *Reviews in Endocrine and Metabolic Disorders* 16: 341–357.

Szép, A., Kertész, S., László, Z., Szabó, G. and Hodúr, C., 2012. Advanced treatment of pharmaceutical wastewater by nanofiltration and ozonation. *Acta Technicia Corviniensis – Bulletin of Engineering* 5: 25–27.

Tai, Z., Ma, H., Liu, B., Yan, X. and Xue, Q., 2012. Facile synthesis of Ag/GNS-g-PAA nanohybrids for antimicrobial applications. *Colloids and Surfaces B Biointerfaces* 89: 147–151.

Ternes, T.A., Meisenheimer, M., McDowell, D., Sacher, F., Brauch, H.J., Haist-Gulde, B., Preuss, G., Wilme, U. and Zulei-Seibert, N., 2002. Removal of pharmaceuticals during drinking water treatment. *Environmental Science & Technology* 36: 3855–3863.

Tu, Y., Lv, M., Xiu, P., Huynh, T., Zhang, M., Castelli, M., Liu, Z., Huang, Q., Fan, C., Fang, H. and Zhou, R., 2013. Destructive extraction of phospholipids from *Escherichia coli* membranes by graphene nanosheets. *Nature Nanotechnology* 8: 594–601.

US EPA (United States Environmental Protection Agency), 2016. *Life Cycle Inventory (LCI) Data – Treatment Chemicals, Construction Materials, Transportation, On-site Equipment, and Other Processes for Use in Spreadsheets for Environmental Footprint Analysis (SEFA)*.Technical Report EPA/600/R-16/176. US EPA, Cincinnati, OH.

Van der Bruggen, B. and Vandecasteele, C., 2002. Modelling of the retention of uncharged molecules with nanofiltration. *Water Research* 36: 1360–1368.

Van der Bruggen, B. and Vandecasteele, C., 2003. Removal of pollutants from surface water and groundwater by nanofiltration: overview of possible applications in the drinking water industry. *Environmental Pollution* 122: 435–445.

Vergili, I., 2013. Application of nanofiltration for the removal of carbamazepine, diclofenac and ibuprofen from drinking water sources. *Journal of Environmental Management* 127: 177–187.

Verliefde, A.R.D., Heijman, S.G.J., Cornelissen, E.R., Amy, G., Van der Bruggen, B. and van Dijk, J.C., 2007. Influence of electrostatic interactions on the rejection with NF and assessment of the removal efficiency during NF/GAC treatment of pharmaceutically active compounds in surface water. *Water Research* 41: 3227–3240.

Vieno, N., Tuhkanen, T. and Kronberg, L., 2006. Removal of pharmaceuticals in drinking water treatment: effect of chemical coagulation. *Environmental Technology* 27(2): 183–192.

Vieno, N., Tuhkanen, T. and Kronberg, L., 2007. Elimination of pharmaceuticals in sewage treatment plants in Finland. *Water Research* 41: 1001–1012.

Villanueva, C.M., Kogevinas, M. and Grimalt, J.O., 2003. Haloacetic acids and trihalomethanes in finished drinking waters from heterogeneous sources. *Water Research* 37(4): 953–958.

Vogel, D., Simon, A., Alturki, A., Bilitewski, B., Price, W.E. and Nghiem, L., 2010. Effects of fouling and scaling on the retention of trace organic contaminants by a nanofiltration membrane: the role of cake-enhanced concentration polarisation. *Separation and Purification Technology* 73: 256–263.

Vona, A., di Martino, F., Garcia-Ivars, J., Pico, Y., Mendoza-Roca, J.A. and Iborra-Clar, M.I., 2015. Comparison of different removal techniques for selected pharmaceuticals. *Journal of Water Process Engineering* 5: 48–57.

Wang, S., Hongqi, S., Ha-Ming, A. and Moses, T., 2013. Adsorptive remediation of environmental pollutants using novel graphene-based nanomaterials. *Chemical Engineering Journal* 226: 336–347.

Wang, X., Li B., Zhang T. and Li X.Y., 2015. Performance of nanofiltration membrane in rejecting trace organic compounds: experiment and model prediction. *Desalination* 370: 7–16.

Wei, X., Wang, Z., Fan, F., Wang, J. and Wang, S., 2010. Advanced treatment of a complex pharmaceutical wastewater by nanofiltration: membrane foulant identification and cleaning. *Desalination* 251: 167–175.

Xu, C., Wang, X., Yang, L. and Wu, Y., 2009. Fabrication of a graphene–cuprous oxide composite. *Journal of Solid State Chemistry* 182(9): 2486–2490.

Xu, C., Cui, A., Xu, Y. and Fu, X., 2013. Graphene oxide–TiO_2 composite filtration membranes and their potential application for water purification. *Carbon* 62: 465–471.

Yang, J. and Qiu, K., 2010. Preparation of activated carbons from walnut shells via vacuum chemical activation and their application for methylene blue removal. *Chemical Engineering Journal* 165: 209–217.

Yang, X., Zhang, X., Ma, Y., Huang, Y., Wang, Y. and Chen, Y., 2009. Superparamagnetic graphene oxide-Fe_3O_4 nanoparticles for controlled targeted drug carriers. *Journal of Materials Chemistry* 21: 2710–2714.

Yang, S.T., Chen, S., Chang, Y., Cao, A., Liu, Y. and Wang, H., 2011. Removal of methylene blue from aqueous solution by graphene oxide. *Journal of Colloid and Interface Science* 359: 24–29.

Yang, L., Ma, X. and Guo, N., 2012. Sodium alginate/Na^+-rectorite composite microspheres: preparation, characterization, and dye adsorption. *Carbohydrate Polymers* 90: 853–858.

Yang, G.C.C., Chen, Y.C., Yang, H.X. and Yen, C.H., 2016. Performance and mechanisms for the removal of phthalates and pharmaceuticals from aqueous solution by graphene-containing ceramic composite tubular membrane coupled with the simultaneous electrocoagulation and electrofiltration process. *Chemosphere* 155: 274–282.

Yoon, Y., Westerhoff, P., Snyder, S.A. and Wert, E.C., 2006. Nanofiltration and ultrafiltration of endocrine disrupting compounds, pharmaceuticals and personal care products. *Journal of Membrane Science* 270: 88–100.

Yoon, K.Y., Hoon Byeon, J., Park, J.H., Hwang, J., 2007. Susceptibility constants of *Escherichia coli* and *Bacillus subtilis* to silver and copper nanoparticles. *Science of the Total Environment* 373: 572–575.

Zhang, K., 2012. Fabrication of copper nanoparticles/graphene oxide composites for surface-enhanced Raman scattering. *Applied Surface Science* 258: 7327–7329.

Zhang, X., Liu, Y., Sun, C., Ji, H., Zhao, W., Sun, S., Zhao, C., Bhatnagar, A., Sillanpää, M. and Vandenbroucke, A.M., 2015. Graphene oxide-based polymeric membranes for broad water pollutant removal. *RSC Advances* 5: 100651–100662.

Abbreviations

^{1}H-NMR	Proton nuclear magnetic resonance
ADP	Abiotic depletion
AOP	Advanced oxidation process
BSA	Bovine serum albumin
CFU	Colony-forming units
CML	Institute for Environmental Science
Cu-rGO	Reduced graphene oxide–copper composite
CuNP	Copper nanoparticle
DCB	1,4-Dichlorobenzene
DCU	Dublin City University
DI	Deionised
EDX	Energy-dispersive X-ray spectroscopy
EG	Expanded graphite
FO	Forward osmosis
FRR	Flux recovery ratio
FTIR	Fourier transform infrared
GAC	Granular-activated carbon
GCC	Graphene–copper composite
GO	Graphene oxide
GRM	Graphene-related material
GWP	Global warming protection
HA	Humic acid
HOP	Hazardous organic pollutant
IMS	Industrial methylated spitits
IPA	Isopropyl alcohol
LCA	Life cycle assessment
LCI	Life cycle inventory
LCIA	Life cycle impact assessment
LogK_{ow}	Octanol water partition coefficient
LYZ	Lysozyme
MB	Methylene blue
MD	Membrane distillation
MF	Microfiltration
MIC	Minimum inhibitory concentration
MWCO	Molecular weight cut-off
NF	Nanofiltration
NIPS	Non-solvent induced phase separation
NMP	*N*-methyl-2-pyrrolidone
NOM	Natural organic matter
PBS	Phosphate-buffered saline
PMMA	Polymethyl methacrylate
PCOP	phytochemical oxidation potential
PPCP	Pharmaceuticals and personal care product
ppm	Parts per million
PSf	Polysulfone
PV	Pervaporation
PVP	Polyvinylpyrrolidone
QPSf	Quaternised polysulfone
rGO	Reduced graphene oxide
RO	Reverse osmosis
rpm	Revolutions per minute
RT	Room temperature
SEM	Scanning electron microscopy
TEM	Transmission electron microscopy
TFC	Thin film composite
TGA	Thermogravimetric analysis
TTIP	Titanium isopropoxide
UF	Ultrafiltration
UV	Ultraviolet
UV-Vis	Ultraviolet-visible
WWTP	Wastewater treatment plant

Appendix 1 Selected Outputs of the Project

Publications

Lawler, J., 2017. Graphene-based nanosheet functionalized membranes – industrial applications. In Wright, D. (ed.), *Nanosheets: Types, Applications and Research Insights*. Nova Science Publishers, Hauppage, NY, pp. 1–40.

Kumar, M., Gholamvand, Z., Morrissey, A., Nolan, K., Ulbricht, M. and Lawler, J., 2016. Preparation and characterization of low fouling novel hybrid ultrafiltration membranes based on the blends of GO/TiO_2 nanocomposite and polysulfone for humic acid removal. *Journal of Membrane Science* 506: 38–49.

Kumar, M., McGlade, D., Ulbricht, M. and Lawler, J., 2015. Quaternized polysulfone and graphene oxide nano-sheet derived low fouling novel positively charged hybrid ultrafiltration membranes for protein separation. *RSC Advances* 63(5): 51208–51219.

Kumar, M., McGlade, D. and Lawler J., 2014. Functionalised chitosan derived novel positively charged organic–inorganic hybrid ultrafiltration membranes for protein separation. *RSC Advances* 42(4): 21699–21711.

Conference Presentations – Oral

McGlade, D., Morrissey, A., Nolan, K., Lawler, J. and Quilty, B., 2016. A graphene–copper composite film as an anti-bacterial agent for potential water treatment applications. Environ 2016, University of Limerick, Limerick.

McGlade, D., Morrissey, A., Nolan, K., Lawler, J. and Quilty, B., 2016. A graphene–copper composite as an anti-bacterial agent for potential water treatment applications. Advanced Materials World Congress 2016, Stockholm.

McGlade, D., Morrissey, A., Nolan, K., Lawler, J. and Quilty, B., 2015. A graphene–copper composite as an anti-bacterial agent for potential water treatment applications, Environ 2015, IT Sligo, Sligo.

Morrissey, A., Nolan, K., Gholamvand, Z., Keane, D. and O'Dwyer, R., 2014. Using nanomaterials to remove emerging micro-pollutants from water. 247th American Chemical Society National Meeting & Exposition, 16–20 March, Dallas, TX.

Conference Presentations – Poster

McGlade, D., Morrissey, A., Nolan, K., Lawler, J. and Quilty, B., 2014. Investigation of the antimicrobial activity of graphene and graphene composites for use in drinking water treatment. Environ 2014, 26–28 February, Trinity College Dublin, Dublin.

McGlade, D., Morrissey, A., Nolan, K., Lawler, J. and Quilty, B., 2014. Investigation of the anti-microbial activity of graphene and graphene composites for use in drinking water treatment. Graphene Study 2014, Obergurgl, Austria.

McGlade, D., Morrissey, A., Nolan, K., Lawler, J. and Quilty, B., 2013. Investigation of the anti-microbial activity of graphene oxide and reduced graphene oxide. Environ 2013, National University of Ireland, Galway, Galway.

McGlade, D., Morrissey, A., Nolan, K., Lawler, J. and Quilty, B., 2013. Investigation of the anti-microbial activity of graphene and graphene composites for use in drinking water treatment. ATWARM 2013, The Helix, Dublin City University, Dublin.

Planned Publications

McGlade, D., Morrissey, A., Nolan, K., Lawler, J. and Quilty, B., 2017. The antibacterial activity of graphene materials: a review. For submission to *Colloids and surfaces B: Biointerfaces*.

McGlade, D., Morrissey, A., Nolan, K., Lawler, J. and Quilty, B., 2017. Production, characterisation and antibacterial activity of graphene–copper composite films. For submission to *Colloids and Surfaces B: Biointerfaces*.

Jaquet, Y., Gunes, B., Kumar, M., Yavorskky, A., McGlade, D., Quilty, B., Morrissey, A., Nolan, K. and Lawler, J., 2017. Adsorption of methylene blue onto dried and pH activated alginate-graphene oxide beads. For submission to *Chemical Engineering Journal*.

Jaquet, Y., Gunes, B., Kumar, M., Yavorskky, A., McGlade, D., Quilty, B., Morrissey, A., Nolan, K. and Lawler, J., 2017. Removal of pharmaceuticals from aqueous solutions using dried and ph activated alginate-graphene oxide beads. For submission to *Journal of Hazardous Materials*.

Other

Morrissey, A., 2014. New technology uses sunlight to purify water. *Business Standard*, 23 March 2014. Available online: http://www.business-standard.com/article/news-ani/new-technology-uses-sunlight-to-purify-water-114032300289_1.html (accessed 30 April 2016).

Appendix 2 Detailed Analysis of LCIA

A2.1 Global Warming and Acidification

Global warming potential per MB and famotidine removal is 0.02 and 0.054 kg CO_2 equivalent, respectively (Figure A2.1). Acidification potential per MB and famotidine is 1×10^{-4} and 2.69×10^{-4} kg SO_2 equivalent (Figure A2.2). The Hummers process, which is used to prepare the GO, accounts for >90% of the total GWP and acidification potential. The H_2O_2 input is responsible for 60% of the GWP; H_2SO_4 (16.5%), graphite production (8%) and HCl production (5%) are the other primary contributors to this category. H_2SO_4 production accounts for almost 80% of the acidification, with H_2O_2 the next largest contributor potential, accounting for over 11% of the total.

A2.2 Photochemical Oxidation and Ozone Depletion

Photochemical oxidation potential per MB and famotidine removal is 6.66×10^{-6} and 1.75×10^{-5} kg ethane equivalent, respectively (Figure A2.3). The primary contributors in this category are H_2SO_4 (63%) and H_2O_2 production (25%). The actual photochemical oxidation potential (PCOP) impact is subject to regional sensitivities. H_2O_2 and H_2SO_4 production datasets used in this study are based on French and aggregated EU-28 data, respectively. Climatic conditions have a large influence on the PCOP cause–effect chain. Photochemical oxidation occurs most commonly in locations where there are high concentrations of nitrogen oxides and volatile organic carbons, and in atmospheres of high sunlight, stagnant air and low precipitation. These conditions occur more commonly on mainland Europe; they are not commonplace in Ireland. Therefore, while it is conceivable that the production of H_2O_2 and H_2SO_4 in Ireland may produce similar potentials, the actual effect of PCOP emissions may be much lower than in Europe. Ozone depletion potential per MB and famotidine removal is 1.43×10^{-13} and 3.76×10^{-13} kg R11 equivalent, respectively (Figure 2.7). The main contributors are H_2O_2 (57%) and H_2SO_4 production (24%). Normalised ozone depletion potential values are orders of magnitude lower than other impact category outputs (Figure A2.4) as a result of human efforts to reduce the use and, ultimately, emissions of chlorofluorocarbons over the last three decades. Further efforts to reduce ozone depletion potential should focus on reducing emissions of bromine source gases.

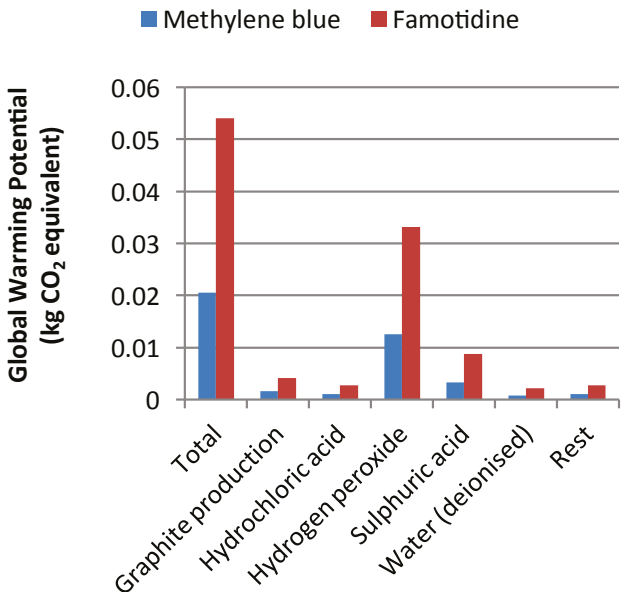

Figure A2.1. Global warming potential.

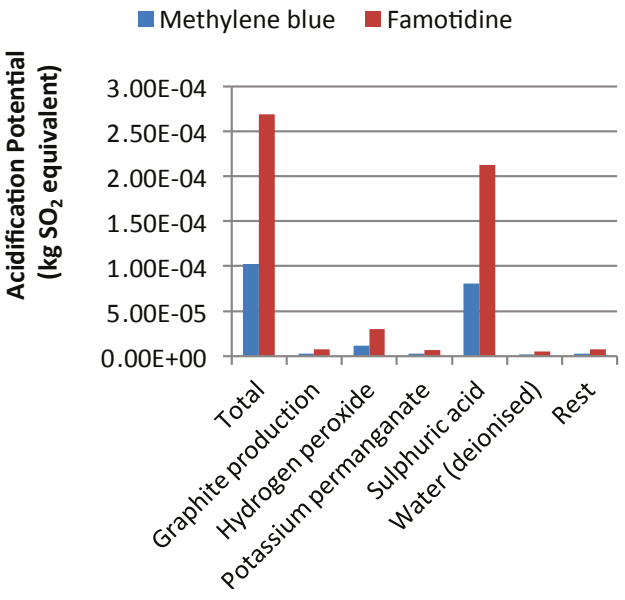

Figure A2.2. Acidification potential.

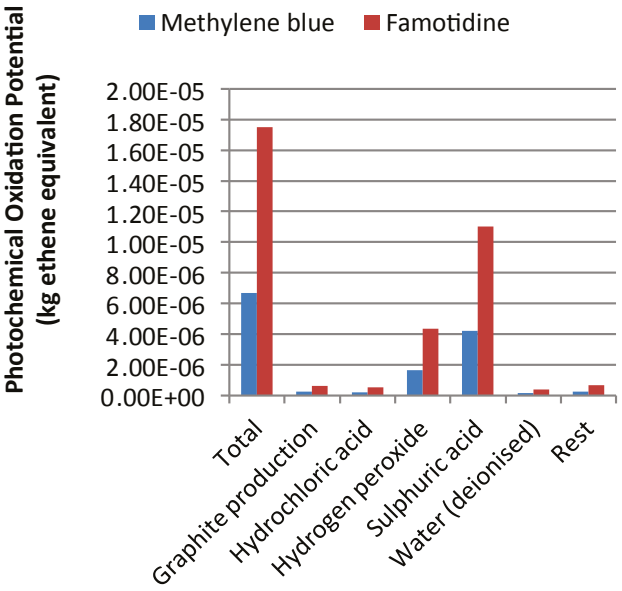

Figure A2.3. Photochemical oxidation potential.

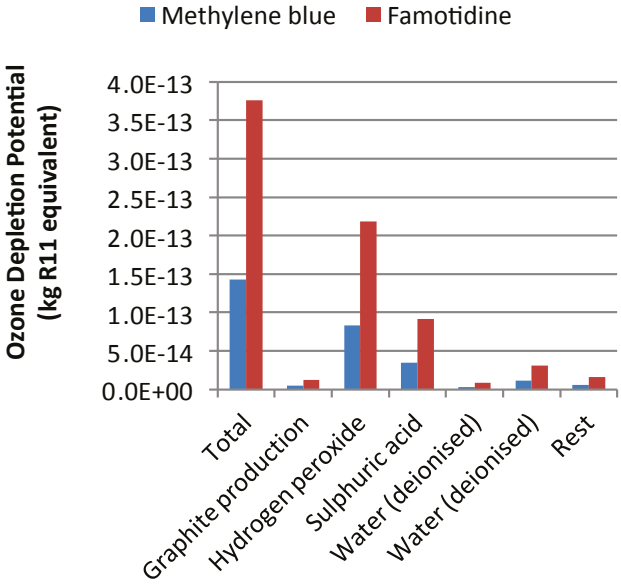

Figure A2.4. Ozone depletion potential.

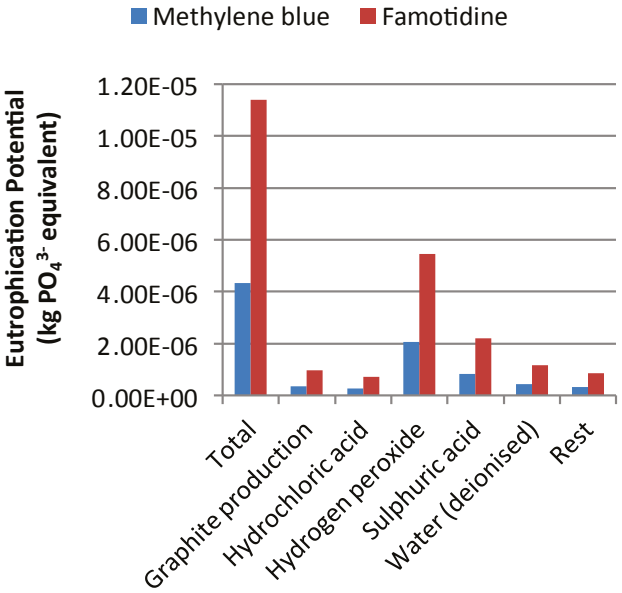

Figure A2.5. Eutrophication potential.

A2.3 Eutrophication

Eutrophication potential per MB and famotidine removal is 4.34×10^{-6} and 1.14×10^{-5} kg PO_4^{3-} equivalent, respectively (Figure A2.5). H_2O_2 production accounts for 47% of total eutrophication potential and is the largest contributor to this category. H_2SO_4 production (19%), DI water (10%) and graphite production (8%) make up the most of the remaining potential. Eutrophication is a regionally sensitive environmental intervention with an end-point impact that is dependent on several local parameters, such as the existing background concentrations of eutrophying substances and receiving compartment (air, water, soil) variation. It is worth pointing out once more that the CML methodology defines only the potential for environmental impact and not the actual end-point effect. Therefore, while the values presented here provide a good basis for comparing systems' environmental profiles, assessment of the actual impact would require a more extensive localised data acquisition exercise as per environmental risk assessment practices.

A.2.4 Ecotoxicity

Ecotoxicity potential presented in units of kg of 1,4-dichlorobenzene (DCB) equivalent is further divided into freshwater (Figure A2.6), human (Figure A2.7), marine (Figure A2.8) and terrestrial (Figure A2.9) toxicity potential. The primary contributors to impact potential are H_2O_2 (17–83% of total potential) and H_2SO_4 (2.6–60% of total potential) production. Of the four toxicity categories, the marine exhibits the largest potential at 0.78 kg DCB/mg MB removed, and 2 kg DCB/mg famotidine removed. Human, terrestrial and freshwater toxicity potentials for MB and famotidine removal are 7.16×10^{-4} and 1.88×10^{-3}, 1.48×10^{-4} and 3.88×10^{-3}, and 8.64×10^{-5} and 2.2×10^{-4} kg DCB equivalence, respectively.

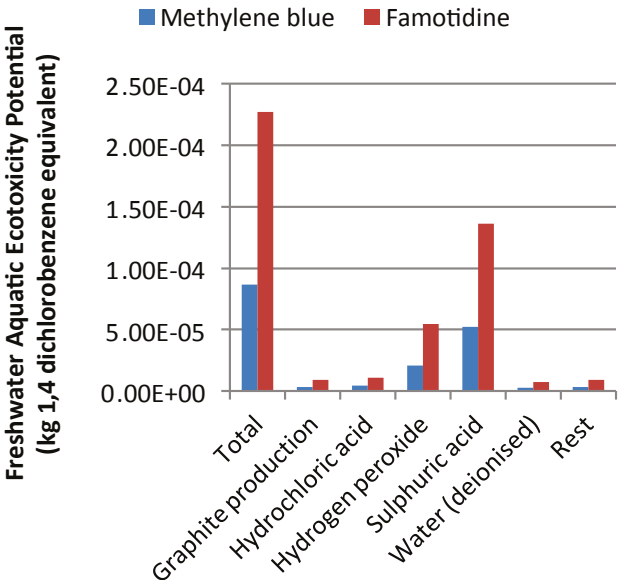

Figure A2.6. Freshwater aquatic ecotoxicity potential.

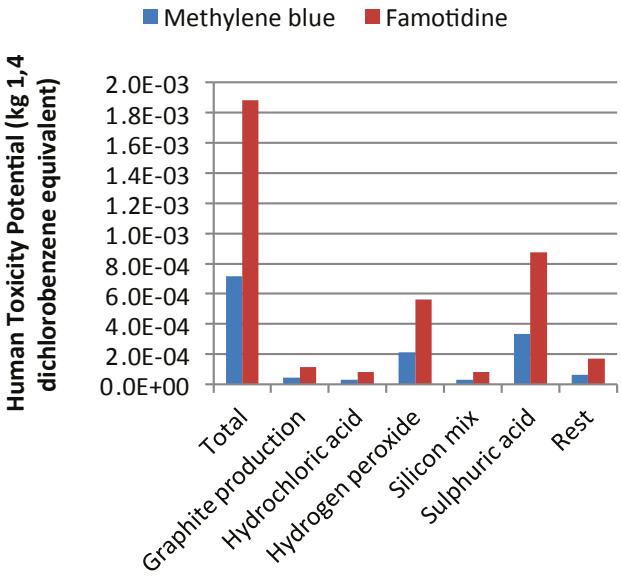

Figure A2.7. Human toxicity potential.

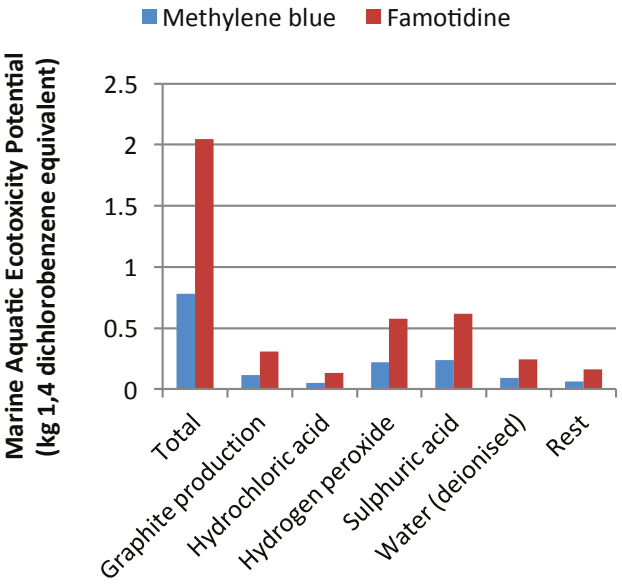

Figure A2.8. Marine aquatic ecotoxicity potential.

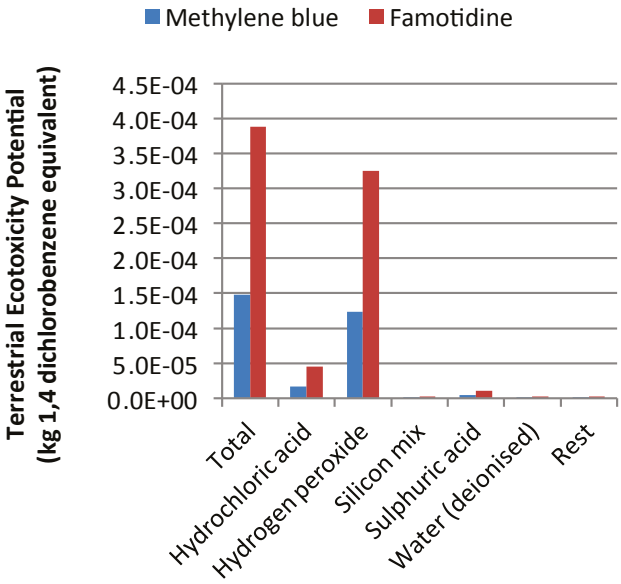

Figure A2.9. Terrestrial ecotoxicity potential.

A2.5 Abiotic Resource Depletion

Abiotic resource depletion is presented in two different forms. The impact of the elemental abiotic depletion (ADP) category (ADPe) is measured relative to the ultimate reserves of a substance and is expressed in units of antimony equivalence (kg Sb_{eqv}) (Figure A2.10). In this category, it is the quantity of Cu consumed that accounts for the largest percentage of potential impact at 77%, with minor contributions from other inputs.

The impact of the fossil ADP category is based on the exergy content of a substance expressed in units of MJ/kg (Figure A2.11). As with many of the other impact categories, it is the production of H_2O_2 and H_2SO_4 that provides over 90% of the total potential impact.

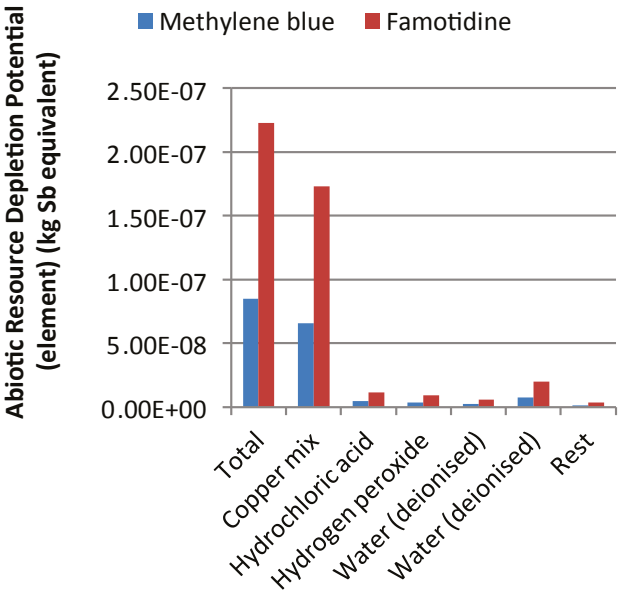

Figure A2.10. ADP potential (element).

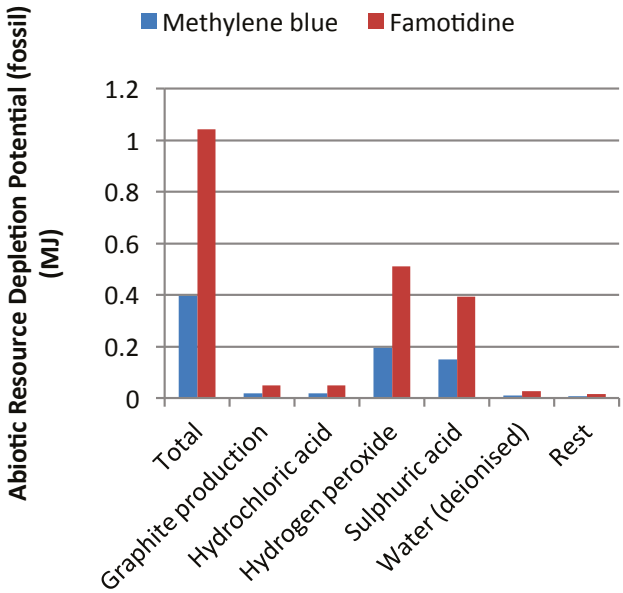

Figure A2.11. ADP potential (fossil).

EPA Research Report 234

One-step Drinking Water Treatment Using Filtration and Nanostructured Composites

Authors: Anne Morrissey, Declan McGlade, Kieran Nolan, Brid Quilty and Jenny Lawler

This report provides a summary of the findings of the research on the design, development and testing of a novel drinking water treatment system using a combination of filtration and nanostructured composites for the removal of inorganic, organic and microbiological contaminants from water. The system developed is based on a novel graphene adsorptive biocide composite used in combination with a filtration membrane separation system and addresses the limitations of disinfection methods that use TiO_2 and UV.

Identify Pressures

Sustainable access to clean, safe drinking water has been a key concern in Ireland in recent years, with instances of boil water notices due to the presence of microbial contaminants such as *Cryptosporidium parvum* and *E. coli*, being all too frequent. Many drinking water treatment plants do not have the technical capacity to fully eliminate these microbial contaminants. In addition, emerging micropollutants of concern, such as diclofenac, a commonly used nonsteroidal anti-inflammatory drug, are also not fully eliminated in a drinking water treatment process. While levels found in drinking water sources are typically very low (of the ng/L to µg/L order of magnitude), the effects of long term exposure to low levels of these chemicals is unknown.

In order to assure water quality, the development and application of treatment technologies that are capable of removing microbial contaminants, pharmaceutical and personal care products and Hazardous organic materials is apparent. While community access to drinking water varies between public water supplies, group water schemes and private water supplies, there is a need for a variety of drinking water treatment technologies, that can remove both microbial and other micropollutants in the same system, particularly for small water supply schemes. A solution to these pressures is addressed in this report.

Inform Policy

Environmental quality standards for a list of priority substances in surface waters is published in Annex II of the Directive on Environmental Quality Standards (Directive 2008/105/EC) (EQSD). In addition to the priority list, the need for a second list, called a **Watch List**, was also established for the purpose of supporting future prioritisation exercises. This watch list now comprises of 10 substances as identified in the EU Commission Implementing Decision 2015/495, one of which is diclofenac. This report provides useful information that can aid policy, enforcement and engineering stakeholders work towards an efficient, low cost small scale drinking water treatment system.

Develop Solutions

The key output from this project is an innovative modular drinking water treatment system that can be used for small scale drinking water treatment. The overall system, which incorporates a preliminary ultra-filtration step followed by a prototype consisting of 9 graphene-copper composite coated membranes, was shown to be effective in the adsorption of small organic molecules and the removal and inactivation of microorganisms such as *E. Coli* and *Cryptosporidum parvum*. This design can be improved by selecting membranes that are tailored to the pollutant characteristics and by the inclusion of a nano-filtration post-treatment step on a temporary basis to manage standalone pollution events. Other recommended design improvements to avoid membrane rupture, is to use a more porous or "holey" design, similar to a buchner funnel, that better facilitates the distribution of pressure across the membrane.

EPA Research: McCumiskey House, Richiew, Clonskeagh, Dublin 14.

Phone: 01 268 0100
Twitter: @EPAResearchNews
Email: research@epa.ie

www.epa.ie

EPA Research Webpages
www.epa.ie/researchandeducation/research/